Time-resolved swarm studies in gases with emphasis on electron detachment and ion conversion

Please check the document version of this publication:

TIME-RESOLVED SWARM STUDIES IN GASES
WITH EMPHASIS ON
ELECTRON DETACHMENT AND ION CONVERSION

WEN, CHUAN

TIME-RESOLVED SWARM STUDIES IN GASES
WITH EMPHASIS ON
ELECTRON DETACHMENT AND ION CONVERSION

TIME-RESOLVED SWARM STUDIES IN GASES
WITH EMPHASIS ON
ELECTRON DETACHMENT AND ION CONVERSION

PROEFSCHRIFT

TER VERKRIJGING VAN DE GRAAD VAN DOCTOR
AAN DE TECHNISCHE UNIVERSITEIT EINDHOVEN,
OP GEZAG VAN DE RECTOR MAGNIFICUS,
PROF. IR. M. TELS, VOOR EEN COMMISSIE
AANGEWEZEN DOOR HET COLLEGE VAN
DEKANEN IN HET OPENBAAR TE VERDEDIGEN
OP DINSDAG 26 SEPTEMBER 1989 TE 14.00 UUR

DOOR

WEN, CHUAN

GEBOREN TE XI'AN, CHINA

Dit proefschrift is goedgekeurd door de

promotor: Prof. dr. ir. P. C. T. van der Laan

co-promotor: Dr. ir. J. M. Wetzer

To my predecessors
who opened the subject
and
to my successors
who will see further than I

Wen, Chuan

CONTENTS

PUBLICATIONS INCLUDED:

[1] C. Wen, and J.M. Wetzer. Conf. Record of the 1988 IEEE Int. Symp. on Electrical Insulation, Boston, June 5-8, pp.108-111.

[2] C. Wen, and J.M. Wetzer. Proc. 9th Int. Conf. on Gas Discharges and Their Applications, Venezia, Sept. 19-23, 1988, pp.367-370.

[3] C. Wen, and J.M. Wetzer. IEEE Trans. on Electrical Insulation, Vol. 23, No. 6, Dec., 1988, pp.999-1008.

[4] C. Wen, and J.M. Wetzer. IEEE Trans. on Electrical Insulation, Vol. 24, No. 1, Feb., 1989, pp.143-149.

[5] C. Wen, and J.M. Wetzer. Proc. 19th Int. Conf. on Phen. in Ionized Gases, Belgrade, July 10-14, 1989, Vol. 3, pp.592-593.

[6] J.M. Wetzer, and C. Wen. Proc. 5th Int. Symp. on High Voltage Engineering, Braunschweig, Aug. 24-28, 1987. Paper 15.06.

[7] J.M. Wetzer, and C. Wen. Proc. 6th Int. Symp. on High Voltage Engineering, New Orleans, Aug. 28-Sept. 1, 1989. Paper 23.03.

[8] J.M. Wetzer, C. Wen, and P.C.T. van der Laan. Conf. Record of the 1988 IEEE Int. Symp. on Electrical Insulation, Boston, June 5-8, pp.355-358.

SUMMARY

Insulating gases used in power systems may occasionally suffer electrical breakdown. Such a breakdown occurs as the result of excessive charge growth, in which various collisional processes are involved. Knowledge on these fundamental collisional processes, and on the transport properties of electrons and ions, is therefore of great importance for the understanding of gaseous breakdown. The aim of the present work is to investigate the processes responsible for the avalanche growth. The emphasis is on electron detachment and ion conversion processes, and their impact on the avalanche properties and on the dielectric behavior of the gases studied. These two processes determine the production rate of "delayed" electrons and are called delaying processes. The experimental technique used is the so-called time-resolved swarm method.

A thorough analysis of bandwidth limitations of the time-resolved current measurement has been carried out, which has resulted in improvements of the measuring system. The main features of the present system are: (1) a TEA N_2 laser (wavelength 337.1 nm) with a very short pulse duration (0.6 ns) for releasing primary electrons ($10^6 \sim 10^7$) from the cathode; (2) a subdivided measuring electrode which favors both sensitivity and frequency response; (3) a fast 9 bit digitizer (bandwidth $0 \sim 1$ GHz) for recording avalanche current waveforms; and (4) a careful layout of the whole measuring system which minimizes electromagnetic interference, traveling wave effects, and the effects of stray capacitance and inductance. The time-resolution of the setup is 1.4 ns.

A hydrodynamic model has been set up that accounts for electron and ion drift, electron diffusion, ionization, attachment, electron detachment and ion conversion. Analytical solutions have been obtained for this model, and for several special cases (with and without diffusion, with and without delaying processes). Fitting programs have been developed to derive swarm parameters from measured current waveforms, in particular from the electron component of the current.

Fast swarm experiments have been performed in N_2, SF_6, dry air, O_2, $1-C_3F_6$, $c-C_4F_8$ and CCl_2F_2. Depending on the gas under study,

swarm parameters such as the electron drift velocity, the electron longitudinal diffusion coefficient, the effective ionization coefficient, and the detachment and conversion coefficients have been determined from the evaluation of the measured avalanche current waveforms with appropriate theoretical models. The results are interpreted in terms of the responsible collisional processes.

Special effort has been paid to $1-C_3F_6$ and $c-C_4F_8$. In the literature these two gases have been reported to possess an abnormal dielectric behavior: they show unexpected pressure dependences of the dielectric strength and of the "apparent" swarm parameters, which cannot be explained by the conventional approach (an experiment with insufficient or no time resolution, and a model without delaying processes). With the present fast avalanche setup, we have clearly observed the occurrence of delaying processes in these gases. The evaluation of the measured avalanche current waveforms shows that these delaying processes are responsible for the reported abnormal dielectric behavior.

SAMENVATTING

Isolerende gassen, zoals toegepast in de energietechniek, kunnen
ongewenst elektrische doorslag vertonen. Deze doorslag is het gevolg
van een buitensporige aangroei van lading. Hierbij zijn verschillende
botsings-processen betrokken. Kennis over deze processen, alsook over
de transport-grootheden van elektronen en ionen, is daarom van groot
belang voor een goed begrip van doorslag in gassen. Doel van dit
promotie-onderzoek is om de processen te onderzoeken die
verantwoordelijk zijn voor de aangroei van lawines. Hierbij ligt de
nadruk op "electron detachment" of "loslating" (negatieve ionen staan
hun elektron weer af) en "ion conversion" of "konversie" (instabiele
negatieve ionen gaan over in stabiele negatieve ionen), alsook op de
effekten van deze processen op de lawine-eigenschappen en op het
dielektrische gedrag van de bestudeerde gassen. De twee genoemde
processen bepalen de mate waarin "vertraagde" elektronen worden
geproduceerd, en worden vertragende processen genoemd. De gehanteerde
experimentele techniek is de zogenaamde tijdopgeloste lawine-meting.

Een grondige analyse van de bandbreedte-beperkingen van de
tijdopgeloste stroommeting is uitgevoerd. Dit heeft geleid tot een
aantal verbeteringen van de meetopstelling. De belangrijkste
eigenschappen van het huidige meetsysteem zijn: (1) elektronen (1~10
miljoen) worden uit de kathode vrijgemaakt met behulp van een TEA N_2
laser (golflengte 337.1 nm) met een korte pulsduur (0.6 ns);
(2) gevoeligheid en bandbreedte zijn optimaal door het gebruik van
een opgedeelde meetelektrode; (3) de golfvorm wordt vastgelegd met
een snelle 9 bit digitizer (bandbreedte 0~1 GHz); en
(4) elektromagnetische storingen, lopende-golf effekten en de
effekten van parasitaire kapaciteiten en zelfindukties zijn minimaal
door een zorgvuldig ontwerp van het meetsysteem. De tijdoplossing van
de meetopstelling is 1.4 ns.

Een hydrodynamisch model is opgezet dat de volgende processen in
rekening brengt: drift van elektronen en ionen, diffusie van
elektronen, ionizatie, aanhechting, loslating en konversie. Een
analytische oplossing is verkregen voor het komplete model, en voor
enkele speciale gevallen (met en zonder diffusie, met en zonder

vertragende processen). Fitting programma's zijn ontwikkeld om lawine-parameters te bepalen uit de golfvorm van de gemeten stroom, en in het bijzonder uit de elektronen-komponent van deze stroom.

Tijdopgeloste lawine-metingen zijn uitgevoerd in N_2, SF_6, droge lucht, O_2, $1-C_3F_6$, $c-C_4F_8$ en CCl_2F_2. Afhankelijk van het bestudeerde gas zijn lawine-grootheden, zoals de driftsnelheid en de longitudinale diffusie-koefficient van elektronen, de effektieve ionizatie-koefficient en de koefficienten voor loslating en konversie, bepaald door de golfvorm van de lawine-stroom te analyseren aan de hand van geschikte modellen. De resultaten zijn geinterpreteerd in termen van de verantwoordelijke botsings-processen.

Speciale aandacht is uitgegaan naar $1-C_3F_6$ en $c-C_4F_8$. Volgens de literatuur worden deze twee gassen gekenmerkt door abnormaal dielektrisch gedrag: ze vertonen een onverwachte druk-afhankelijkheid in de doorslagveldsterkte en in de "schijnbare" lawine-parameters, welke niet verklaard kan worden volgens de gangbare benadering van lawines (een opstelling met een te gering of geen tijdoplossend vermogen, en een model waarin geen vertragende effekten in rekening zijn gebracht). Met de hier gerapporteerde tijdopgeloste metingen is het optreden van vertragende processen in deze gassen duidelijk waargenomen. De analyse van de gemeten stroom-golfvormen laat zien dat deze vertragende processen verantwoordelijk zijn voor het gerapporteerde abnormale dielektrische gedrag.

4

CHAPTER 1

INTRODUCTION

1.1 General aspects of gaseous insulation

Gases are widely used as a dielectric in power systems to provide insulation. During the operation of these systems, the insulating gas may, however, break down electrically; the gas then shows a rapid (milliseconds to nanoseconds) transition from a perfect insulator to an almost perfect conductor (Llewellyn-Jones, 1983). Such electrical breakdown of gases may occur, for instance, as a result of either external (lightning) or internal (switching) overvoltages.

The breakdown voltage (or dielectric strength) of a certain gas in a practical system depends not only on the inherent (physical and chemical) properties of the gas but also on the gas pressure and temperature, the waveform of the applied voltage, the electrode material and geometry, field inhomogeneities and surface properties of electrodes and insulators (Meek and Craggs, 1978). In addition, environmental conditions such as dust, moisture and pollution may strongly influence the electrical insulation behavior of air gaps in open air substations and of overhead transmission lines (Feser and Schmid, 1987). In this context, gas-insulated substations (GIS) and transmission cables (GITC) have rapidly gained worldwide acceptance in power systems because of their advantages. These advantages include the reduction of system size, the reduced sensitivity to environmental conditions and the possibility of using compressed gases or gas-mixtures with a higher dielectric strength than that of atomspheric air (Garrity and Vora, 1980).

At present, sulphur hexafluoride, SF_6, is commonly used in GIS systems. This gas has, however, its problems (Christophorou and co-workers, 1982): (a) it is sensitive to non-uniform fields, particles and rough surfaces; (b) it may form harmful by-products during the spark, and (c) it is relatively expensive. Therefore, with the demands for higher voltages for energy transmission, "new" gases or gas-mixtures with insulating characteristics superior to SF_6 are being considered as replacements of, or admixtures to, SF_6 (James and co-workers, 1978; James and co-workers, 1980; Wootton and co-workers,

1980).

1.2 Implications of electron detachment and ion conversion

Gaseous breakdown occurs as the result of excessive charge growth, in which various collisional processes such as ionization, attachment, detachment and conversion are involved. A detailed description of these collisional processes is presented in chapter 2.

Ionization and attachment are often considered the predominant processes. In that case all electrons are contained in the avalanche head. In many cases, however, also electron detachment and ion conversion processes play an important role in the growth of the pre-breakdown avalanches; therefore the formation and loss of unstable negative ions cannot be neglected.

Electron detachment from unstable negative ions provides delayed electrons and, as a consequence, alters the spatial distribution of electrons in the swarm. Electrons then are not only contained in the avalanche head, but the avalanche has a distinct tail. This will affect the breakdown characteristics of gases in case of streamer breakdown since this mechanism depends on the field distortion caused by the charge distribution of the swarm. On the other hand, ion conversion (from unstable negative ions to stable ones) reduces the probability of releasing electrons from the unstable negative ions and is actually a process that competes with electron detachment.

The electron detachment and ion conversion processes often cause surprising pressure dependences of the dielectric strength, and of the "apparent" swarm parameters (see Verhaart and van der Laan (1984) for humid air, and Wen and Wetzer (1988a) for $1-C_3F_6$).

Electron detachment, at a much slower rate, can also be important for the production of the first electrons that initiate breakdown. This "slow" electron detachment strongly affects the statistical time-lag for impulse breakdown (Somerville and Tedford, 1982).

1.3 Methods for the study of avalanches in insulating gases

To understand and predict the insulating behavior of a certain insulating gas, basic studies are obviously required. Such basic studies can, in general, be classified into two categories: (I) the study of breakdown behavior, and (II) the study of pre-breakdown

6

processes.

The first category investigates directly the breakdown behavior of insulating gases under a number of conditions, such as different kinds of field configurations (uniform and non-uniform fields), different gas pressures and different voltage waveforms (AC, DC, impulse and fast transient). This kind of study can provide information on what breakdown strength a certain insulating gas may possess under certain conditions but does not provide insight into the inhibition and control of breakdown and, as a result, does not allow scaling.

As a complement to the first category, the second category attempts to elucidate the relative importance of various processes, during the pre-breakdown stage, which lead to a gas discharge. Such avalanche studies can contribute significantly to the understanding of the dielectric behavior and to the knowledge on how to predict and control electrical breakdown of insulating gases. Furthermore, avalanche studies have also found their applications in many related technologies such as gas lasers, gaseous switching and plasma etching (Christophorou and Hunter, 1984).

Various methods, both experimental and theoretical, are used for the study of avalanches in insulating gases. In this section we only describe briefly the principles and limitations of some of these methods. Detailed accounts can be found in many references (see, for instance, Christophorou, 1984; Fletcher, 1981; Huxley and Crompton, 1974; Meek and Craggs, 1978; Raether, 1964).

1.3.1 Experimental methods

There are in principle two different types of experimental methods: the measurement of the gap current and the measurement of the photon flux. In each method there are, however, two different approaches: steady state and time resolved.

Steady-state Townsend method (SST). This method (see, for instance, Meek and Craggs, 1978) detects the steady-state current in a parallel-plate gap caused by the multiplication of the primary electrons under the influence of the applied (uniform) electric field. The primary electrons are released continuously by, for example, ultraviolet illumination of the cathode.

7

Swarm parameters, such as the ionization and attachment coefficients, are derived from the measured steady-state current as a function of gap distance. If the anode consists of annular segments and the primary electrons are released from a small cathode area, the transverse diffusion coefficient may also be derived from the ratio of the current collected by each segment to the overall current (Fletcher, 1981).

Due to the absence of temporal resolution, such a method can only provide information on the final result of many different, and possibly successive, reactions between electrons and gas molecules. The evaluation of the measured steady-state current (as a function of gap distance) is restricted to the use of a simple model which includes only ionization and attachment processes. More complex models cannot be verified with the steady-state experiments. The method therefore provides only "apparent" swarm parameters. The interpretation of such "apparent" swarm parameters is often ambiguous and may lead to incorrect conclusions. For instance, secondary electrons produced by positive ions or photons striking the cathode, and electrons produced by electron detachment, all contribute to the total current which can yield false values for the ionization coefficient. Similarly, the negative ions formed by electron attachment and those formed by ion conversion cannot be distinguished, which can lead to false values for the attachment coefficient.

To obtain more information on the physical processes in avalanches and to determine swarm parameters more realistically, one should record the fast time history of electrons and ions. This can be achieved by the so-called time-resolved swarm method.

Time-resolved swarm method (TRS). This method (also called electrical method or pulsed Townsend discharge method (Christophorou, 1984; Raether, 1964)) is based upon the detection of the time-dependent current due to the electrons and ions drifting across a parallel-plate gap under the influence of the applied (uniform) electric field. The primary electrons are released from the cathode by a pulsed ultraviolet source in a very short time interval (this work), or are produced in the gas by a short pulse of γ-radiation (Schmidt and co-workers, 1980).

8

Swarm parameters are obtained from the evaluation of the measured transient current by means of an appropriate theoretical model (see chapter 3).

The time-resolved swarm method presents a more direct way to study the various processes involved, since it enables the observation of the temporal avalanche growth, and thereby the study of the production and loss mechanisms of both electrons and ions. If the time resolution of the experiment is sufficiently high, rapid successive processes (for instance, fast attachment followed by fast detachment) may show up in the current waveform, and a more complete set of swarm parameters can be derived. These fast processes are of more than academic interest as long as they modify the electron distribution in the swarm and thereby the streamer breakdown threshold (Wen and Wetzer, 1988b). In fact, it has been shown in many cases that the identification of various fast processes in avalanches is very useful for the interpretation of the pressure dependences of the breakdown behavior of several insulating gases, such as humid air (Verhaart and van der Laan, 1984) and $1-C_3F_6$ (Wen and Wetzer, 1988a; Wetzer and Wen, 1987). Furthermore, also for the observation and evaluation of diffusion of electrons, a high time-resolution is of paramount importance.

Steady-state photon flux method (SSPF). This method (see, for instance, Meek and Craggs, 1978) is based upon the observation of the emitted light due to decay of gas species excited by electrons with sufficiently high energy. Primary electrons are continuously being released from the cathode as in the steady-state current measurement. The photon flux is observed at different positions across a parallel-plate gap.

The detected photon flux can pinpoint the location of electrons and as such give the electron distribution across the gap which is of importance in understanding the breakdown mechanism. A limitation is the very low photon flux encountered in many gases. Another uncertainty is the quantitative relation between the detected photon flux and the number density of electrons. This relation depends in general on the electron velocity distribution (or "temperature" if the temperature-concept is valid at all). Furthermore, the electron distribution obtained is integrated over time and does not

9

necessarily represent the distribution within a single avalanche.

Time of flight method (TOF). This method (see, for instance, Fletcher, 1981) also detects, at different positions across a parallel-plate gap, the light emitted by excited molecules in the gas. Primary electrons are, in this case, released from the cathode in a very short time interval as in the time-resolved swarm experiment. Therefore the behavior of a single swarm is observed as a function of distance as well as time. From such information swarm parameters can be obtained but the analysis is complicated because of uncertainties in the conversion of the photon distribution into an electron distribution. The problem of detection sensitivity for such a single shot experiment is even more important than for steady-state measurements. This problem can be overcome by performing repetitive measurements (Brennan and Teich, 1988).

1.3.2 Theoretical methods

Theoretical investigations are important for the understanding and the modeling of the electrical discharge behavior of insulating gases. Theoretical methods can be based either on a microscopic or on a macroscopic description of the electron swarm in the gas. The microscopic models give a relation between the cross sections and the velocity distribution on the one hand, and macroscopic, or swarm, parameters on the other. Macroscopic models presume that the processes can be described by swarm parameters. For a microscopic description, the commonly used methods are the Boltzmann equation analysis or the Monte Carlo simulation.

The Boltzmann equation analysis (BEA). In the Boltzmann equation analysis (see, for instance, Huxley and Crompton, 1974), a set of cross sections of relevant elastic and inelastic collisions is collected for the gas under consideration, based on available data from theory and experiment. These cross sections are used in the Boltzmann equation to derive the velocity distribution function. Swarm parameters such as the electron drift velocity, ionization and attachment coefficients can then be calculated and are compared with the experimental swarm data. If the agreement is poor, the set of cross sections should be reexamined.

The Monte Carlo simulation (MCS). An alternative theoretical

10

method that relates the cross sections and the velocity distribution function to swarm parameters is the Monte Carlo simulation (see, for instance, Christophorou, 1984). This technique simulates the actual motion and collisions of the electrons in the swarm by following the trajectories for a large number of electrons. Appropriate averages over the spatial coordinates and the velocity components of the electrons then allow the swarm parameters to be obtained.

Both the Boltzmann equation analysis and Monte Carlo simulation allow us to obtain the velocity distribution and the swarm parameters once a complete set of cross sections is known. Accurate data on swarm parameters is required to check whether the set of cross sections used is correct and complete.

Macroscopic model. In this thesis we use the macroscopic description, and thereby assume that avalanche growth can be described by swarm parameters and continuity equations. This description provides a direct coupling between the processes involved, and the resulting charge distribution and current waveform. The macroscopic model can be verified by time–resolved current measurements. The continuity equations are used to evaluate the measured avalanche current waveforms, and to simulate the effects of various processes on the charge growth, the charge distribution and the current waveform of the avalanche. A detailed description of these macroscopic models is given in chapter 3.

1.4 Objectives of the present work

In the present study the time–resolved swarm method is employed for the observation of electron avalanches in insulating gases. The bandwidth limitations of this method, however, are in general not sufficiently understood. In addition, the associated theoretical models used for the evaluation of the measured avalanche current waveforms in the literature are often inadequate. The present work therefore, first of all, aims at:

(a) a better understanding of the bandwidth limitations of time–resolved current measurements and possible improvements of the experimental techniques;

(b) the development of appropriate theoretical models applicable to the evaluation of swarm parameters from the measured avalanche

current waveforms.

With this improved TRS method and the developed models we aim at:

(c) a better understanding of the various processes in avalanches, in particular of electron detachment and ion conversion, during the pre-breakdown stage of a gas discharge; and

(d) the determination of realistic swarm parameters in several interesting insulating gases.

CHAPTER 2

FUNDAMENTAL COLLISIONAL PROCESSES IN AVALANCHES

2.1 Introduction

Electrical breakdown in gases is the result of collisions between electrons or photons and gas molecules. These collisions may produce an increasing number of new electrons (and ions) which may eventually lead to the establishment of a self-sustaining mechanism (i.e. independent of external sources of primary electrons or photons). The production and loss mechanisms of electrons and ions are governed by the reaction rates at which these collisional processes occur, and the transport properties of electrons and ions. Knowledge on fundamental collisional processes in the gas and at electrodes, and on the transport properties of electrons and ions, is therefore of importance in understanding the breakdown behavior of gases.

In the formation of avalanches, five species are considered in the gas apart from the neutral gas molecules. These species are: photons, electrons, positive ions, unstable negative ions and stable negative ions respectively. Each species can be produced through several processes. Positive ions, for instance, can be produced through ionization by photon impact or by electron impact. Stable negative ions can be formed through electron attachment, or through stabilization and charge transfer. In this chapter we discuss only those collisional processes that describe the interactions among these five species and the neutral gas molecules. Other collisional processes are described by, for instance, Christophorou (1984), and Meek and Craggs (1978).

The processes considered here are:
(a) ionization by photon and electron impact;
(b) secondary emission at the cathode by the incidence of photons and positive ions;
(c) electron attachment and ion conversion (i.e., formation and conversion of negative ions);
(d) electron detachment (i.e., loss of negative ions); and
(e) transport properties of electrons and ions.

13

2.2 Electron and positive ion formation

2.2.1 Ionization by photon impact

When a photon with sufficiently high energy ($h\nu$) collides with a gas molecule (A), the molecule can be ionized as to yield a positive ion and an electron:

$$h\nu + A \longrightarrow A^+ + e \qquad\qquad (2.2.1)$$

This is called photoionization and is the reverse process of radiative electron-ion recombination.

Photoionization, as well as photodetachment (see section 2.3), are important mechanisms in streamer breakdown (Meek and Craggs, 1978).

2.2.2 Ionization by electron impact

When electrons move through a gas under the influence of the applied electric field, they can collide with gas molecules either elastically or inelastically. If the collisions are elastic, the total kinetic energy is conserved. If, however, the collisions are inelastic, some of the kinetic energy of the electrons is transferred into potential energy of the molecules. Only if this transferred energy is greater than the ionization potential, ionization of gas molecules can occur.

If we also include dissociative ionization of a gas molecule AB, we can express the ionization processes due to electron impact by the following reactions:

$$\text{single:} \qquad e + AB \longrightarrow AB^+ + 2e \qquad (2.2.2)$$
$$\text{dissociative:} \ e + AB \longrightarrow A^+ + B + 2e \qquad (2.2.3)$$
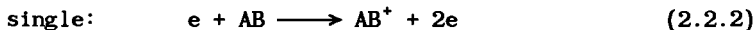
Dissociative ionization, as well as double or multiple ionization (Märk, 1984) requires, however, a higher electron energy than single ionization.

The ionization coefficient for ionization by electron impact, α, is defined as the mean number of ionizing collisions of one electron traveling a unit length in the direction of the field. Throughout

14

this thesis the unit length is chosen 1 cm.

2.2.3 Secondary emission at the cathode

When positive ions or photons (produced as a result of the excitation and subsequent decay of gas molecules) hit the cathode they can release secondary electrons, provided that the energy of the positive ion or photon exceeds the work-function of the cathode material.

In a time-resolved swarm experiment, the secondary electrons caused by the incidence of secondary photons on the cathode leave the cathode much earlier than the secondary electrons caused by the incidence of positive ions, due to the quite different drift velocities of the two species. This information is lost in a steady-state Townsend method.

2.3 Negative ion formation and loss

2.3.1 Electron attachment and negative ion stabilization

Dissociative attachment. When an electron collides with a gas molecule AB, the molecule can be split into a negative ion A^- and a neutral molecule B. This is called dissociative attachment and is expressed as:

$$e + AB \longrightarrow A^- + B \qquad (2.3.1)$$

Non-dissociative attachment. A non-dissociative attachment process can be expressed as:

$$e + AB \longrightarrow AB^- \qquad (2.3.2)$$

Three-body attachment, stabilization and charge transfer. The three-body attachment process that produces a stable negative ion:

$$e + A + B \longrightarrow A^- + B \qquad (2.3.3)$$

is often considered to occur in two stages (Meek and Craggs, 1978): an electron is captured by a gas molecule A to form an unstable

15

negative ion A^{-*}:

$$e + A \longrightarrow A^{-*} \qquad\qquad (2.3.4)$$

If this unstable negative ion further collides with a third-body B, it may be stabilized into a stable negative ion:

$$A^{-*} + B \longrightarrow A^- + B \qquad\qquad (2.3.5)$$

or molecule B may become a negative ion upon charge transfer:

$$A^{-*} + B \longrightarrow A + B^- \qquad\qquad (2.3.6)$$
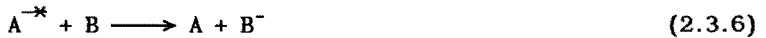
It is therefore, more convenient to define these two-stage processes separately, i.e., to define the reaction in Eq. (2.3.4) as a normal two-body attachment process forming an unstable negative ion, and define the reactions in Eqs. (2.3.5) and (2.3.6) as stabilization and charge transfer respectively. Further, the last two reactions (stabilization and charge transfer) can also be called a "conversion" process which converts an unstable negative ion, through the collision with a third body, into a stable negative ion. From the measurement of the gap current stabilization and charge transfer cannot be distinguished.

According to the above description, we use a coefficient η_{ns} to represent all attachment processes that produce stable negative ions (the reactions in Eqs. (2.3.1) and (2.3.2)) and another coefficient η_{nu} to represent all attachment processes that produce unstable negative ions (the reaction in Eq. (2.3.4)). Both coefficients η_{ns} and η_{nu} are defined as the mean number of attachment processes produced by one electron traveling 1 cm in the direction of the field. The total attachment coefficient is $\eta=\eta_{ns}+\eta_{nu}$.

It should be mentioned that in the models described in chapter 3, sections 3.2 and 3.4, detachment is not regarded and therefore all negative ions formed are assumed to be stable ones and hence η used there is η_{ns}. In the models described in sections 3.3 and 3.5 we have

16

assumed that all attachment processes only form unstable negative ions, and that stable negative ions are formed through conversion processes. Therefore the coefficient η used there is η_{nu}. The incorporation of direct stable negative ion formation (i.e., $\eta_{ns} \neq 0$) into these models is straightforward (see Verhaart, 1982), but is not done here because it would increase the uncertainty for the parameter determination from the measured current waveforms.

We describe stabilization and charge transfer processes by a conversion coefficient β which is defined as the mean number of conversion processes per unstable negative ion *in a time an electron travels 1 cm in the direction of the field.*

Note that the above definition of the conversion coefficient β (as well as the definition of the detachment coefficient δ that will follow) is different from the definition used in the literature (see, for instance, Llewellyn–Jones, 1967; Meek and Craggs, 1978) where β and δ are related to the ion drift velocity. For avalanche studies it is more convenient to relate β and δ to the electron drift velocity, because then all coefficients relate to one time scale given by the drift velocity of the electron swarm. The advantage of referring all coefficients to the electron drift velocity is that one can determine all coefficients (or combinations of these coefficients, see chapter 3) from the evaluation of the electron component of the avalanche current only. The ion drift velocity is not required. Furthermore, this electron component is more important than the ion component because the electrons are directly responsible for breakdown.

2.3.2 Electron detachment

Autodetachment. An unstable negative ion may spontaneously lose its captured electron, after a mean lifetime τ, provided that it is not collisionally stabilized:

$$A^{-*} \xrightarrow{\dfrac{1}{\tau}} A + e \qquad (2.3.7)$$

If, however, the mean time between collisions of the unstable negative ion with the neutral gas molecules is much shorter than τ,

17

then reaction in Eq. (2.3.7) is unlikely (Schmidt and Van Brunt, 1982).

Collisional detachment. When an unstable negative ion AB^{-*} collides with a gas molecule C, several kinds of collisional detachment processes may occur:

direct detachment: $AB^{-*} + C \longrightarrow AB + C + e$ (2.3.8)

associative detachment: $AB^{-*} + C \longrightarrow ABC + e$ (2.3.9)

dissociative detachment: $AB^{-*} + C \longrightarrow A + B + C + e$ (2.3.10)
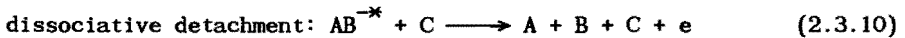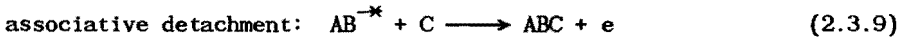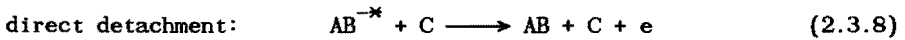
Collisional detachment seems to be the most likely mechanism under normal gas-discharge conditions, especially when the unstable negative ion acquires an appreciable energy from the electric field between collisions (Schmidt and Van Brunt, 1982).

The detachment coefficient for both autodetachment and collisional detachment, δ, is defined as the mean number of detachment processes per unstable negative ion *in a time an electron travels 1 cm in the direction of the field.*

Photodetachment. Photodetachment can be expressed as:

$$h\nu + A^{-*} \longrightarrow A + e \qquad (2.3.11)$$

This process is, however, unlikely in a practical electrode configuration unless intense light sources are used to irradiate the gas, or radiation is emitted by the discharge itself with sufficient intensity such as in streamer breakdown (Schmidt and Van Brunt, 1982). It may be useful as a possible diagnostic in locating and identifying negative ions in an electrode gap (for instance in O_2 by Teich and Morris (1987a, 1987b)).

2.4 Drift and diffusion of electrons and ions in a uniform field

2.4.1 Drift of electrons and ions

We consider a parallel-plate electrode configuration as shown in Fig. 2.4.1, in which a cloud of primary electrons is released from

18

the cathode by, for example, ultraviolet illumination in a negligibly
short time interval.
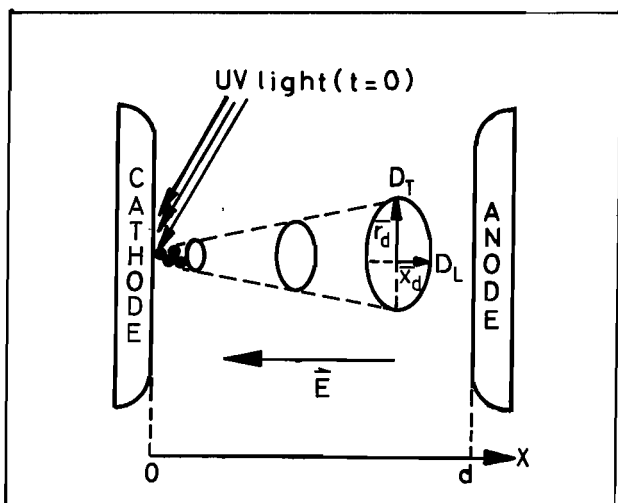
Figure 2.4.1

The drift and diffusion of an electron swarm
in a parallel-plate discharge gap.

These primary electrons first cross a small non-equilibrium region
near the cathode where they still retain some memory of the initial
conditions (Blevin, 1985), and where no steady velocity distribution
has been established yet. Note that a similar non-equilibrium region
exists near the anode. An experimental indication of the
non-equilibrium region at the cathode is the peak at the beginning of
waveforms recorded with high time-resolution, which is observed in
case of attaching gases (see Figs. 5.4.4a and 5.4.4b for SF_6, and
Figs. 5.6.1a and 5.6.1b for O_2 in chapter 5). This peak, that is not
observed in non-attaching gases such as N_2, can be explained by the
fact that the primary electrons which have just been released from
the cathode have little energy and, consequently, can easily be
attached to gas molecules. This results in a fast drop of the initial
current.

After crossing this non-equilibrium region the primary electrons
move as a swarm towards the anode under the influence of the applied

19

electric field in the equilibrium region, and the swarm can be described by the continuity equations and by constant swarm parameters. Due to electron diffusion the electron cloud (swarm) grows in size as shown in Fig. 2.4.1.

In the equilibrium region, although every electron in the swarm moves with its own velocity, the electron swarm as a whole moves with a drift velocity v_e parallel to the direction of the field. This drift velocity v_e is defined as the averaged velocity of all electrons in the swarm.

Another drift velocity also important for the description of avalanche growth is the center-of-mass drift velocity:

$$W_r = \frac{d\overline{x}(t)}{dt} \tag{2.4.1}$$

where $\overline{x}(t)$ is the center of mass of the swarm at time t.

It has been reported by Sakai and co-workers (1977), Tagashira and co-workers (1977), Taniguchi and co-workers (1978) and Tagashira (1981) who used either a Monte Carlo simulation or an analysis of the Boltzmann equation, that the averaged velocity v_e in the presence of ionization and electron diffusion is in general smaller than the center-of-mass drift velocity W_r. Their simulations in both N_2 and Ar suggest that this difference can be as high as 25% at high E/p (electric field over gas pressure).

When the primary electrons move towards the anode in the gap as shown in Fig. 2.4.1, they may collide with gas molecules and, as a consequence, may produce positive and negative ions. These ions will also drift in the gap, however with a drift velocity v_i much smaller than the electron drift velocity v_e.

The motion of ions is normally described in terms of the ion mobility, K_i, where $K_i = v_i/E$. The mobility is usually referred to standard conditions of temperature and pressure (s.t.p) by (Meek and Craggs, 1978):

$$K_o = v_i (E/p)^{-1} (760)^{-1} \frac{273}{T} \quad cm^2 V^{-1} s^{-1} \tag{2.4.2}$$

where T is the temperature in K, p is the gas pressure in Torr at temperature T, and E is the electric field in V/cm.

2.4.2 Diffusion of electrons

Diffusion of electrons is described by the general diffusion equation:

$$\vec{j} = -D \cdot \nabla \rho_e \qquad (2.4.3)$$

where $\vec{j}$ is the number of electrons passing a unit area per unit time and ρ_e is the electron number density. The minus sign indicates that the flow occurs in the direction of decreasing density. The proportionality constant D is called the (scalar) diffusion coefficient.

For the description of electron swarms in homogeneous fields it is useful to distinguish between two electron diffusion components. The transverse diffusion coefficient, D_T, describes the diffusion of the swarm in the direction perpendicular to the electric field E. The longitudinal diffusion coefficient, D_L, describes the diffusion of the swarm in the direction parallel to E. These two components can be expressed by (Tagashira, 1981):

$$D_T = \frac{1}{2} \cdot \frac{d(\overline{r}_d^2)}{dt} \qquad (2.4.4)$$

$$D_L = \frac{1}{2} \cdot \frac{d(\overline{x}_d^2)}{dt} \qquad (2.4.5)$$

where $\overline{r}_d$ and $\overline{x}_d$ are the averaged distances from the center of the cloud of electrons, as shown in Fig. 2.4.1.

In a time-resolved swarm experiment, only the longitudinal diffusion coefficient D_L is important. The electrons which diffuse perpendicular to the field direction arrive at the anode at the same time. In addition, in this work the primary electron cloud released from the cathode is shaped as a thin "disk" and not as a small sphere. Relatively speaking, the diffusion perpendicular to the

E-field direction (D_T) is therefore less important than the diffusion parallel to the E-field direction (D_L). Moreover, at atmospheric pressure, the velocity distribution of the electrons in the gap is nearly isotropic, and the difference between D_T and D_L is negligible. In this work we therefore consider only longitudinal diffusion, and use only one coefficient D.

Diffusion of ions is not incorporated in the present work. The emphasis is on the evaluation of the electron component of the current which is hardly affected by ion diffusion. In addition, the experimental observation of ion diffusion is complicated because: (1) the ion diffusion coefficient is much smaller than the electron diffusion coefficient; (2) the initial distribution of ions is not a simple disk as is the initial electron distribution; and (3) different ionic species, with different drift velocities, are involved.

2.4.3 Boundary conditions

Since in all swarm experiments the swarm is contained within a volume enclosed by metal electrodes (anode and cathode), it is necessary to discuss the boundary conditions imposed by these electrodes.

The motion of electrons and ions in regions very close to the electrodes is no longer random and cannot be described by the continuity equations. When particles interact with the metal surfaces of the electrodes it is often assumed that the surfaces act as perfectly absorbing plates, i.e., electrons and ions do not return into the gas when they have hit the electrodes. For such a perfectly absorbing boundary surface S, the boundary condition is (Kailash Kumar and co-workers, 1980; Skullerud, 1977):

$$f(\vec{r}, \vec{v}, t)\Big|_{\vec{r} \text{ on } S} = 0 \quad \text{for } \cos\theta = \frac{\vec{v}}{|\vec{v}|} \cdot \vec{n} > 0 \qquad (2.4.6)$$

where $f(\vec{r}, \vec{v}, t)$ is the velocity distribution function of the charge carriers, $\vec{r}$ and $\vec{v}$ are the position and velocity vectors respectively, $\vec{n}$ is the unit vector normal to S and directed away from the

22

electrode, and θ is the angle between the velocity vector $\vec{v}$ and the unit vector $\vec{n}$.

The condition in Eq. (2.4.6) implies a change in velocity distribution near the electrodes, and can therefore not be incorporated in the continuity equations. As a matter of fact the continuity equations are not valid in the non-equilibrium regions near the electrodes.

Another boundary condition is often used instead (Aschwanden, 1985; Brambring, 1964; Huxley and Crompton, 1974; Lowke, 1962; Schlumbohm, 1965):

$$\rho(\vec{r}, t)\Big|_{\vec{r} \text{ on } S} = 0 \qquad (2.4.7)$$

where $\rho(\vec{r}, t)$ is the number density of the charge carriers. This condition is based on the extrapolation of the particle density profile to a distance behind S approximately equal to the mean free path λ (McDaniel, 1964). Skullerud (1977) stated that the condition in Eq. (2.4.7) introduces errors in calculated density profiles.

Equation (2.4.7) is not only inaccurate but also violates Maxwell's laws. We consider the situation of a cloud of electrons moving without ionizing or attaching collisions across a gap as shown in Fig. 2.4.2.

These electrons may diffuse either perpendicular or parallel to the E-field direction, but the total number of electrons (or the total charge) is constant. For every closed surface S we may state that:

$$\iint\limits_{S} (\vec{J} + \frac{\partial \vec{D}}{\partial t}) \cdot d\vec{S} = 0 \qquad (2.4.8)$$

where $\vec{J}$ is the material current density and $\frac{\partial \vec{D}}{\partial t}$ is the displacement current density. Integration over a sufficiently long time interval gives no net contribution by the displacement current. Therefore, over a sufficiently long period of time the charge entering the

closed surface (through S_1) equals the charge leaving the closed surface (through S_2). If we choose surface S_1 just outside of the anode, Eq. (2.4.7) implies that no net charge is flowing through the external circuit, which is obviously inconsistent with Maxwell's equations.
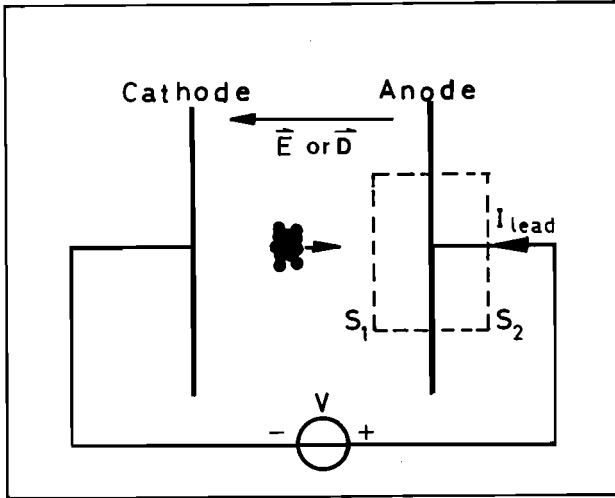
Figure 2.4.2

A constant number of electrons crossing a
gap without ionizing or attaching collisions.

Although some other boundary conditions have been suggested in the literature, none of them is satisfactory in general (Kailash Kumar and co-workers, 1980). Basically, the hydrodynamic (macroscopic) approach is no longer valid near the electrodes because of the lack of an isotropic velocity distribution.

In view of the above fact, we assume that the electrodes simply act as counting plates as if they were perfectly transparent grids (Verhaart, 1982). This condition (which is consistent with Maxwell's equations) gives an incorrect picture of reality only in a very thin layer near the electrode surfaces.

CHAPTER 3

THEORY OF DENSITY DISTRIBUTIONS AND TRANSIENT
CURRENTS OF ELECTRONS AND IONS IN AVALANCHES

3.1 Introduction

In this chapter we describe macroscopic models based on the continuity equations of the charged particles. In order to derive swarm parameters from the measured transient currents of electrons and ions, it is necessary to set up a macroscopic model which adequately describes the processes involved. Such a model is usually represented by a set of partial differential equations describing the space- and time-dependent density distributions of electrons and ions in the gas, and the corresponding initial and boundary conditions. Once the solutions of these equations are obtained, one can calculate the avalanche current in the external circuit and derive swarm parameters by means of curve fitting, i.e., by fitting the theoretically calculated transient current to the measured one.

Moreover, the calculation of the density distributions and transient currents of electrons and ions can also provide detailed information on how electrons and ions are distributed in the gap, and how the transient currents of electrons and ions look like, for a given set of swarm parameters. We may thereby study the effects of various individual processes on the avalanche growth, more quickly than could be done in experiments.

In this chapter we consider an electron "disk" of negligible thickness released at time t=0 from the cathode of a parallel-plate electrode system at fairly low E/p (electric field over gas pressure) values so that no secondary emission is present. This is a valid approximation for the time-resolved swarm measurements described later, where the primary electrons are released in a very short time interval (0.6 ns). In some cases, at high E/p values, secondary emission does occur but can readily be distinguished, and corrected for, from the measured total avalanche current (see Fig. 5.3.1c in chapter 5).

The approach described in this chapter is different from earlier work reported in the literature in three respects. Firstly, the

method of characteristic lines is introduced to solve the partial differential equations. Secondly, the drift of ions during the electron transit time is incorporated. Finally, the solutions presented are complete in the sense that no time limit is imposed.

Before we describe the models, we define some general quantities such as the numbers and number densities of the charged particles, and their relations to the current in the external circuit.

We consider a parallel-plate gap configuration, and the corresponding coordinate system, as shown in Fig. 3.1.1. At time t=0, n_o primary electrons are released instantaneously by UV illumination from an area S on the cathode. These primary electrons will drift, as a swarm, towards the anode under the influence of the applied electric field. During their drift, these primary electrons may produce new electrons, positive ions and negative ions upon collisions with neutral gas molecules (such as those described in chapter 2).
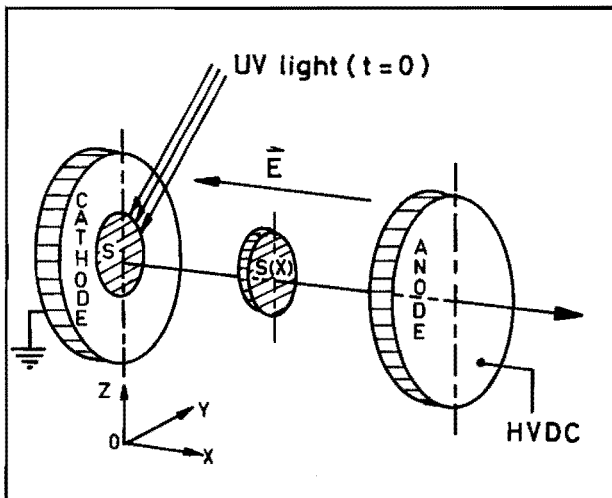
Figure 3.1.1
A parallel-plate gap configuration.

Apart from the neutral molecules, four species of particles are considered: electrons (index e), positive ions (index p), unstable negative ions (index nu) and stable negative ions (index ns)

respectively. Compared to the stable negative ion, the unstable negative ion has a short lifetime and is able either to release its electron, or to be converted into a stable ion, within the ion's transit time. The stable negative ion is either formed directly through electron attachment or indirectly through ion conversion from an unstable negative ion.

We denote $\rho_j(x,y,z,t)$ (unit: cm^{-3}) as the number density of species j (j=e, p, nu, ns) present in the gap at time t and at location (x,y,z). Integration of $\rho_j(x,y,z,t)$ over y and z will yield the number density $\rho_j(x,t)$ (unit: cm^{-1}):

$$\rho_j(x,t) = \iint\limits_{yz} \rho_j(x,y,z,t)dydz \qquad (3.1.1)$$

The total number of species j present in the whole gap at time t is:

$$n_j(t) = \int_0^d \rho_j(x,t)dx \qquad (3.1.2)$$

Since we are only interested in the variation of the densities in the x-direction, the direction of the E-field, we can describe the situation with the $\rho_j(x,t)$ densities.

The current flowing in the external circuit, $i_j(t)$, due to the species j alone, can be derived from the energy balance concept. The work required to move the charge $q=en_j(t)$, moving with a constant drift velocity v_j, over a distance dx, during a time interval dt equals $qEdx=en_j(t)Ev_jdt$, where we have used the relation $v_j=dx/dt$. Here E is the constant electric field strength between the two parallel plates at a distance d and at a constant voltage U. The energy is provided by the external circuit, i.e.:

$$en_j(t)Ev_jdt = Ui_j(t)dt \qquad (3.1.3)$$

Hence $i_j(t)$ is:

$$i_j(t) = \frac{en_j(t)Ev_j}{U} = \frac{en_j(t)v_j}{d} = \frac{en_j(t)}{T_j} \qquad (3.1.4)$$

where T_j is the transit time of species j.

3.2 Avalanches in which ionization and attachment processes occur

In this section we consider the avalanches in which only ionization and attachment processes occur. The incorporation of diffusion of electrons is presented in section 3.4.

The species of charged particles involved are electrons (index e), positive ions (index p) and (stable) negative ions (index n). The continuity equations for these charged particles are:

$$\frac{\partial\rho_e(x,t)}{\partial t} + v_e\frac{\partial\rho_e(x,t)}{\partial x} = (\alpha-\eta)v_e\rho_e(x,t) \qquad (3.2.1a)$$

$$\frac{\partial\rho_p(x,t)}{\partial t} - v_p\frac{\partial\rho_p(x,t)}{\partial x} = \alpha v_e\rho_e(x,t) \qquad (3.2.1b)$$

$$\frac{\partial\rho_n(x,t)}{\partial t} + v_n\frac{\partial\rho_n(x,t)}{\partial x} = \eta v_e\rho_e(x,t) \qquad (3.2.1c)$$

Here $\rho_j(x,t)$ is the number density of species j across the gap at time t, v_j is the drift velocity of species j (j=e, p, n). α and η are the coefficients for ionization and attachment defined in chapter 2. Note that here $\eta=\eta_{ns}$; only stable negative ions are formed because detachment is not accounted for. All velocities v_j have positive values, and the direction of the charge carrier movement is indicated by the sign in the above equations.

The initial and boundary conditions imposed on Eq. (3.2.1a) are:

$$\rho_e(x,0) = n_0D(x) \qquad (3.2.2a)$$

$$\rho_e(x,t) = 0 , \qquad (t>T_e) \qquad (3.2.2b)$$

where n_0 is the number of primary electrons released from the cathode at time t=0 and D(x) is the Dirac function (unit: cm^{-1}). $T_e=d/v_e$ is the electron transit time. Equation (3.2.2a) states that the primary

28

electrons are released at time t=0 instantaneously as a Dirac pulse. Equation (3.2.2b) indicates that no electrons exist in the gap after T_e (all electrons have disappeared into the anode).

In the swarm coordinate system, i.e., for $x-v_e t=$constant, one does not have to account for the electron drift, and the left-hand-side of Eq. (3.2.1a) reduces to one time derivative. The simplified equation describes the temporal evolution of the electrons along a prescribed trajectory, the characteristic line, given by $x-v_e t=h_e=$constant. Formally, this transformation is performed by introducing a variable substitution:

$$x = h_e + v_e t \qquad (3.2.3a)$$
$$t = t \qquad (3.2.3b)$$

The characteristic lines ($h_e=$constant) are shown schematically in Fig. 3.2.1. The line $h_e=0$ (or $x=v_e t$) corresponds to the electrons released at t=0. The lines $h_e>0$ (not shown in Fig. 3.2.1) and $h_e<0$ corresponds to earlier (t<0) and later (t>0) electrons respectively.
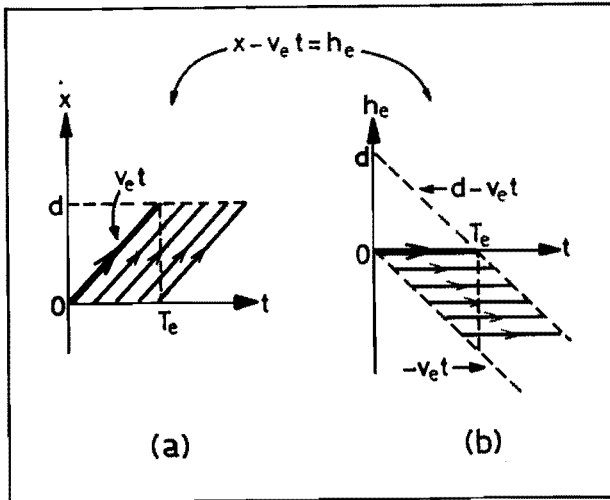
Figure 3.2.1

The characteristic lines of Eq. (3.2.1a) for

the electrons within the region: $0\leq x\leq d$ and $t\geq 0$.

In the new (h_e, t) system, the electron number density $\rho_e(x, t)$ can be written as:

$$\rho_e(x, t) = \rho_e(h_e + v_e t, t) \overset{\Delta}{=} \tilde{\rho}_e(h_e, t) \qquad (3.2.4)$$

where $\tilde{\rho}_e(h_e, t)$ and $\rho_e(x, t)$ have identical values if x and h_e are related according to Eq. (3.2.3a).

The partial derivative $\dfrac{\partial \tilde{\rho}_e(h_e, t)}{\partial t}$ is related to the partial derivatives $\dfrac{\partial \rho_e(x, t)}{\partial x}$ and $\dfrac{\partial \rho_e(x, t)}{\partial t}$ (see, for example, Bronshtein and Semendyayev, 1985) by:

$$\frac{\partial \tilde{\rho}_e(h_e, t)}{\partial t} = \frac{\partial \rho_e(x, t)}{\partial x} \cdot \frac{\partial x}{\partial t} + \frac{\partial \rho_e(x, t)}{\partial t} \cdot \frac{\partial t}{\partial t}$$

$$= \frac{\partial \rho_e(x, t)}{\partial x} \cdot v_e + \frac{\partial \rho_e(x, t)}{\partial t} \qquad (3.2.5)$$

With this substitution, Eq. (3.2.1a) becomes:

$$\frac{\partial \tilde{\rho}_e(h_e, t)}{\partial t} = (\alpha - \eta) v_e \tilde{\rho}_e(h_e, t) \qquad (3.2.6)$$

For any constant value of h_e, and for an electron cloud starting at $t=0$, the solution of Eq. (3.2.6) is:

$$\tilde{\rho}_e(h_e, t) = \tilde{\rho}_e(h_e, 0) \exp[(\alpha - \eta) v_e t] \qquad (3.2.7)$$

Transformation to the original coordinate system (x, t) according to Eq. (3.2.3) gives:

$$\rho_e(x, t) = \rho_e(x - v_e t, 0) \exp[(\alpha - \eta) v_e t] \qquad (3.2.8)$$

for $0 \leq x \leq d$ and $t \geq 0$.

The solution shows that the number density of electrons at

position x and at time t is caused by the exponential growth of the electrons at position $x-v_e t$ and at time $t=0$.

The application of the initial condition in Eq. (3.2.2a) to this general solution gives the specific solution:

$$\rho_e(x,t) = n_o D(x-v_e t)\exp[(\alpha-\eta)v_e t] \qquad (3.2.9)$$

As a result of this initial condition, a solution different from zero is found only along the special characteristic line $x-v_e t=0$, drawn as a bold line in Fig. 3.2.1. With the condition in Eq. (3.2.2b), the solution for the electron number density $\rho_e(x,t)$ can finally be written as:

$$\rho_e(x,t) = \begin{cases} n_o D(x-v_e t)\exp(\overline{\alpha}v_e t) , & (t \leq T_e) \qquad (3.2.10a) \\ \\ 0 , & (t > T_e) \qquad (3.2.10b) \end{cases}$$

where $\overline{\alpha}=\alpha-\eta$ is the effective ionization coefficient. With this solution for $\rho_e(x,t)$, also the number densities for positive and (stable) negative ions can be obtained by solving Eqs. (3.2.1b) and (3.2.1c).

The solution of Eq. (3.2.1b) for positive ions is obtained similarly along the characteristic lines $x+v_p t=h_p=$constant. The characteristic lines for positive ions are shown schematically in Fig. 3.2.2.

After transformation to the (h_p,t) coordinate system the solution is obtained as:

$$\tilde{\rho}_p(h_p,t) = \alpha v_e \int_0^t \rho_e(h_p-v_p\tau,\tau)d\tau \qquad (3.2.11)$$

From Fig. 3.2.2b we can derive that for each constant h_p, with $h_p \leq d+v_p T_e$, positive ions exist only for $t \geq h_p/(v_e+v_p)$. Equation (3.2.11) can therefore be written as:

$$\tilde{\rho}_p(h_p, t) = \alpha v_e \int_{\frac{h_p}{v_e + v_p}}^{t} \rho_e(h_p - v_p \tau, \tau) d\tau \qquad (3.2.12)$$
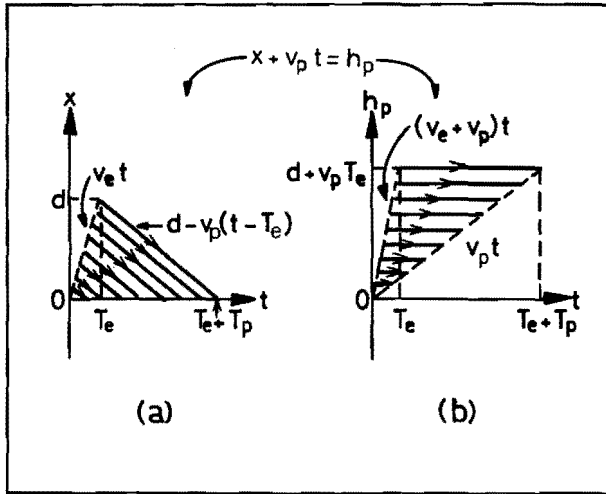
Figure 3.2.2

The characteristic lines of Eq. (3.2.1b) for the positive ions within the region: $0 \leq x \leq d$ and $0 \leq t \leq T_e + T_p$.

Transformation of this solution to the original (x, t) coordinate system gives:

$$\rho_p(x, t) = \alpha v_e \int_{\frac{x + v_p t}{v_e + v_p}}^{t} \rho_e(x + v_p t - v_p \tau, \tau) d\tau \qquad (3.2.13)$$

Substitution of Eq. (3.2.10a) into Eq. (3.2.13) yields:

$$\rho_p(x,t) = \alpha v_e \int_{\frac{x+v_p t}{v_e+v_p}}^{t} n_o D(x+v_p t-v_p\tau-v_e\tau)\exp(\overline{\alpha v}_e\tau)d\tau$$

$$= \frac{\alpha v_e n_o}{v_e+v_p}\exp(\overline{\alpha v}_e \frac{x+v_p t}{v_e+v_p}) \qquad (3.2.14)$$

The validity regions for $\rho_p(x,t)$ can easily be seen from Fig. 3.2.2 as: $0{\leq}x{\leq}v_e t$ if $t{\leq}T_e$ and $0{\leq}x{\leq}d-v_p(t-T_e)$ if $T_e{<}t{\leq}T_e+T_p$. Here $T_p=d/v_p$ is the positive ion transit time.

In the same way we obtain the solution of Eq. (3.2.1c) for the negative ions. The characteristic lines are $x-v_n t=h_n=$constant, and are shown schematically in Fig. 3.2.3. We find:

$$\rho_n(x,t) = \frac{\eta v_e n_o}{v_e-v_n}\exp(\overline{\alpha v}_e \frac{x-v_n t}{v_e-v_n}) \qquad (3.2.15)$$

for $v_n t{\leq}x{\leq}v_e t$ if $t{\leq}T_e$ and $v_n t{\leq}x{\leq}d$ if $T_e{<}t{\leq}T_n$. Here $T_n=d/v_n$ is the negative ion transit time.
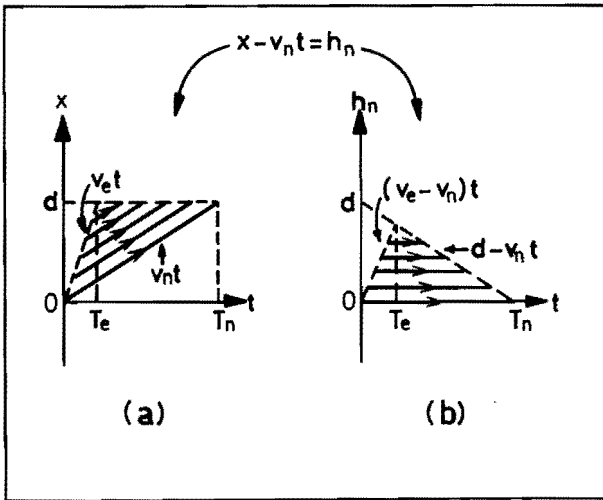
Figure 3.2.3

The characteristic lines of Eq. (3.2.1c) for the negative ions within the region: $0{\leq}x{\leq}d$ and $0{\leq}t{\leq}T_n$.

The numbers of electrons $n_e(t)$, positive ions $n_p(t)$ and (stable) negative ions $n_n(t)$ present in the gap at time t can be obtained by integration, taking into account the regions in which these densities are valid.

For $t \leq T_e$, we obtain:

$$n_e(t) = \int_0^d n_o D(x - v_e t) \exp(\bar{\alpha} v_e t) dx$$

$$= n_o \exp(\bar{\alpha} v_e t) , \qquad (t \leq T_e) \qquad (3.2.16)$$

$$n_p(t) = \int_0^{v_e t} \frac{\alpha v_e n_o}{v_e + v_p} \exp(\bar{\alpha} v_e \frac{x + v_p t}{v_e + v_p}) dx$$

$$\left[= \frac{\alpha n_o}{\bar{\alpha}} [\exp(\bar{\alpha} v_e t) - \exp(\bar{\alpha} \frac{v_e v_p}{v_e + v_p} t)] \quad \text{if } \bar{\alpha} \neq 0 \qquad (3.2.17a) \right.$$

$$(t \leq T_e)$$

$$\left. = \alpha \frac{v_e}{v_e + v_p} n_o v_e t \qquad\qquad \text{if } \bar{\alpha} = 0 \qquad (3.2.17b) \right.$$

$$n_n(t) = \int_{v_n t}^{v_e t} \frac{\eta v_e n_o}{v_e - v_n} \exp(\bar{\alpha} v_e \frac{x - v_n t}{v_e - v_n}) dx$$

$$\left[= \frac{\eta n_o}{\bar{\alpha}} [\exp(\bar{\alpha} v_e t) - 1] \qquad \text{if } \bar{\alpha} \neq 0 \qquad (3.2.18a) \right.$$

$$(t \leq T_e)$$

$$\left. = \eta v_e n_o t \qquad\qquad\qquad \text{if } \bar{\alpha} = 0 \qquad (3.2.18b) \right.$$

For $t > T_e$, we obtain:

$$n_e(t) = 0 , \qquad (t > T_e) \qquad (3.2.19)$$

$$n_p(t) = \int_0^{d-v_p(t-T_e)} \frac{\alpha v_e n_o}{v_e+v_p} \exp(\bar{\alpha} v_e \frac{x+v_p t}{v_e+v_p}) dx$$

$$\begin{array}{ll} = \dfrac{\alpha n_o}{\bar{\alpha}}[\exp(\bar{\alpha} v_e \dfrac{d+v_p T_e}{v_e+v_p})-\exp(\bar{\alpha}\dfrac{v_e v_p}{v_e+v_p}t)] & \text{if } \bar{\alpha}\neq 0 \\[4mm] & \hspace{1cm} (3.2.20a) \\[2mm] & (t>T_e) \\[2mm] = \alpha\dfrac{v_e}{v_e+v_p}n_o[d-v_p(t-T_e)] & \text{if } \bar{\alpha}=0 \hspace{0.5cm} (3.2.20b) \end{array}$$

$$n_n(t) = \int_{v_n t}^{d} \frac{\eta v_e n_o}{v_e-v_n} \exp(\bar{\alpha} v_e \frac{x-v_n t}{v_e-v_n}) dx$$

$$\begin{array}{ll} = \dfrac{\eta n_o}{\bar{\alpha}}[\exp(\bar{\alpha} v_e \dfrac{d-v_n t}{v_e-v_n})-1] & \text{if } \bar{\alpha}\neq 0 \hspace{0.5cm} (3.2.21a) \\[4mm] & (t>T_e) \\[2mm] = \eta\dfrac{v_e}{v_e-v_n}n_o(d-v_n t) & \text{if } \bar{\alpha}=0 \hspace{0.5cm} (3.2.21b) \end{array}$$

Finally, the electron and ion components of the avalanche current in the external circuit are obtained from Eq. (3.1.4):

$$i_e(t) = \frac{e n_e(t)}{T_e} \hspace{4cm} (3.2.22)$$

$$i_i(t) = \sum_j \frac{e n_j(t)}{T_j} , \hspace{1cm} (j=p, n) \hspace{2cm} (3.2.23)$$

The present expressions for $n_p(t)$ and $n_n(t)$ are more complete than those described previously (Meek and Craggs, 1978; Raether, 1964; Verhaart, 1982) because the drift motion of both positive and negative ions during the first electron transit time T_e has been taken into account in the present derivation.

Figure 3.2.4 shows the number-density distributions for each species (e, p, n) in the gap for three different situations: $\bar{\alpha}<0$, $\bar{\alpha}=0$

and $\bar{\alpha} > 0$. The corresponding currents are shown in Fig. 3.2.5.
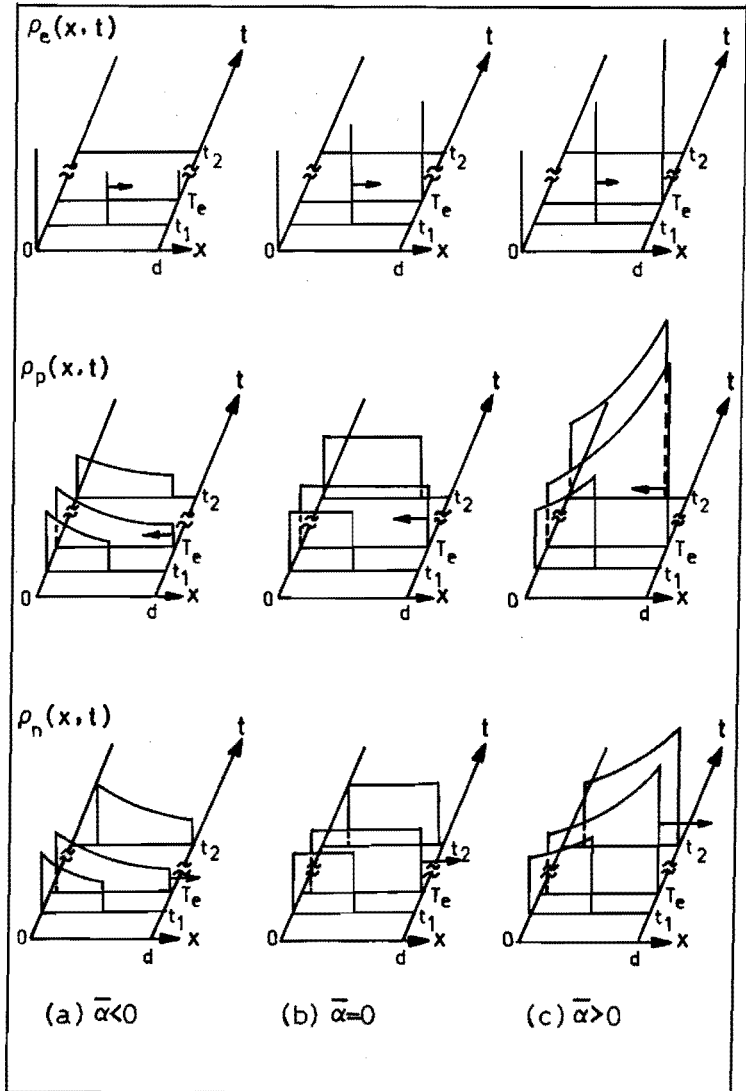
Figure 3.2.4

Number-density distributions for electrons (ρ_e), positive ions (ρ_p) and (stable) negative ions (ρ_n) in the gap for an avalanche with only ionization and attachment. Here T_e is the electron transit time.
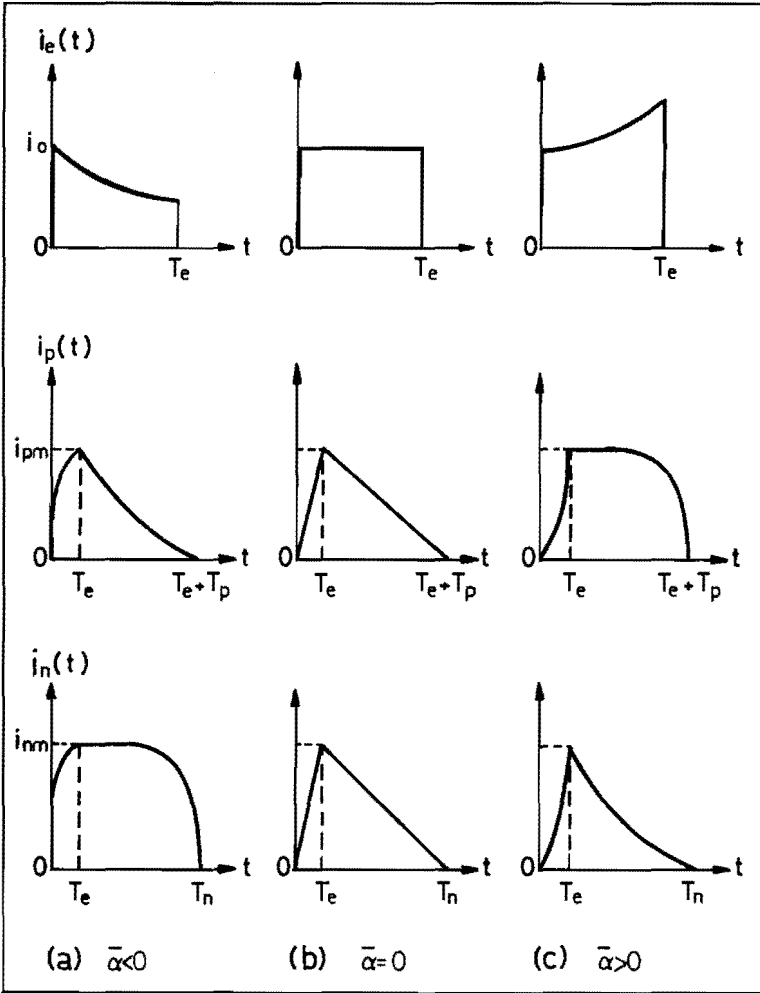
Figure 3.2.5

Electron (i_e), positive ion (i_p) and (stable) negative ion (i_n) components of the avalanche current in the external circuit for an avalanche with only ionization and attachment. Here $i_o = e n_o / T_e$. $i_{pm} = i_p(T_e)$ and $i_{nm} = i_n(T_e)$. The index m denotes the maximum value. Note that, for clarity, in the figures for $i_p(t)$ and $i_n(t)$ the period $0 \sim T_e$ is drawn much larger than it is in reality.

3.3 Avalanches in which ionization, attachment, detachment and conversion processes occur*

3.3.1 The model

In this section we consider the avalanches in which, besides ionization and attachment processes, electron detachment and ion conversion processes also occur. Diffusion of electrons is not considered here, but is incorporated later (section 3.5).

The species considered are: electrons (index e), positive ions (index p), unstable negative ions (index nu) and stable negative ions (index ns). We assume that all negative ions formed via attachment processes are unstable ions. However, direct stable negative ion formation could easily be incorporated in the present model.

Before the first electrons reach the anode of the parallel-plate gap, shown in Fig. 3.1.1, after the electron transit time T_e, the following set of linear first order differential equations describes the temporal evolution of the four components if the drift motion of ions (for $t < T_e$) is neglected (Verhaart, 1982; Verhaart and van der Laan, 1984):

$$\frac{dn_e(t)}{dt} = (\alpha - \eta)v_e n_e(t) + \delta v_e n_{nu}(t) \qquad (3.3.1a)$$

$$\frac{dn_p(t)}{dt} = \alpha v_e n_e(t) \qquad (3.3.1b)$$

$$\frac{dn_{nu}(t)}{dt} = \eta v_e n_e(t) - (\delta + \beta)v_e n_{nu}(t) \qquad (3.3.1c)$$

$$\frac{dn_{ns}(t)}{dt} = \beta v_e n_{nu}(t) \qquad (3.3.1d)$$

Here $n_j(t)$ is the total number of species j (j=e, p, nu, ns) present in the gap at time $t \leq T_e$. α, η, δ and β are the ionization, attachment, detachment and conversion coefficients, as defined in chapter 2. Note that here $\eta = \eta_{nu}$ and $\eta_{ns} = 0$ since all negative ions formed through attachment are assumed to be unstable.

We assume that n_o primary electrons are released from the cathode in an infinitely short time interval, i.e., $n_e(0) = n_o$. For times not exceeding T_e, one does not have to account for the neutralization of the charged particles at the anode. In this case the solution for the total number of electrons is given by (Verhaart, 1982; Verhaart and van der Laan, 1984):

$$n_e(t) = \frac{n_o}{A_1 - A_2}[(A_1 + \delta + \beta)\exp(A_1 v_e t) - (A_2 + \delta + \beta)\exp(A_2 v_e t)]$$
$$(t \leq T_e) \qquad (3.3.2)$$

Here

$$A_{1,2} = \frac{1}{2}[(\alpha - \eta) - (\delta + \beta) \pm \sqrt{(\alpha - \eta + \delta + \beta)^2 + 4\eta\delta}] \qquad (3.3.3)$$

and A_1 takes the positive sign.

The solutions for $n_p(t)$, $n_{nu}(t)$ and $n_{ns}(t)$ for times t up to T_e can also be derived from Eqs. (3.3.1a) $\sim$ (3.3.1d) as:

$$n_p(t) = \frac{\alpha n_o}{A_1 - A_2}[(1 + \frac{\delta + \beta}{A_1})\exp(A_1 v_e t) - (1 + \frac{\delta + \beta}{A_2})\exp(A_2 v_e t)]$$

$$+ \frac{\alpha(\delta + \beta)n_o}{A_1 A_2}. \qquad\qquad (t \leq T_e) \qquad (3.3.4)$$

$$n_{nu}(t) = \frac{\eta n_o}{A_1 - A_2}[\exp(A_1 v_e t) - \exp(A_2 v_e t)], \qquad (t \leq T_e) \qquad (3.3.5)$$

$$n_{ns}(t) = \frac{\eta\beta n_o}{(A_1 - A_2)A_1}\exp(A_1 v_e t) - \frac{\eta\beta n_o}{(A_1 - A_2)A_2}\exp(A_2 v_e t) + \frac{\eta\beta n_o}{A_1 A_2}$$
$$(t \leq T_e) \qquad (3.3.6)$$

The electron and ion components of the current in the external circuit can then be written as:

$$i_e(t) = \frac{e n_e(t)}{T_e} \qquad (3.3.7)$$

$$i_i(t) = \sum_j \frac{en_j(t)}{T_j} \,, \qquad (j = p,\ nu,\ ns) \qquad (3.3.8)$$

where T_p, T_{nu} and T_{ns} are the transit times of positive ions, unstable and stable negative ions, respectively.

For times exceeding T_e one should take into account the loss (neutralization) of the charged particles at the electrodes. Due to delaying processes such as detachment, electrons are distributed over the gap rather than situated only in the head of the avalanche. One should therefore determine the number-density distribution $\rho_j(x,t)$ across the gap.

If we also take into account the drift motion of ions for $t \leq T_e$, the number densities of electrons and ions are described by the following set of partial differential equations:

$$\frac{\partial \rho_e(x,t)}{\partial t} + v_e \frac{\partial \rho_e(x,t)}{\partial x} = (\alpha-\eta)v_e\rho_e(x,t) + \delta v_e\rho_{nu}(x,t) \qquad (3.3.9a)$$

$$\frac{\partial \rho_p(x,t)}{\partial t} - v_p \frac{\partial \rho_p(x,t)}{\partial x} = \alpha v_e\rho_e(x,t) \qquad (3.3.9b)$$

$$\frac{\partial \rho_{nu}(x,t)}{\partial t} + v_{nu} \frac{\partial \rho_{nu}(x,t)}{\partial x} = \eta v_e\rho_e(x,t) - (\delta+\beta)v_e\rho_{nu}(x,t) \qquad (3.3.9c)$$

$$\frac{\partial \rho_{ns}(x,t)}{\partial t} + v_{ns} \frac{\partial \rho_{ns}(x,t)}{\partial x} = \beta v_e\rho_{nu}(x,t) \qquad (3.3.9d)$$

where $\rho_j(x,t)$ is the number density distribution in the gap and v_j (a positive value) is the drift velocity of species j ($j=e,\ p,\ nu,\ ns$).

In order to correlate measured and calculated current waveforms, also for times exceeding one electron transit time T_e, Verhaart (1982) and Verhaart and van der Laan (1984) developed a numerical model to simulate the current waveform on the basis of the above continuity equations. The swarm parameters were then determined from experiments by a (time-consuming) comparison between measured and numerically simulated waveforms.

In this section we present a general analytical solution valid also for $t > T_e$. This analytical solution can be obtained by solving

the continuity equations (3.3.9a) to (3.3.9d) with the appropriate boundary conditions. Equations (3.3.9a) and (3.3.9c) are coupled and should be solved simultaneously. Equations (3.3.9b) and (3.3.9d) can then be solved using the derived solutions for $\rho_e(x,t)$ and $\rho_{nu}(x,t)$. The method to solve Eqs. (3.3.9a) and (3.3.9c) simultaneously was presented by Llewellyn-Jones (1967) or Meek and Craggs (1978). They, however, used different definitions of the coefficients. In the following approach undelayed and delayed electrons are treated separately.

Undelayed electrons are those released from the cathode that have not yet been attached, or those produced by other undelayed electrons through ionization. Hence all undelayed electrons are found in the head of the avalanche $(x=v_e t)$. Delayed electrons are the result of detachment, or the result of ionization caused by delayed electrons. Hence all delayed electrons are found in the tail of the avalanche $(x<v_e t)$.

If n_o primary electrons are released from the cathode in an infinitely short time interval, the number density of the undelayed electrons is obviously given by (see section 3.2):

$$\rho_e^{und}(x,t) = n_o D(x-v_e t)\exp[(\alpha-\eta)x] \; , \quad (t\leq T_e) \qquad (3.3.10a)$$

$$\rho_e^{und}(x,t) = 0 \; , \qquad\qquad\qquad (t>T_e) \qquad (3.3.10b)$$

Here $D(\tau)$ is the Dirac function (unit: cm^{-1}).

The region where delayed electrons and unstable negative ions are found is given by $v_{nu}t\leq x\leq v_e t$ if $t\leq T_e$ and $v_{nu}t\leq x\leq d$ if $T_e<t\leq T_{nu}$ (see also Fig. 3.3.1). In order to solve the differential equations for the delayed electrons and for the unstable negative ions, we need to specify the boundary conditions at $x=v_e t$ and $x=v_{nu}t$. The unstable negative ions along the characteristic line $x=v_e t$ are produced by undelayed electrons which are being attached in the process and at the same position x, hence (see also Llewellyn-Jones, 1967; Raether, 1964):

$$\rho_{nu}(v_e t, t) = \frac{n_o \eta v_e}{v_e - v_{nu}} \exp[(\alpha - \eta)v_e t] \ , \qquad (v_e t \leq d) \qquad (3.3.11)$$
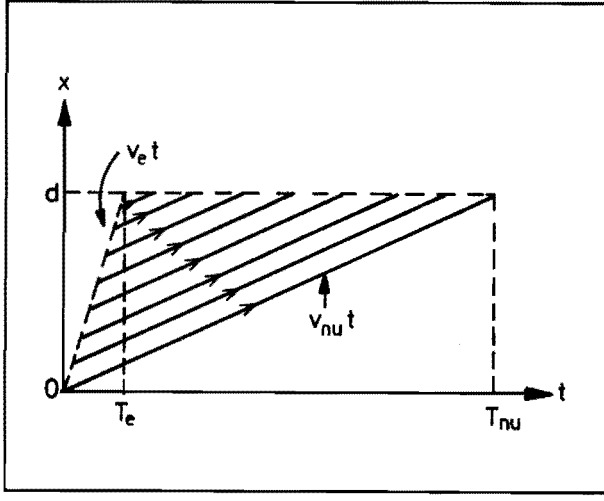
Figure 3.3.1

The region where delayed electrons and unstable negative ions exist. The lines with arrows are the characteristic lines for the unstable negative ions.

The unstable negative ions along the characteristic line $x = v_{nu} t$ are those formed by attachment at $t=0$ that have not yet undergone detachment or conversion, hence (see also Llewellyn-Jones, 1967; Raether, 1964):

$$\rho_{nu}(v_{nu} t, t) = \frac{n_o \eta v_e}{v_e - v_{nu}} \exp[-(\delta + \beta)v_e t] \qquad (3.3.12)$$

In order to derive the solutions for delayed electrons and unstable negative ions, we do not use the method of characteristic lines here, but we directly apply the method proposed by Llewellyn-Jones (1967):

42

$$\rho_e^{del}(x,t) = \frac{n_o y \exp(f)}{2(v_e t - x)} I_1(y) \qquad (3.3.13)$$

$$\rho_{nu}(x,t) = \frac{n_o \eta v_e \exp(f)}{v_e - v_{nu}} I_o(y) \qquad (3.3.14)$$

Here:

$$y = 2\frac{v_e}{v_e - v_{nu}}\sqrt{\eta\delta(v_e t - x)(x - v_{nu} t)} \qquad (3.3.15)$$

$$f = \frac{v_e}{v_e - v_{nu}}[(\alpha - \eta)(x - v_{nu} t) - (\delta + \beta)(v_e t - x)] \qquad (3.3.16)$$

while $I_n(y)$ ($n=0$, 1) is the nth order modified Bessel function:

$$I_n(y) = (\frac{y}{2})^n \sum_{k=0}^{\infty} \frac{1}{k!(k+n)!}(\frac{y}{2})^{2k} \qquad (3.3.17)$$

The same Bessel function also shows up in a stochastic treatment of the electron current by Steutel (1986) for the situation without ion conversion.

The number densities of positive ions and stable negative ions can readily be derived from $\rho_e(x,t)$ (note that $\rho_e = \rho_e^{und} + \rho_e^{del}$) and $\rho_{nu}(x,t)$ with Eqs. (3.3.9b) and (3.3.9d), and the appropriate boundary conditions, as:

$$\rho_p(x,t) = \alpha v_e \int_0^t \rho_e(x + v_p t - v_p \tau, \tau) d\tau \qquad (3.3.18)$$

$$\rho_{ns}(x,t) = \beta v_e \int_0^t \rho_{nu}(x - v_{ns} t + v_{ns} \tau, \tau) d\tau \qquad (3.3.19)$$

These solutions are derived along the characteristic lines $x + v_p t = h_p = $ constant of Eq. (3.3.9b) and $x - v_{ns} t + v_{ns} = h_{ns} = $ constant of

Eq. (3.3.9d). These characteristic lines are shown in Fig. 3.3.2 and Fig. 3.3.3.
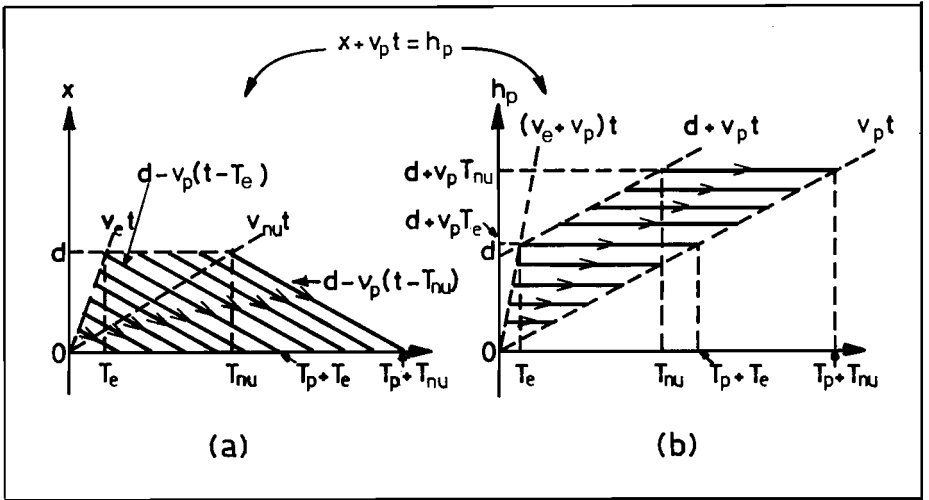
Figure 3.3.2

The characteristic lines of Eq. (3.3.9b) for the positive ions within the region: $0 \leq x \leq d$ and $0 \leq t \leq T_p + T_{nu}$.

The range of validity of Eq. (3.3.19) for the stable negative ions (see Fig. 3.3.3) is similar to that of the unstable negative ions: $v_{ns} t \leq x \leq v_e t$ if $t \leq T_e$ and $v_{ns} t \leq x \leq d$ if $T_e < t \leq T_{ns}$. For the positive ions in Eq. (3.3.18) we obtain the validity range (see Fig. 3.3.2) as: $0 \leq x \leq v_e t$ if $t \leq T_e$. $0 \leq x \leq d$ if $T_e < t \leq T_{nu}$ and $0 \leq x \leq d - v_p(t - T_{nu})$ if $T_{nu} < t \leq T_p + T_{nu}$. For regions outside the validity ranges all densities are zero.

The validity range can be incorporated in Eq. (3.3.18) through the integration limits:

$$\rho_p(x,t) = \alpha v_e \int_{\frac{x+v_p t}{v_e + v_p}}^{t} \rho_e(x + v_p t - v_p \tau, \tau) d\tau \qquad (3.3.20)$$

for $0 \leq x \leq v_e t$ if $t \leq T_e$ and for $0 \leq x \leq d - v_p(t - T_e)$ if $T_e < t \leq T_p + T_e$

(characteristic lines starting from $x = v_e t$, or $h_p = (v_e + v_p) t$, in Fig. 3.3.2), and:

$$\rho_p(x, t) = \alpha v_e \int_{t - \frac{d-x}{v_p}}^{t} \rho_e^{del}(x + v_p t - v_p \tau, \tau) d\tau \qquad (3.3.21)$$

for $\max[0, d - v_p(t - T_e)] \leq x \leq \min[d, d - v_p(t - T_{nu})]$ if $T_e < t \leq T_p + T_{nu}$ (characteristic lines starting from $x = d$, or $h_p = d + v_p t$, in Fig. 3.3.2). Here $\max[A, B]$ and $\min[A, B]$ are the maximum and minimum values of A and B respectively.
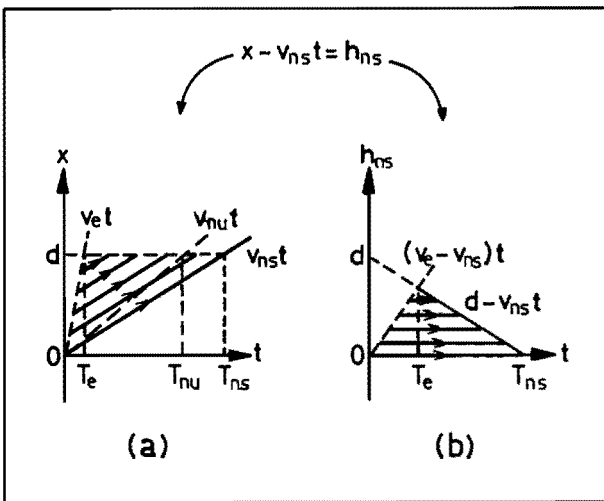
Figure 3.3.3

The characteristic lines of Eq. (3.3.9d) for the stable negative ions within the region: $0 \leq x \leq d$ and $0 \leq t \leq T_{ns}$.

Similarly Eq. (3.3.19) can be further written as:

$$\rho_{ns}(x,t) = \beta v_e \int_{\frac{x-v_{ns}t}{v_e-v_{ns}}}^{t} \rho_{nu}(x-v_{ns}t+v_{ns}\tau,\tau)d\tau \qquad (3.3.22)$$

for $v_{ns}t \leq x \leq v_e t$ if $t \leq T_e$ and for $v_{ns}t \leq x \leq d$ if $T_e \leq t \leq T_{ns}$ (characteristic lines starting from $x=v_e t$, or $h_{ns}=(v_e-v_{ns})t$, in Fig. 3.3.3).

The total numbers of electrons and ions in the gap are finally obtained from:

$$n_j(t) = \int_0^d \rho_j(x,t)dx \ , \qquad (j=e, p, nu, ns) \qquad (3.3.23)$$

where $\rho_j(x,t)=0$ for x and t values outside the validity ranges mentioned above.

One may also incorporate the validity ranges in the integration limits:

$$n_e(t) = \int_{v_{nu}t}^{\min[v_e t,d]} \rho_e(x,t)dx \qquad \text{for } t \geq 0 \qquad (3.3.24)$$

$$n_p(t) = \int_0^{\min[v_e t,d,d-v_p(t-T_{nu})]} \rho_p(x,t) \qquad \text{for } t \geq 0 \qquad (3.3.25)$$

$$n_{nu}(t) = \int_{v_{nu}t}^{\min[v_e t,d]} \rho_{nu}(x,t)dx \qquad \text{for } t \geq 0 \qquad (3.3.26)$$

$$n_{ns}(t) = \int_{v_{ns}t}^{\min[v_e t,d]} \rho_{ns}(x,t)dx \qquad \text{for } t \geq 0 \qquad (3.3.27)$$

With the charge carrier numbers calculated from Eq. (3.3.23) (or Eqs. (3.3.24) ~ (3.3.27)) the electron and ion components of the

current can be calculated from Eqs. (3.3.7) and (3.3.8) at any time.

It is verified that the two approaches presented, the general approach (Eq. (3.3.23) or Eqs. (3.3.24) ~ (3.3.27)) and the one limited to $t \leq T_e$ (Eqs. (3.3.2) ~ (3.3.6)), agree for $t \leq T_e$. The present approach, however, also includes ion drift during the first electron transit time. Furthermore, the general analytical approach is in agreement with the numerical approach presented earlier by Verhaart (1982) and Verhaart and van der Laan (1984). It is, however, more convenient to use the analytical solution in the curve fitting procedure.

3.3.2 Effects of detachment and conversion processes on the avalanche electron distribution

In the "classical" description of electron swarms, it is assumed that ionizing and attaching collisions are predominant and therefore that all electrons are contained in the avalanche head. However, due to detachment, swarms may have a distinct tail of electrons. This will affect streamer breakdown since this breakdown mechanism depends on the space-charge field distortion due to the swarm and thereby on the spatial distribution of the electrons in the avalanche. In that case detachment and conversion processes should be taken into account.

In case of Townsend breakdown, the total number of the charge carriers in the gap is decisive rather than their spatial distribution. In that case even a model including only ionization and attachment will predict the breakdown field strength correctly.

An example of how detachment and conversion processes influence the avalanche electron distribution across the gap is given in Fig. 3.3.4 for humid air with different water vapor pressures. The swarm parameters are chosen from Verhaart and van der Laan (1984): $\alpha=9.2$ cm^{-1}, $\eta=7.7$ cm^{-1}, $\delta=1.03$ cm^{-1}, and β is varied from 2.82 ~ 19.95 cm^{-1} for water vapor pressures from 0.05 ~ 7.5 Torr. Note that in Fig. 3.3.4 the peak of undelayed electrons (a Dirac pulse) is reduced in height. The tail in the electron distribution results from the delayed electrons produced by detachment processes. When the water vapor pressure is increased, and thereby the probability of conversion from unstable negative ions to stable ones

is enlarged, the tail is reduced in height and duration. This indicates that the contribution of delayed electrons to the avalanche growth becomes less. The conversion process immobilizes a certain amount of the electrons, forming harmless stable negative ions. This is consistent with the observation that the breakdown voltage of humid air increases with humidity (see, for instance, Meek and Craggs, 1978).
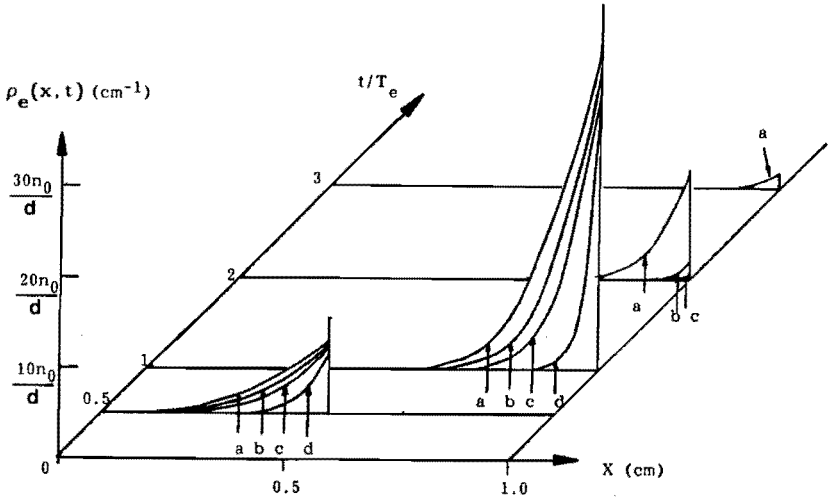
Figure 3.3.4

The influence of detachment and conversion processes on the electron distribution across the gap in humid air. Here $E=28.00$ kV/cm, $p=778$ Torr, $d=1.0$ cm, $T_e=80$ ns, $\alpha=9.2$ cm^{-1}, $\eta=7.7$ cm^{-1}, and $\delta=1.03$ cm^{-1}. Note that, for clarity, the peak of undelayed electrons is reduced in height. The corresponding electron currents are shown in Figs. 3.3.5i to l.

(a) $p_{H_2O}=0.05$ Torr, $\beta=2.82$ cm^{-1};

(b) $p_{H_2O}=0.85$ Torr, $\beta=4.66$ cm^{-1};

(c) $p_{H_2O}=1.79$ Torr, $\beta=6.82$ cm^{-1};

(d) $p_{H_2O}=7.5$ Torr, $\beta=19.95$ cm^{-1}.

3.3.3 Effects of detachment and conversion processes on the avalanche current waveform

With the model presented, the effects of detachment and conversion

processes on the current waveform can be studied. Some simulations of the electron current with different values of δ and β at constant values for $\alpha=9.2$ cm^{-1} and $\eta=7.7$ cm^{-1} as in the previous example are shown in Fig. 3.3.5.

$\beta=2.82$ cm^{-1} $\Longrightarrow \delta$ increase

$\delta=1.03$ cm^{-1} $\longrightarrow \beta$ increase
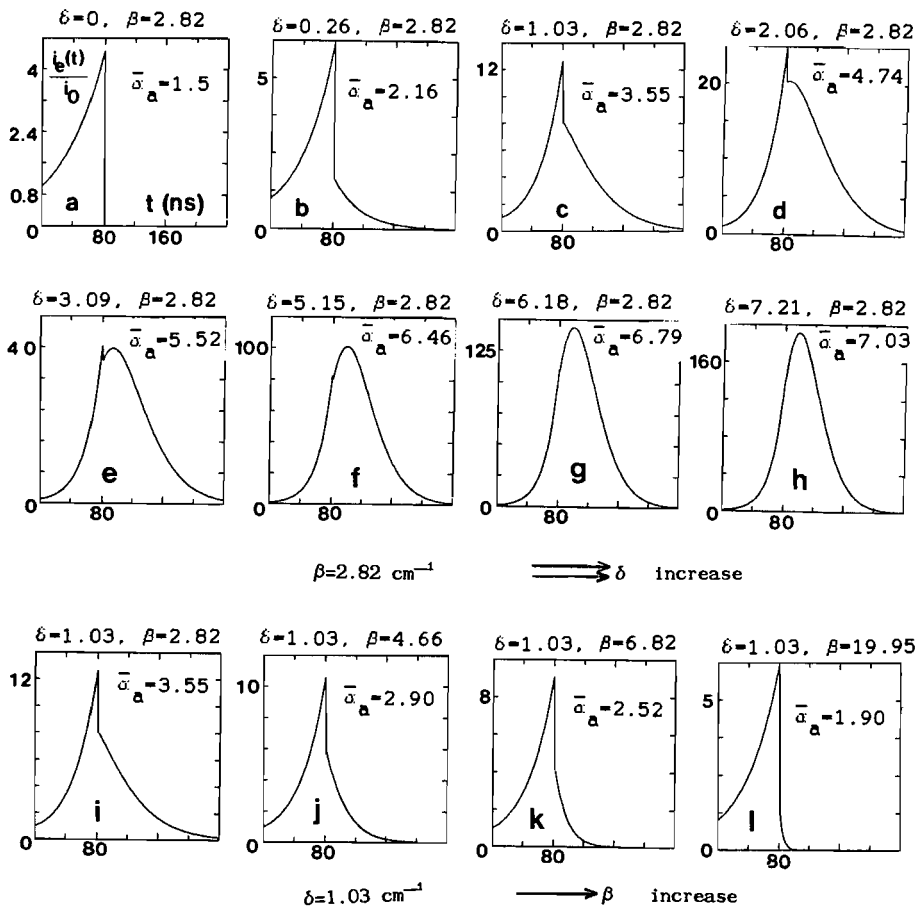
Figure 3.3.5

Effects of detachment and conversion processes on the avalanche electron current waveform calculated with the present model at constant values of $\alpha=9.2$ cm^{-1}, $\eta=7.7$ cm^{-1}, and at $T_e=80$ ns. Here $\bar{\alpha}_a$ is defined in Eq. (3.3.28). Note that the parameters used in Figs. 3.3.5i to l are the same as those used in Fig. 3.3.4.

In Figs. 3.3.5a to h, the effect of detachment is shown at a relatively low conversion coefficient $\beta=2.82$ cm^{-1}. Detachment acts as a secondary ionization mechanism which strongly affects the slope and the magnitude of the waveform, even after the electron transit time T_e. With increasing detachment coefficient, the current slope and magnitude rise accordingly.

The effect of detachment on the apparent transit time is shown in Figs. 3.3.5e to h. At high detachment coefficients or, more correctly, at high values of the product $\eta\delta$, the apparent transit time increases (the actual drift velocity is the same in all cases) because most, or all, electrons are being delayed by the consecutive attachment and detachment processes. This effect is counteracted by conversion processes, since conversion limits the number of unstable negative ions and, consequently, the number of detached electrons.

The stabilizing effect of conversion process is demonstrated by Figs. 3.3.5i to l where δ is kept constant at $\delta=1.03$ cm^{-1}. The reduction of the tail of the electron distribution in Fig. 3.3.4 when the humidity is increased, corresponds to a reduced aftercurrent. In addition the overall magnitude of the current decreases when β is increased.

In Fig. 3.3.6 the double exponential shape of the electron current, as described by Eq. (3.3.2), is easily identified. In cases like this a model including only ionization and attachment cannot describe the waveform. In many other cases the differences are not so obvious; detailed calculations and an experimental setup with a very good time resolution are required to recognize the presence of detachment and conversion processes.

With a two-parameter model, without detachment and conversion, apparent values α_a, η_a and $\bar{\alpha}_a$ are derived. If we define $\bar{\alpha}_a$ in such a way that this two-parameter model predicts the right number of electrons n_e that reach the anode, we find:

$$\bar{\alpha}_a = \alpha_a - \eta_a = \frac{1}{d}\ln(\frac{n_e}{n_o}) \qquad (3.3.28)$$

The total charge, Q_e, that flows in the external circuit as a result

of these electrons moving through the gap is then given by:

$$Q_e = \int_0^\infty i_e(t)dt = \frac{en_o}{\bar{\alpha}_a d}[\exp(\bar{\alpha}_a d)-1] \qquad (3.3.29)$$
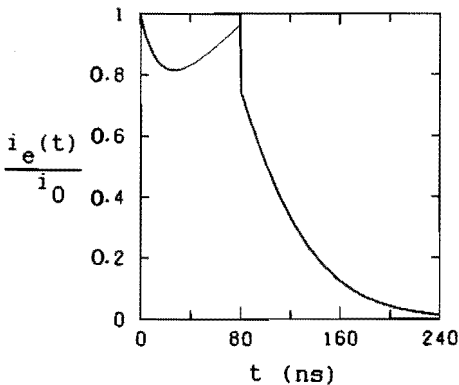
Figure 3.3.6
An example showing the double exponential shape of the electron current (see Eq. (3.3.2)). Here $\alpha=6.14$ cm^{-1}, $\eta=7.7$ cm^{-1}, $\delta=1.03$ cm^{-1}, $\beta=2.82$ cm^{-1} and $T_e=80$ ns.

With our four-parameter model (α, η, δ and β) we can determine n_e, or Q_e, for any set of parameters, and calculate $\bar{\alpha}_a$ from Eq. (3.3.28) or Eq. (3.3.29), which give identical results. This apparent value $\bar{\alpha}_a$ correctly predicts the total number of electrons in the avalanche but, as indicated in Fig. 3.3.5, may significantly deviate from the real one ($\bar{\alpha}=\alpha-\eta$). In some cases $\bar{\alpha}_a$ may still describe the avalanche waveform to a first approximation. The insights gained will however be poor, and the values found cannot be extrapolated to conditions other than the experimental ones, since scaling laws require knowledge of the individual processes involved. Furthermore, in case of streamer breakdown, the apparent effective ionization coefficient may not be consistent with the breakdown strength observed.

We have shown earlier for 1-C_3F_6 (Wen and Wetzer, 1988a) that the apparent ionization coefficient $\bar{\alpha}_a$ is related to the four parameters α, η, δ and β through:

$$\bar{\alpha}_a = \alpha - \eta + \frac{\delta\eta}{\delta+\beta} \qquad (3.3.30)$$

The validity of this relation is not restricted to $1-C_3F_6$ but applies to all cases where the four-parameter model is valid.

3.3.4 Swarm parameter determination from fast swarm experiments

A fitting program is developed on the basis of the present model to obtain swarm parameters from the measured time-resolved current waveform. The question rises whether the parameters can be determined uniquely. The solutions presented show that the swarm parameters show up in the expression for the electron current component in three combinations:

$$c_1 = \alpha - \eta \; ; \qquad c_2 = \delta + \beta \; ; \qquad c_3 = \eta\delta \qquad (3.3.31)$$

Hence, not all four parameters can be identified individually from the electron current only.

An analysis of the ion current would help, but is not straightforward. The ion current is composed of contributions of different kinds of positive and negative ions with different drift velocities. Later it will be illustrated that the ion component is not only more difficult to evaluate but also provides less information on the individual processes. In this work the ion current is not analyzed.

Nevertheless, the three quantities mentioned above fully describe the development of the electron component of the avalanche. Since the electron component is crucial for the occurrence of breakdown, these three quantities themselves are meaningful.

$c_1 = \alpha - \eta$ is easily identified as *the "real" effective ionization coefficient*, which differs from the "apparent" values obtained from a model including only ionization and attachment.

$c_2 = \delta + \beta$ describes *the loss rate of unstable negative ions* which were formed by attachment.

$c_3 = \eta\delta$ may be interpreted as *a secondary, delayed, ionization parameter*, describing the number of attached electrons which are released.

3.4 Avalanches in which ionization, attachment and electron diffusion processes occur

In this section we consider the avalanches in which ionization and attachment processes occur (no detachment and conversion), and in which electron diffusion is no longer negligible. Diffusion of ions is not taken into account for the reasons mentioned before (in chapter 2, section 2.4). Detachment and conversion processes are incorporated later (in section 3.5).

In this section we focus on the electron number density in the gap and the electron current in the external circuit. We consider the broadening of the "disk" of electrons while it crosses the gap; in our case only the longitudinal diffusion is important (see chapter 2, section 2.4).

The species involved are electrons (index e), positive ions (index p) and (stable) negative ions (index n). The following continuity equations describe the number densities of the charged particles (Brambring, 1964; Schlumbohm, 1965; de Urquijo–Carmona and co-workers, 1985):

$$\frac{\partial \rho_e(x,t)}{\partial t} + v_e \frac{\partial \rho_e(x,t)}{\partial x} = \bar{\alpha} v_e \rho_e(x,t) - \bar{\alpha} D \frac{\partial \rho_e(x,t)}{\partial x} + D \frac{\partial^2 \rho_e(x,t)}{\partial x^2}$$

(3.4.1a)

$$\frac{\partial \rho_p(x,t)}{\partial t} - v_p \frac{\partial \rho_p(x,t)}{\partial x} = \alpha v_e \rho_e(x,t) - \alpha D \frac{\partial \rho_e(x,t)}{\partial x}$$

(3.4.1b)

$$\frac{\partial \rho_n(x,t)}{\partial t} + v_n \frac{\partial \rho_n(x,t)}{\partial x} = \eta v_e \rho_e(x,t) - \eta D \frac{\partial \rho_e(x,t)}{\partial x}$$

(3.4.1c)

Here $\rho_j(x,t)$ and v_j (a positive value) are the number density and the drift velocity of species j (j=e, p, n), α and η are the ionization and attachment coefficients, $\bar{\alpha}=\alpha-\eta$ is the effective ionization coefficient, D is the electron (longitudinal) diffusion coefficient. All coefficients are defined in chapter 2. Note that η used here equals η_{ns} since only stable negative ions are considered (no detachment).

The second terms on the right-hand-side of Eqs. (3.4.1a) ~ (3.4.1c) reflect the (second order) effect of electron diffusion on the production of electrons and ions: as a result of diffusion the number of ionizing or attaching collisions per electron changes.

Since we focus on the solution for electrons, we will consider only Eq. (3.4.1a) which can be rewritten as:

$$\frac{\partial \rho_e(x,t)}{\partial t} + W_r \frac{\partial \rho_e(x,t)}{\partial x} = \overline{\alpha} v_e \rho_e(x,t) + D \frac{\partial^2 \rho_e(x,t)}{\partial x^2} \qquad (3.4.2)$$

where $W_r = v_e + \overline{\alpha} D$; Tagashira (1985) calls this quantity the center-of-mass drift velocity of the electron swarm. Note that this so-called center-of-mass drift velocity W_r is only equal to the averaged electron drift velocity v_e if $\overline{\alpha} = 0$ or $D=0$.

To solve Eq. (3.4.2) with the initial condition $\rho_e(x,0)=n_0 D(x)$, where $D(x)$ is the Dirac function (unit: cm^{-1}), we first consider the situation of $\overline{\alpha} = 0$. The solution of the equation (where U represents ρ_e for this particular case):

$$\frac{\partial U(x,t)}{\partial t} + W_r \frac{\partial U(x,t)}{\partial x} = D \frac{\partial^2 U(x,t)}{\partial x^2} \qquad (3.4.3)$$

is (Huxley and Crompton, 1974; Verhaart, 1982):

$$U(x,t) = \frac{n_o}{\sqrt{4\pi Dt}} \exp\left[-\frac{(x-W_r t)^2}{4Dt}\right] \qquad (3.4.4)$$

For $\overline{\alpha} \neq 0$ it can be shown that $U(x,t)\exp(\overline{\alpha} v_e t)$ satisfies Eq. (3.4.2) if $U(x,t)$ satisfies Eq. (3.4.3). Therefore the solution of Eq. (3.4.2) is:

$$\rho_e(x,t) = \frac{n_0 \exp(\overline{\alpha} v_e t)}{\sqrt{4\pi Dt}} \exp\left[-\frac{(x-W_r t)^2}{4Dt}\right] \qquad (3.4.5)$$

The number of electrons present in the gap at time t is:

$$n_e(t) = \int_0^d \rho_e(x,t)dx$$

$$= \frac{n_0 \exp(\overline{\alpha v}_e t)}{\sqrt{4\pi Dt}} \int_0^d \exp[-\frac{(x - W_r t)^2}{4Dt}]dx$$

It was shown by Brambring (1964) and Gilardini (1972) that one can replace the lower integration limit 0 by $-\infty$ without introducing a significant error. We then find:

$$n_e(t) = \frac{n_0 \exp(\overline{\alpha v}_e t)}{2} \text{erfc}(\lambda) \qquad (3.4.6)$$

where

$$\lambda = \frac{W_r t - d}{\sqrt{4Dt}} = \frac{(v_e + \overline{\alpha}D)t - d}{\sqrt{4Dt}} \qquad (3.4.7)$$

and $\text{erfc}(\lambda)$ is the complementary error function which is defined as:

$$\text{erfc}(\lambda) = \frac{2}{\sqrt{\pi}} \int_\lambda^\infty \exp(-u^2)du \qquad (3.4.8)$$

To check the validity of Eq. (3.4.6), we consider a special situation with D=0. For D=0, $\lambda \rightarrow -\infty$ if $v_e t \leq d$ and $\lambda \rightarrow +\infty$ if $v_e t > d$. Since $\text{erfc}(-\infty)=2$ and $\text{erfc}(+\infty)=0$, Eq. (3.4.6) becomes:

$$n_e(t) = n_0 \exp(\overline{\alpha v}_e t) , \qquad (t \leq T_e) \qquad (3.4.9a)$$

$$n_e(t) = 0 , \qquad (t > T_e) \qquad (3.4.9b)$$

This result is identical to Eqs. (3.2.16) and (3.2.19) described in section 3.2 where electron diffusion was not considered.

The electron component of the avalanche current in the external

55

circuit is again:

$$i_e(t) = \frac{en_e(t)}{T_e}$$

(3.4.10)

with $n_e(t)$ as in Eq. (3.4.6).
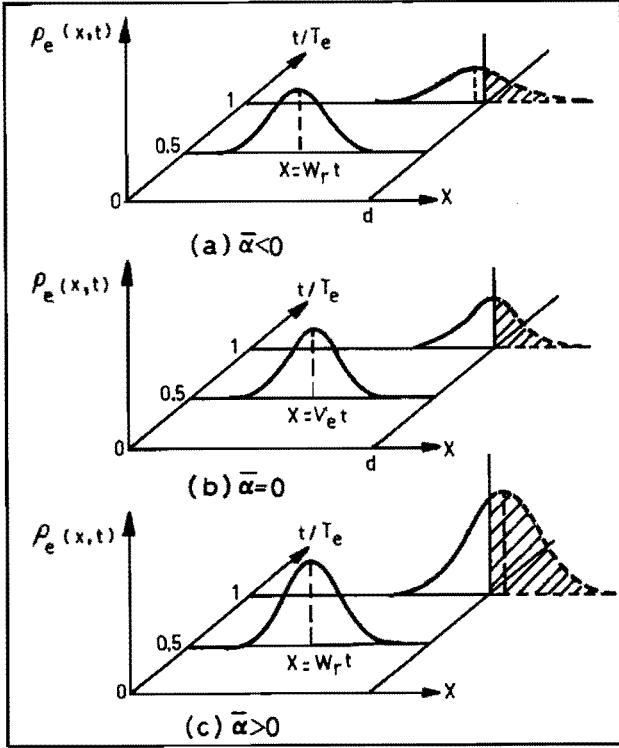
Figure 3.4.1

Electron number density distributions across the gap for an avalanche in which ionization, attachment and electron diffusion occur. The shaded area indicates those electrons which have already entered the anode (at x=d). Note that W_r equals v_e only when $\bar{\alpha}=0$ or D=0.

Figure 3.4.1 shows the electron number density distribution

$\rho_e(x,t)$ for three different situations: $\overline{\alpha}<0$, $\overline{\alpha}=0$ and $\overline{\alpha}>0$. The corresponding electron currents are shown in Fig. 3.4.2.

calculated electron current (µA)

(a) $\alpha-\eta=-1$ cm^{-1}

(b) $\alpha-\eta=0$ cm^{-1}

(c) $\alpha-\eta=3$ cm^{-1}

time(ns)
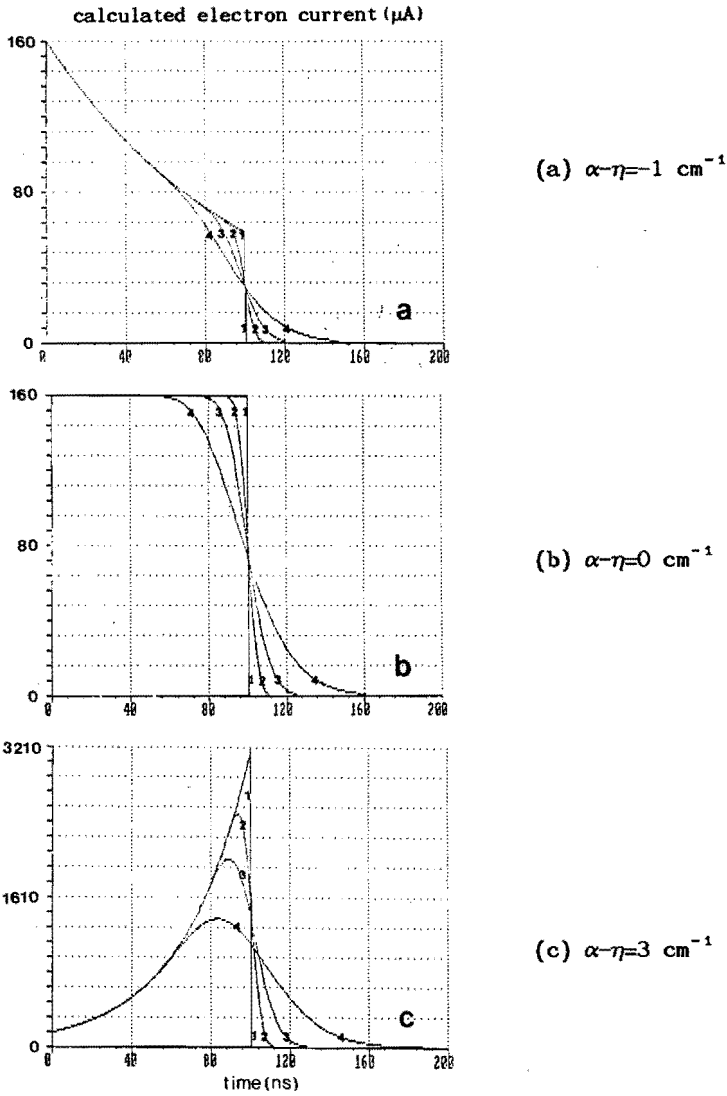
Figure 3.4.2

The electron component of the current waveform for an avalanche in which ionization, attachment and electron diffusion occur.

Here $n_0=10^8$, d=1 cm, $T_e=100$ ns, $\overline{\alpha}$ (cm^{-1}): (a) -1, (b) 0, (c) 3, D (cm^2/s): (1) 0, (2) 8x10^3, (3) 4x10^4, (4) 2x10^5.

3.5 Avalanches in which ionization, attachment, detachment, conversion and electron diffusion processes occur

In this section we consider the avalanches in which ionization, attachment, detachment, and conversion processes occur, and in which electron (longitudinal) diffusion is no longer negligible. Diffusion of ions is, again, not considered.

The species involved are electrons (index e), positive ions (index p), stable negative ions (index ns) and unstable negative ions (index nu). Again we assume that all negative ions formed via electron attachment, are unstable ions which can either undergo electron detachment or ion conversion. Therefore the attachment coefficient η used in the following equations is η_{nu}.

The following partial differential equations are used to describe the number-density distributions of electrons and ions:

$$\frac{\partial \rho_e(x,t)}{\partial t} + v_e \frac{\partial \rho_e(x,t)}{\partial x} = \bar{\alpha} v_e \rho_e(x,t) - \bar{\alpha} D \frac{\partial \rho_e(x,t)}{\partial x} + \delta v_e \rho_{nu}(x,t)$$

$$+ D \frac{\partial \rho_e^2(x,t)}{\partial x^2} \qquad (3.5.1a)$$

$$\frac{\partial \rho_p(x,t)}{\partial t} - v_p \frac{\partial \rho_p(x,t)}{\partial x} = \alpha v_e \rho_e(x,t) - \alpha D \frac{\partial \rho_e(x,t)}{\partial x} \qquad (3.5.1b)$$

$$\frac{\partial \rho_{nu}(x,t)}{\partial t} + v_{nu} \frac{\partial \rho_{nu}(x,t)}{\partial x} = \eta v_e \rho_e(x,t) - \eta D \frac{\partial \rho_e(x,t)}{\partial x}$$

$$- (\delta+\beta) v_e \rho_{nu}(x,t) \qquad (3.5.1c)$$

$$\frac{\partial \rho_{ns}(x,t)}{\partial t} + v_{ns} \frac{\partial \rho_{ns}(x,t)}{\partial x} = \beta v_e \rho_{nu}(x,t) \qquad (3.5.1d)$$

Here $\rho_j(x,t)$ and v_j (a positive value) are the number density and the drift velocity of species j (j=e, p, nu, ns), α, η, δ and β are the ionization, attachment, detachment and conversion coefficients, $\bar{\alpha}=\alpha-\eta$ is the effective ionization coefficient and D is the electron (longitudinal) diffusion coefficient. All coefficients are defined in

chapter 2.

The second terms on the right-hand-side of Eqs. (3.5.1a)~(3.5.1c) again reflect the effect of electron diffusion on the production of electrons and ions.

In this section, we concentrate on the solutions for electrons. The solutions for the distributions of electrons and unstable negative ions are, however, coupled. We therefore solve Eqs. (3.5.1a) and (3.5.1c) simultaneously. It is estimated that, for times in the order of the electron transit time T_e $(0 \leq t \lesssim 2T_e)$, the drift term $v_{nu} \dfrac{\partial \rho_{nu}(x,t)}{\partial x}$ and the diffusion term $-\eta D \dfrac{\partial \rho_e(x,t)}{\partial x}$ in Eq. (3.5.1c) are negligible compared to the other terms in the same equation. Equations (3.5.1a) and (3.5.1c) can be rewritten as:

$$\frac{\partial \rho_e(x,t)}{\partial t} + W_r \frac{\partial \rho_e(x,t)}{\partial x} = \overline{\alpha} v_e \rho_e(x,t) + \delta v_e \rho_{nu}(x,t) + D \frac{\partial \rho_e^2(x,t)}{\partial x^2}$$

$$(3.5.2a)$$

$$\frac{\partial \rho_{nu}(x,t)}{\partial t} = \eta v_e \rho_e(x,t) - (\delta + \beta) v_e \rho_{nu}(x,t) \qquad (3.5.2b)$$

where $W_r = v_e + \overline{\alpha} D$.

The solution for the electron number density $\rho_e(x,t)$ can be obtained from Eqs. (3.5.2a) and (3.5.2b) by means of the Laplace and Fourier transform techniques (see the appendix) as:

$$\rho_e(x,t) = \frac{n_0 \exp(\frac{W_r x}{2D})}{4\pi i \sqrt{D}} \int_{c-i\infty}^{c+i\infty} \frac{\exp(st - \frac{x}{\sqrt{D}}\sqrt{\frac{W_r^2}{4D} + \Gamma})}{\sqrt{\frac{W_r^2}{4D} + \Gamma}} \, ds \qquad (3.5.3)$$

Here s is a complex variable, c is a real constant and:

$$\Gamma = s - \overline{\alpha} v_e - \frac{\eta \delta v_e^2}{s + (\delta + \beta) v_e} \qquad (3.5.4)$$

The complete derivation of Eq. (3.5.3) is given in the appendix.

The number of electrons present in the gap at time t, and the electron component of the current are again obtained from:

$$n_e(t) = \int_0^d \rho_e(x,t)dx \qquad (3.5.5)$$

and:

$$i_e(t) = \frac{en_e(t)}{T_e} \qquad (3.5.6)$$

CHAPTER 4

EXPERIMENTAL SETUP FOR TIME-RESOLVED SWARM MEASUREMENT

4.1 Introduction

The time-resolved swarm method is used in the present study, primarily in view of the fact that this method provides detailed information on various processes in the avalanche growth.

As has been described in chapter 1, the time-resolution of the setup should be sufficiently high to allow the identification, from the measured avalanche current waveform, of fast collisional processes between electrons and gas molecules, and of diffusion, primarily of electrons. Such an identification is important for the verification of the four-parameter model presented, and thereby for the understanding of the breakdown mechanisms in insulating gases.

In the following sections we firstly describe the principle of the time-resolved swarm method. Secondly we present a thorough analysis of the bandwidth limitations of this method. Finally we describe the present setup in detail.

4.2 The principle of the time-resolved swarm method

Figure 4.2.1 shows schematically the principle of a time-resolved swarm method. A parallel-plate electrode gap is enclosed in a gas vessel. A stable DC high voltage source is connected, through a damping resistor R_d, to the anode, so that a uniform electric field is formed in between the two parallel plates. The cathode surface is illuminated by a single UV light pulse to release primary electrons. Under the influence of the uniform field, these primary electrons move towards the anode. During their drift, these primary electrons may produce positive and negative ions upon collisions with gas molecules (see chapter 2). The drift of these charged particles changes the electric flux ending on both electrodes and, as a consequence, induces a time-dependent current in the external circuit. This transient current flows through a measuring resistor in series with the cathode; the voltage drop is recorded by means of an oscilloscope or a transient digitizer.
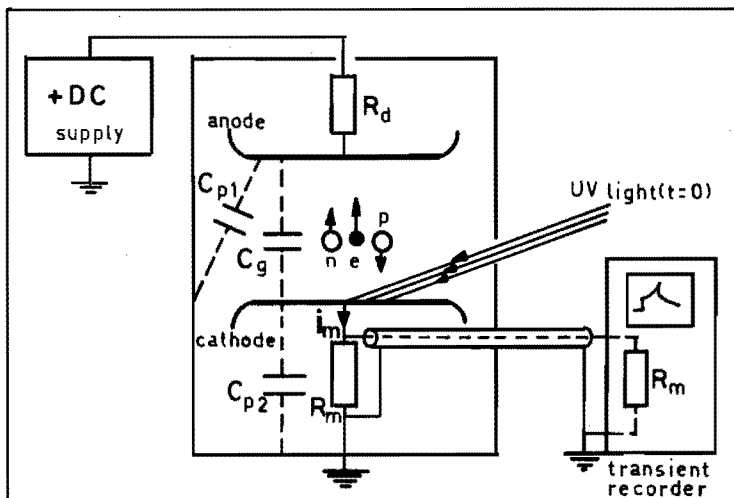
Figure 4.2.1

Schematic diagram of a time-resolved swarm method.
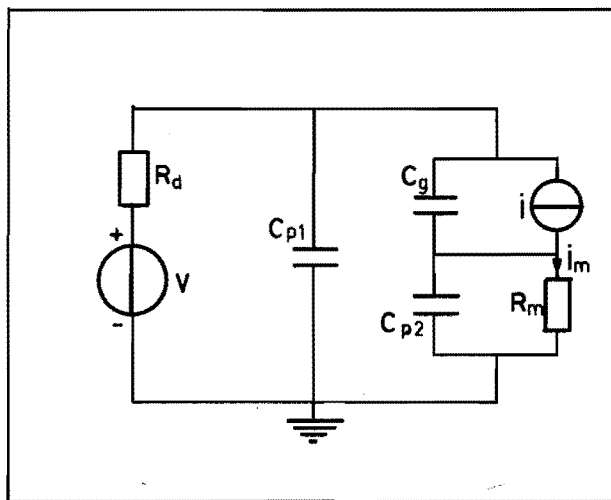
Figure 4.2.2

The equivalent circuit for high frequencies
of the setup shown in Fig. 4.2.1.

To derive the relation between the current, $i_m(t)$, in the measuring circuit and the current, $i(t)$, in the gap, at high frequencies, we use the equivalent circuit shown in Fig. 4.2.2 (inductance effects are incorporated later in section 4.3). Here the gap current is represented by a current source $i(t)$, C_g is the gap capacitance and C_{p1}, C_{p2} are the "parasitic" capacitances as shown in Fig. 4.2.1. For high frequencies, the DC voltage source can be treated as a short circuit. From this equivalent circuit, one can derive the relation between $i_m(t)$ and $i(t)$ in the frequency-domain as:

$$ I_m = \frac{I}{1 + j\omega R_m(C_g+C_{p2}) + \dfrac{j\omega R_d C_g}{1+j\omega R_d C_{p1}} + \dfrac{(j\omega)^2 R_d R_m C_{p2} C_g}{1+j\omega R_d C_{p1}}} \qquad (4.2.1) $$

The current $i(t)$ in the gap due to the motion of the charged particles produces a corresponding current $i_m(t)$ in the external circuit which can be measured.

The amplitude and the phase shift of $i_m(t)$ as compared to $i(t)$, however, strongly depend on the circuit parameters R_m, R_d, C_g, C_{p1} and C_{p2}. These circuit parameters should be chosen such that $i_m(t)$ represents $i(t)$ as accurately as possible. The damping resistor R_d is chosen very large (in our setup $R_d=20$ MΩ) in order to protect both the high voltage source and the measuring equipment in case of a complete gap-breakdown. For most frequencies of interest in the experiment we have $\omega R_d C_{p1} \gg 1$, and Eq. (4.2.1) simplies to:

$$ I_m = \frac{I}{(1+\dfrac{C_g}{C_{p1}}) + j\omega R_m(C_g+C_{p2} + \dfrac{C_{p2}C_g}{C_{p1}})} $$

$$ = \frac{I\dfrac{C_{p1}}{C_{p1}+C_g}}{1+j\omega R_m C_{eq}} \qquad (4.2.2) $$

where

$$C_{eq} = \frac{C_{p1}C_g}{C_{p1}+C_g} + C_{p2} \qquad\qquad (4.2.3)$$

From Eq. (4.2.2) it can be seen that, to avoid a loss of measuring sensitivity, C_{p1} must be chosen large compared to C_g, i.e., $C_{p1} \gg C_g$. Furthermore, to have as small a phase-shift as possible, the circuit RC-time $\tau = R_m C_{eq}$ must be small. The measuring resistor R_m cannot be chosen arbitrarily small because then the voltage across R_m becomes too small. This R_m is often chosen to be 50 Ω to match the impedance of the measuring cable. Obviously C_{eq} should be as small as possible. As can be seen from Eq. (4.2.3), this calls for the same condition $C_{p1} \gg C_g$ and also for a small C_{p2}. All these requirements led Verhaart and van der Laan (1982) to the development of an avalanche setup with a subdivided cathode which favors both sensitivity and frequency response.

The following section presents a more thorough analysis on the bandwidth limitations of the complete measuring system. Note that in the section "Closed current concept" below, C_{p2} is taken zero and C_{p1} is simply denoted by C_p. When applying this concept to the avalanche setup, the different stray capacitances C_{p1} and C_{p2} are accounted for, together with the inductances in the circuit.

4.3 Bandwidth limitations of the time-resolved swarm method

64

BANDWIDTH LIMITATIONS OF GAP CURRENT MEASUREMENTS

J.M. Wetzer, C. Wen, P.C.T. van der Laan
High-Voltage Group
Eindhoven University of Technology
The Netherlands

ABSTRACT

The bandwidth limitations which affect gap current measurements, and which are particularly important for pulsed swarm experiments, are analyzed. Such limitations are caused by the electrode geometry, geometry imperfections and the components and equipment used for signal transport and storage. Recommendations are given to optimize the time resolution. The analysis is applied to a pulsed swarm setup at the Eindhoven University of Technology, where a time resolution of 1.2 to 1.4 ns has been achieved.

INTRODUCTION

Charge carrier motion between electrodes induces currents in the electrode leads. Rapid changes of the discharge, as they occur in the early phases of breakdown, in corona and in partial discharges, may or may not show up in the external current. When a discharge is to be studied by means of current measurements we need a clear correlation between external currents and internal events. We discuss the problem here for the case of pulsed swarm experiments, where a high time resolution is necessary for the analysis of fast processes such as ionization, attachment, detachment or diffusion /1/.

A fundamental bandwidth limitation is related to the electrode geometry. This limitation is, in general, not sufficiently understood. In this paper we consider closed current paths with their impedances to find the high frequency response of gap current experiments. Based on this concept a high frequency equivalent circuit is presented and evaluated for two types of pulsed swarm setups: the conventional type, and the EUT-version with a subdivided electrode.

Other causes for bandwidth limitation include imperfections of the setup, or of the components used. Electrodes may not be strictly parallel, or may have surface irregularities. The pulse width of the light source, used for the release of primary electrons, limits the time resolution. Further, not only amplifiers and oscilloscopes, but also coaxial cables and connectors impose bandwidth limitations.

GEOMETRY RELATED LIMITATIONS

Closed current concept

Figure 1 shows the basic circuit of a pulsed avalanche setup, a homogeneous field gap, in which primary electrons are being released from the cathode, in our case by a pulsed UV-laser. The DC HV voltage source is connected through a large damping resistor R_d very close to the anode. The avalanche current is measured by means of resistor R_m. The (stray) capacitance from anode to ground, C_p is an essential part of this basic circuit.

To calculate the currents induced in the electrode leads we consider two closed surfaces A_1 and A_2, as shown in Fig.1. From Maxwell's laws we may derive that for any closed surface A

$$\oint_A (\vec{j} + \partial \vec{D}/\partial t) \cdot \vec{n} \, dA = 0 \qquad (1)$$

In case of A_1 we find the current in the lead, I_m, to be $-\partial \Psi_{A_1}/\partial t$ where the flux through A_1 changes because of the electron motion. For surface A_2 we learn from Eq.1 that the same current I_m also has to flow through C_p. The damping resistor R_d is large so that it carries only a DC current.

The above description with surface A_1, holds also at the moment that the swarm passes through this surface. The steep increase of the material current when the electrons move out is fully compensated by a simultaneous displacement current. The external current I_m is determined only by the gradual change in flux towards the cathode.
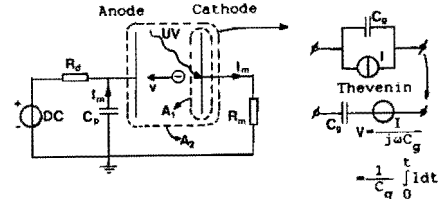
Fig.1 Basic circuit of pulsed avalanche setup illustrating closed current concept.

Since C_p closes the current path it is an essential part of the avalanche circuit. For the basic circuit of Fig.1 the relation between measured current I_m and avalanche current I is given by:

$$I_m/I = (1 + j\omega R_m C_g + \frac{j\omega R_d C_g}{1+j\omega R_d C_p})^{-1} \qquad (2)$$

For low frequency I_m approaches I, and the current is delivered by the source. For fast pulsed experiments the hf-current should not be delivered by the source but by the local circuit, in which C_p is essential. For this frequency range ($\omega R_d C_p \gg 1$) we obtain:

$$I_m/I = (1 + j\omega R_m C_g + C_g/C_p)^{-1} \quad (\omega R_d C_p \gg 1) \qquad (3)$$

In order to optimize both amplitude and bandwidth we should choose $C_p/C_g \gg 1$. Note that by this choice I_m becomes independent on C_p. Resuming, we state:

1. C_p is an essential part of the circuit, and should be chosen large compared to C_g. Without C_p no high-frequency current is measured.
2. Since we have to consider closed current loops that extend outside of the gap, inductance effects should be taken into account, and minimized.

The avalanche setup

Figure 2 shows two types of avalanche measuring setups, the conventional one and the one with subdivided electrode. The advantages of the latter will be illustrated later.
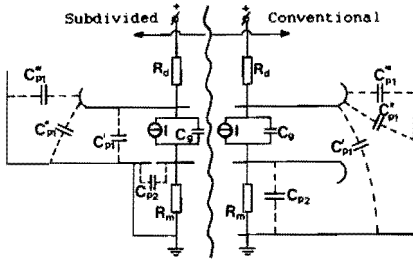
Fig.2 Avalanche measuring setups, left half: subdivided type; right half: conventional type.

As is indicated the stray capacitance C_{p1} is in fact not localized, but distributed. The same holds for the inductance associated with each current path. In our analysis they have been lumped to one capacitance C_{p1} and one inductance L_1, which is reasonable considering that dimensions are small compared to the wavelengths regarded. Further a second stray capacitance C_{p2} is introduced, being the capacitance from measuring electrode to ground, and a second inductance L_2 added by the measuring circuit. The current source representing the avalanche current, with parallel capacitance, is transformed into a voltage source with series capacitance, with the help of Thevenin's theorem (see also Fig.1). The equivalent network used in the present analysis is finally given in Fig.3, and may be applied to both types of setup.

Fig.3 Network model of avalanche setup.

For the analysis of the network response an "idealized" current waveform is introduced as the electron current without diffusion or avalanche growth. The current then takes the form of a square wave:
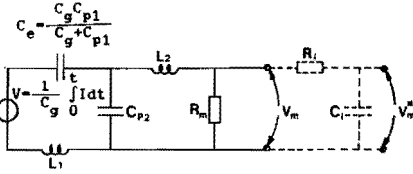
$$I = I_o [U(t) - U(t - T_e)] \qquad (4)$$

Here T_e is the electron transit time (gap distance d divided by electron drift velocity v_e), $U(t)$ is the unit stepfunction and I_o is the electron current amplitude. When transforming the current source with parallel capacitance into a voltage source with series capacitance, we find:

$$V = \frac{I_o t}{C_g} [U(t) - U(t - T_e)] + \frac{I_o T_e}{C_g} U(t - T_e) \qquad (5)$$

In order to compare calculated and measured waveforms, the finite bandwidth of the measuring equipment has to be taken into account. This was approximated by the addition of an integrating network consisting of one resistor R_i and one capacitance C_i (dotted lines in Fig.3). R_i is chosen large compared to R_m.

356

Capacitance effects

Without inductances in the network of Fig.3, the response to the "idealized" avalanche current shows a response time:

$$\tau = R_m (C_e + C_{p2}) \text{ where } C_e = C_g C_{p1}/(C_g + C_{p1}) \qquad (6)$$

For the sake of both sensitivity (as discussed earlier) and response time, C_{p1} should be chosen large compared to C_g, and C_{p2} should be minimized. C_g depends to a large extent on the clearances and dimensions required to withstand the applied voltage and to ensure field homogeneity.

By subdividing the electrode we arrive at lower C_g and C_{p2} values and at a higher C_{p1} value, all of which favor both response time and sensitivity.

Typical values obtained with subdivided cathode are: C_g = 1 pF, C_{p1} > 30 pF, and C_{p2} = 15 pF. With an R_m of 50 Ohm the RC-time is 0.8 ns (200 MHz bandwidth). For a conventional setup typical values achieved (for example /3/) are: C_g = 10 pF, C_{p1} = 25 pF, and C_{p2} = 30 pF. The RC-time (with 50 Ohm resistor) thus yields 1.86 ns (86 MHz bandwidth). In the latter (conventional) case the amplitude drops by 30%, as opposed to only a few percent with subdivided electrode. The RC-times can easily be related to step response risetimes by:

$$t_{10-90\%} = RC \left[\ln\left(\frac{100}{100-90}\right) - \ln\left(\frac{100}{100-10}\right) \right] = 2.2 * RC \qquad (7)$$

It should be noted that the Ramo-Shockley effect requires us to keep the radius of the measuring part of the electrode larger than twice the electrode separation /2/.

Inductance effects

The most important inductance in the network is L_1. First of all L_1, as opposed to L_2, depends to a large extend on the clearances required, and cannot easily be minimized. Secondly the circuit containing L_1 is primarily formed by the capacitances C_g, C_{p1} and C_{p2}, and by L_1 itself. Because no damping resistor is present, oscillations can be excited. The oscillation frequency is given by:

$$f_o = \frac{1}{2\pi\sqrt{L_1 C}} \text{ with } C = \frac{C_g C_{p1} C_{p2}}{C_g C_{p1} + C_g C_{p2} + C_{p1} C_{p2}} \qquad (8)$$

With a subdivided electrode, C approaches C_g, since C_g << C_{p1}, C_{p2}. For a conventional setup, C will be larger.

L_1 values have been estimated with a concentric cylinder approximation:

$$L = \frac{\mu_o \ell}{2\pi} \ln\left(\frac{r_2}{r_1}\right) = (200 \text{ nH/m}) \ell \cdot \ln\left(\frac{r_2}{r_1}\right) \qquad (9)$$

Here ℓ is the cylinder length, r_1 and r_2 are the radii of inner and outer conductor respectively. For the subdivided type we find a value in the order of 5-10 nH, for the conventional type a value of over 25 nH is obtained. The oscillation frequency derived is about 2 GHz for the subdivided type, and below 400 MHz for the conventional type.

Usually the measuring apparatus operates as a low pass filter, and attenuates the resonances. Additional filtering would slow down the response time. It is therefore essential that f_o is well above the relevant frequency range. This calls for minimization of L_1. Also in this respect, subdivision of the electrode is advantageous.

Model calculations confirm the oscillation frequency found in Eq.(8), but also show some damping as a result

of the measuring circuit containing R_m. An increase of L_1 results in a lower f_o (see Eq.(8)), and a higher amplitude.

The effect of the additional inductance L_2 has been evaluated by performing model calculations for typical sets of parameters with varying L_2. It was found that, provided some effort is taken to minimize L_2 to below about 10 nH, the waveform is very little affected. A higher value of L_2 tends to reduce the oscillation amplitude, however at the cost of bandwidth.

EUT-avalanche setup

Figure 4 shows the simulation of the step response for the avalanche setup of the Eindhoven University of Technology /2/, which is of the subdivided type. The capacitance values are measured, whereas inductance values are estimated from Eq.(9). In the experiment the 50 Ohm measuring cable is terminated at both ends to avoid reflections, thus giving an R_m of 25 Ohm.
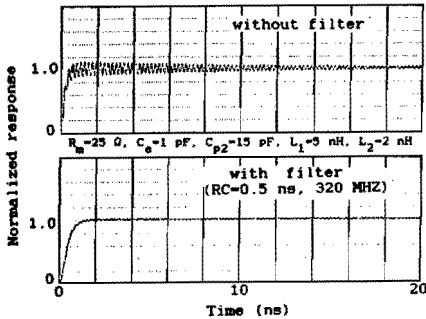

Fig.4 Simulated response of EUT-avalanche setup with subdivided cathode. Upper trace without filter, lower trace with filter.

The simulation shows a (10-90%) risetime of 1.37 ns, which is consistent with the experimentally observed risetime of 1.4-1.5 ns /1,4/, especially when we consider the additional bandwidth limitations to be discussed later. Another feature observed from the experiment is a certain linewidth of the screen trace, which is not observed when the equipment is tested with a fast pulse generator. According to our calculations this linewidth is caused by oscillations in the avalanche circuit. The oscillations are partly suppressed by the filter (RC = 0.5 ns, bandwidth 320 MHz), and may be suppressed further, however not without a loss in bandwidth.

Simulations for typical parameter sets for a conventional (not subdivided) setup show a slower response, oscillations at a lower frequency and with a larger amplitude, but with some more damping. Adequate suppression of these oscillations would require a filter with an RC-time larger than 2.5 ns (bandwidth below 65 MHz). According to Eq.(7) this will result in risetimes larger than 5 ns.

GEOMETRY IMPERFECTIONS

An electrode geometry used for avalanche experiments

may have non parallel electrodes or surface irregularities on its cathode. Figure 5 shows two examples. As a result of these imperfections, electrons leaving the cathode at the same time, arrive at the anode with a time difference ΔT_e. This causes a "diffusion-like" distortion of the current waveform. Obviously also the size of the surface irregularity, as compared to the avalanche width, is important.
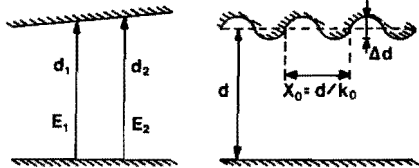
Fig.5 Two examples of geometry imperfections.

In the first situation with slightly non parallel electrodes ($\Delta d/d \ll 1$) the field is still almost homogeneous. A simple analysis yields:

$$T_e = \frac{d}{v_e} = \frac{d}{bE} = \frac{d^2}{bV} \quad \text{so} \quad \frac{\Delta T_e}{T_e} = 2\frac{\Delta d}{d} \qquad (10)$$

Here $b = v_e/E$ is the electron mobility, which may be assumed constant considering the minor field variation involved. For a typical electron drift velocity $v_e = 10^7$ cm/s, a Δd of 100 µm results in a $\Delta T_e = 2$ ns. A falltime of 2 ns corresponds to an RC-time of 0.91 ns, or a bandwidth of 175 MHz. Note that the risetime is not affected.

To treat surface ripples with shorter wavelength (see Fig.5, right hand side), we have to calculate the distorted field. For $\Delta d \ll d$ we obtain:

$$\frac{\Delta T_e}{T_e} = \frac{\Delta d}{d}\{1+\frac{1}{2\pi k_o}\frac{d}{\Delta d}\ln\frac{1+\frac{\pi k_o\Delta d/d}{1-\exp(-4\pi k_o)}}{1-\frac{\pi k_o\Delta d/d}{1-\exp(-4\pi k_o)}}\} \qquad (11)$$

If we further assume that $\exp(-4\pi k_o) \ll 1$, which holds for $k_o > 0.5$ or $x_o < 2d$, we find:

$$\frac{\Delta T_e}{T_e} = \frac{\Delta d}{d}[2+\frac{(\pi k_o\Delta d/d)^2}{3}+\frac{(\pi k_o\Delta d/d)^4}{5}+\cdots] \qquad (12)$$

Hence this result is, to a first approximation, identical to the long wavelength solution of Eq. (10).

The irregularities mentioned may arise from machining, or from the polishing that is required in between measurements to ensure the release of sufficient electrons from the cathode. Figure 6 illustrates the effect of irregularities on the falltime of an avalanche waveform measured in atmospheric nitrogen.
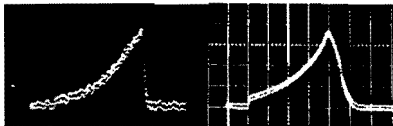
Fig.6 Avalanche current waveform with smooth surface (left $\Delta d < 10$ µm), and with irregular surface (right, $\Delta d < 300$ µm within avalanche width). Nitrogen: p = 750 Torr, d = 10 mm, E/p = 35.3 V/cm.Torr, 20 ns/div.

357

TECHNICAL LIMITATIONS

Apart from the geometry and its imperfections, several technical aspects may limit the bandwidth. We mention the pulse width of the laser used to release the primary electrons, and the signal transport and storage system.

The pulse duration of the laser determines the size of the primary electron swarm and thereby limits the time resolution. The N_2-laser used in the EUT avalanche setup has been manufactured in our group according to the design of Patel /5/. Instead of parallel plate capacitors, however, the capacitor plates are mounted on an aluminum cylinder to obtain a compact design. Measurement of the laser power versus time shows a pulse width (FWHM=full width half maximum) of 0.6 ns. The minimum risetime of the avalanche current will then be 0.65 ns which corresponds to an RC-time of 0.3 ns, or a bandwidth of 540 MHZ.

The signals are stored on a Tektronix (7912 AD) digitizer. The minimum risetime observed when supplying a fast rising pulse from a mercury wetted reed relay is 0.6 ns. The bandwidth in this case may be limited either by the pulse-generator or by the digitizer. The digitizer bandwidth however must be at least 580 MHz (which corresponds to an 0.6 ns risetime).

Due to the skineffect also the 50 Ohm coaxial cable used causes bandwidth limitations (see for example /6/). This contribution has been investigated by repeating the experiments with the mercury wetted reed relay for different types (RG 58 and RG 214) and different lengths of cable (see Fig.7). Other cables will be investigated in the near future. A cable contribution to the risetime can be prevented by the choice of the type of the cable, and by the reduction of the cable length. It was further found that BNC connectors, even in large numbers, did not have a measurable effect on the risetime.
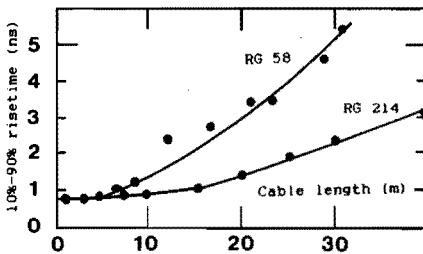

Fig.7 Risetimes versus cable-length for RG58 and RG214 50 ohm coaxial cable.

The risetime of the complete setup, including all contributions mentioned, has been checked experimentally by performing an experiment in vacuum, i.e. with the vessel pumped down to 10^{-7} Torr. Under DC voltage, one electron released from the cathode, or many electrons released simultaneously, induce a linearly increasing current waveform until the electrons reach the anode after a transit time of $T_e = (2m_e d/eE)^{1/2}$. Here m_e and e are the electron's mass and charge respectively. In our experiment we used E = 10 kV/cm and d = 1 cm, resulting in a transit time T_e = 0.34 ns. This is sufficiently short to ensure that this current waveform acts as an impulse excitation of the setup. The measured impulse response is integrated to obtain the step response. Figure 8 shows the measured impulse waveform

and the stepresponse derived by integration. The overall risetime obtained is 1.42 ns, which corresponds to a bandwidth of 250 MHZ.
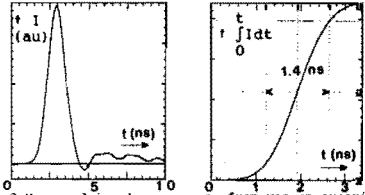
Fig.8 Measured impulse response from vacuum experiment, and stepresponse obtained from integration.

The effect of different independent risetime contributions on the finally obtained risetime can be approximated by:

$$\tau = \sqrt{\sum_i \tau_i^2} \qquad (13)$$

The geometry contribution (1.37 ns) together with the laser contribution (0.65 ns) yields a risetime of 1.52 ns. In combination with a digitizer contribution of 0.6 ns, this yields a risetime of 1.63 ns. Presumably however, this digitizer contribution is overestimated.

CONCLUSIONS AND RECOMMENDATIONS

1. Analysis of the bandwidth of gap current measurements involves the evaluation of closed current paths. The electrode geometry, (stray) capacitances and inductances play a decisive role.
2. In terms of bandwidth and sensitivity, subdivision of the measuring electrode is much better than the classic two-electrode measuring system.
3. After optimization of the geometry with respect to high frequency response, the bandwidth of gap current measurements is limited by the stray capacitance in parallel to the measuring resistor.
4. Geometry imperfections, such as non parallel electrodes or irregular surfaces, cause diffusion-like waveform distortions.
5. Apart from the oscilloscope also the type and length of coaxial cable should be carefully selected when nanosecond risetime measurements are made.
6. A laser triggered pulsed avalanche setup has been developed with an overall risetime of 1.4 ns, corresponding to a bandwidth of 250 MHz. The risetime of the electrical circuit (i.e. when disregarding the finite pulsewidth of the laser) is 1.26 ns, which corresponds to a 280 MHz bandwidth.

ACKNOWLEDGEMENT

LITERATURE

/1/ J.M. Wetzer, C. Wen, 5th.Int.Symp.on High Voltage Eng., Braunschweig, FRG, 1987, paper 15.06.
/2/ H.F.A. Verhaart, P.C.T. van der Laan, J.Appl.Phys., 53(3), March 1982.
/3/ Th. Aschwanden, thesis ETH Zurich, 1985.
/4/ H.F.A. Verhaart, thesis, Eindhoven University of Technology, 1982.
/5/ R.S. Patel, Rev.Sci.Instrum., 49(9), September 1978
/6/ N.S. Nahman, IRE Trans.on Circuit Theory, June 1962

4.4 The experimental setup and the measuring system

The present setup is shown in Fig. 4.4.1, and is basically the same as that described earlier by Verhaart and van der Laan (1982) and Verhaart (1982).
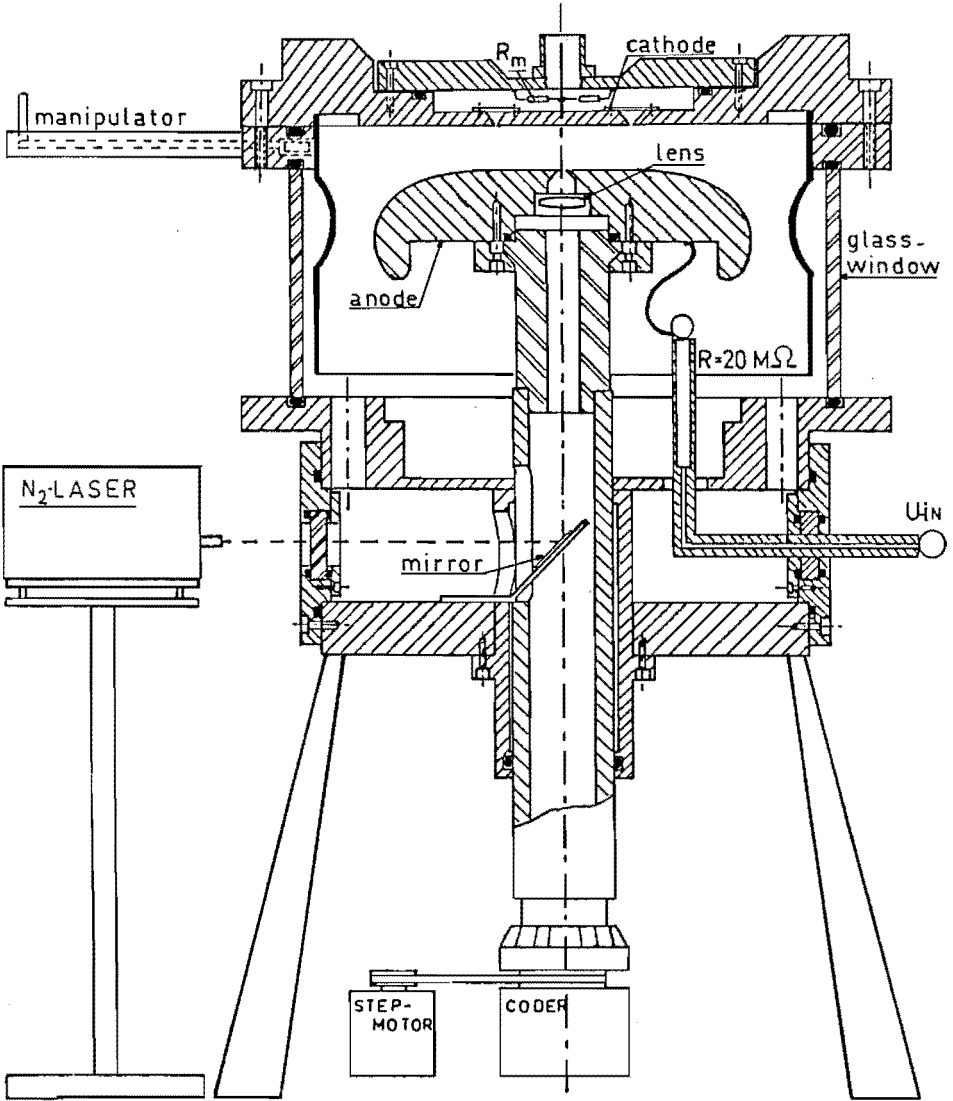
Figure 4.4.1

The experimental setup.

As compared to their setup, the discharge vessel has better vacuum properties and a smaller volume in order to reduce the amount of gas required. The chamber is made of stainless-steel with glass windows on the sides. The chamber can be evacuated by a turbomolecular pump (Pfeiffer, type TPH170) with an electronic drive unit (Pfeiffer, type TCP300) down to 10^{-7} Torr before the gas under consideration is admitted. The vacuum pressure is measured by a cold cathode gauge (Balzers, type PKG010, range $5 \times 10^{-8} \sim 100$ Torr) or a digital pressure meter (Balzers, type TPG300, range $10^{-11} \sim 1000$ mbar (=750 Torr)).

When filled with gas, the pressure is measured by several pressure gauges: five Penwalts, type FA-160 (range 0~20 Torr, 0~50 Torr, 0~100 Torr, 0~450 Torr and 400~800 Torr) and one Balzers, type APG010 (range 0~1200 mbar).

The aluminum anode inside the vessel has a Bruce profile (Bruce, 1947) and a 17 cm diameter. The aluminum cathode is a subdivided disk with a total diameter of 22 cm with a central measuring part of 4 cm in diameter. The outer-part is grounded. The annular gap between the two parts at the cathode surface is 0.1 mm. To minimize the stray capacitance between the central measuring part and the grounded ring (i.e., C_{p2} in Fig. 4.2.1), the edges of the two parts are beveled as shown in Fig. 4.4.1.

The gap distance can be varied by moving the anode up or down along the axis with a step-motor. The distance can be measured outside by a precision meter (Mitutoyo, range 0.01~10 mm). The maximum gap distance which guarantees a reliable measurement is limited due to the Ramo-Shockley effect (Ramo, 1939; Shockley, 1938). This effect was described, amongst others, by Verhaart and van der Laan (1982), Verhaart (1982) and, according to a quite different approach, by Borghesani and co-workers (1986). For a measuring electrode of 4 cm diameter the maximum gap distance is 1.0 cm. The gap distance is fixed at 1.0 cm throughout the present study.

A TEA (transversely excited atmospheric) N_2 laser (wavelength 337.1 nm), constructed in our laboratory, has been used to release primary electrons. The laser pulse duration is 0.6 ns FWHM (full width half maximum). This laser has been described in more detail by Verhaart (1982). The light pulse of the laser strikes the cathode

70

through a hole of 1.5 mm diameter in the center of the anode. A positive lens in front of this pinhole images the light beams upon an area of approximately 1 cm^2 (for a gap distance of 1 cm) from which the "disk" of primary electrons is being released.

To ensure the release of sufficient primary electrons from the cathode, a mechanical manipulator was installed to clean the surface of the cathode in between the measurements. Since this cleaning process may deteriorate the cathode surface, the central measuring part of the cathode was frequently renewed.

The measuring resistor R_m (=50 Ω) was made in a star-configuration (4x200 Ω in parallel) to reduce the inductance.

The damping resistor, R_d, which connects the DC supply to the anode has a value of 20 MΩ and was mounted inside the chamber close to the anode in order to have a well-defined stray capacitance C_{p1}, and to minimize the inductance and the effects of traveling waves.

The DC voltage source is a Wallis, type R603/05p, with an output voltage up to 60 kV and a maximum ripple of 20 ppm peak to peak. The DC voltage applied on the anode is measured by a resistive divider and a digital volt-meter (DigiTec model 2780). The accuracy of this measurement is better than 1% for V>1 kV. To achieve the same accuracy also for V≤1 kV, a Keithley multimeter (type 177 Microvolt DMM) was directly connected to the high voltage lead to measure the applied voltage.

Figure 4.4.2 shows the complete measuring system. The voltage across R_m is measured through a 50 Ω cable (RG 214, length 5 m) by a 9 bit Tektronix 7912 AD digitizer with amplifier unit 7A29 (bandwidth 0~1 GHz) and timebase unit 7B10. The type and the length of the cable was selected according to the description in section 4.3. For very weak signals an additional wideband preamplifier (constructed with Avantek amplifiers GPD 461, 462, 463, bandwidth 250 Hz–500 MHz) was used. To protect both the preamplifier and the digitizer, a pair of silicon diodes (type 1N-4151, capacitance C=2 pF) was mounted back to back in parallel with the measuring resistor R_m.

The gap capacitance and the stray capacitances of this setup were measured at a gap distance of 1.0 cm with a Philips RLC meter (type PM6303). The values obtained are: C_g=1.1 pF, C_{p1}=42.2 pF and C_{p2}=16.1 pF. The equivalent capacitance C_{eq} of the whole measuring

71

circuit is 17.2 pF (Eq. (4.2.3)). Since the cable is terminated at both ends by a 50 Ω resistor, the total or equivalent resistance is 25 Ω. The RC-time of the measuring circuit alone is $\tau = R_m C_{eq} = 0.43$ ns which corresponds to a risetime of 0.95 ns ($2.2 R_m C_{eq}$). As mentioned earlier (section 4.3) the risetime of the complete measuring system has been determined by an experiment in vacuum to be 1.4 ns. The experimental risetime includes the contributions of the electrode geometry (the effects of both capacitances and inductances), the laser pulse width, the digitizer, the preamplifier, the cable and possible imperfections of the electrode surface.
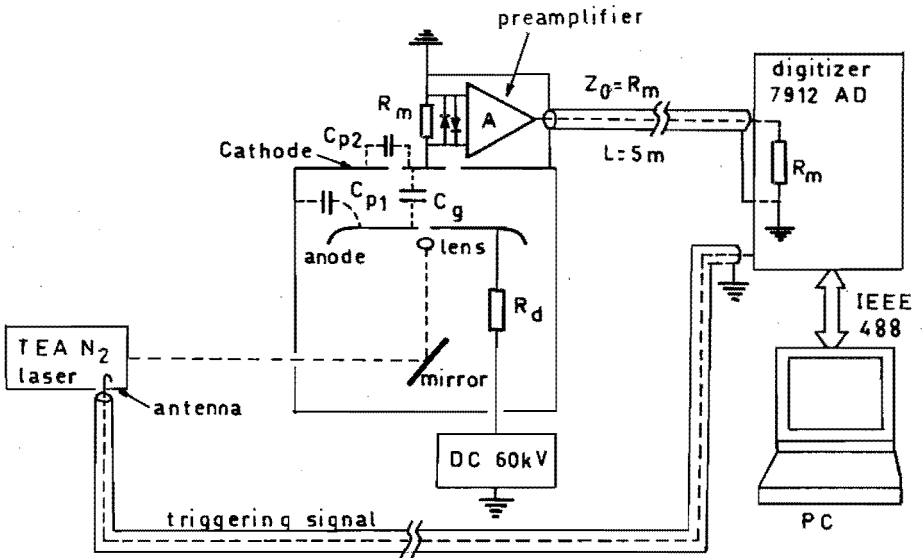
Figure 4.4.2

Schematic diagram of the complete measuring system.

72

CHAPTER 5

EXPERIMENTAL RESULTS AND DISCUSSIONS

5.1 Introduction

The time-resolved swarm technique described in chapter 4 has been used to measure avalanche currents in a number of insulating gases: nitrogen (N_2), sulfur hexafluoride (SF_6), dry air, oxygen (O_2), hexafluoropropene ($1-C_3F_6$), octafluorocyclobutane ($c-C_4F_8$) and dichlorodifluoromethane (CCl_2F_2).

These gases are, or can be used as, electrical insulants. Air and SF_6 are widely used in practical power systems. The gases $1-C_3F_6$, $c-C_4F_8$ and CCl_2F_2 have a higher dielectric strength at practical pressures, and may be promising contenders in the future, as a replacement of, or an admixture to, SF_6. Although for application on a large scale a number of other requirements (such as thermal properties, carbonization and reaction products, toxicity and environmental impacts etc.) should be fulfilled, we here concentrate on the swarm parameters.

In the present work special attention is paid to electronegative gases in which electron detachment and ion conversion processes, next to ionization and attachment processes, contribute to the avalanche growth. Since the production of electrons in avalanches is crucial for the occurrence of gas breakdown, most effort is dedicated to the observation and evaluation of the electron component of the avalanche current waveform. In most cases, the experiments have been carried out at relatively high pressures because in practical systems gases are used at high pressures. At high pressure collisional electron detachment and ion conversion are important, and the neglect of electron diffusion in the theoretical model is justified.

The theoretical models described in chapter 3 have been employed for the evaluation of the measured avalanche current waveforms. The choice of an appropriate model depends on the type of gas (whether or not delaying processes occur) and on the gas pressure (whether or not diffusion is important). We distinguish between what we call "simple" gases and "complex" gases. "Simple" gases are those gases that can be described by ionization and attachment processes only. In "complex"

73

gases also delaying processes such as electron detachment and ion conversion affect the avalanche growth.

At relatively high pressure electron diffusion is negligible. The model described in section 3.2 is then applicable to the "simple" gases. For "complex" gases the model described in section 3.3 should be used. The two models are sometimes referred to as the two-parameter model (α and η) and the four-parameter model (α, η, δ and β).

At sufficiently low pressure all "high pressure" processes (such as collisional electron detachment and ion conversion) have a low probability. Then the model described in section 3.4 is employed for both "simple" and "complex" gases; at these pressures electron diffusion cannot be neglected.

For "complex" gases in the intermediate pressure range, where both electron diffusion and delaying processes should be accounted for, the model presented in section 3.5 should be applied. This situation is, however, not dealt with in this work.

A detailed discussion on the choice of swarm parameters for the evaluation of the measured avalanche current waveforms is given in the following section.

5.2 The choice of swarm parameters for avalanche studies

74

THE CHOICE OF SWARM PARAMETERS FOR AVALANCHE STUDIES

J.M. Wetzer and C. Wen

High-Voltage Group, Eindhoven University of Technology

THE NETHERLANDS

ABSTRACT

In order to choose the appropriate model, and the relevant swarm parameters, for the analysis of avalanche current waveforms, a distinction is made between avalanches without delaying processes, avalanches with delaying processes and "ion-dominated" avalanches. This distinction is based on the appearance of the time-resolved current waveform. We present the different approaches required for the analysis of the different types of avalanches. Application of an inadequate model may result in apparent values for the swarm parameters, including the electron drift velocity, which do not agree with scaling laws.

INTRODUCTION

In the study of swarm parameters of insulating gases we expect from scaling laws that, at least over a considerable range of pressure p and electric field E:
1. the electron drift velocity, v_e, is a function of E/p;
2. the pressure reduced effective ionization coefficient, α/p, is a function of E/p;
3. the limiting E/p is a constant.

This is indeed true for a number of gases (N_2, SF_6). For other gases ($1-C_3F_6$, $c-C_4F_8$) unexpected pressure dependencies have been observed /1,2,3/. We have shown earlier /2,4/ that a derivation of swarm-parameters for C_3F_6 on the basis of a model, which includes detachment and ion-conversion processes, next to ionization and attachment processes, leads to results that agree with the scaling laws.

The evaluation of avalanche currents in $1-C_3F_6$ based on the extended model indicated that the pressure dependence of v_e versus E/p is caused by temporary electron trapping. This results in an averaged velocity below the drift velocity. The pressure dependence in α/p versus E/p is partly caused by the use of the incorrect drift velocity, and partly by the neglect of detachment and conversion processes /5/.

In case of Townsend breakdown, a simplified model that neglects detachment and ion-conversion correctly predicts the limiting E/p since the total number of electrons is important. Scaling however is not possible and the understanding is poor.

In case of streamer breakdown, such a simplified model generally no longer predicts the correct limiting E/p because the spatial distribution of electrons is only correctly described if delaying processes, such as detachment, are incorporated.

Usually the electron component of the current, which can be easily distinguished from the ion component by the difference in amplitude and duration, is analyzed. Recent experiments in $c-C_4F_8$, however, have shown avalanche currents where these two components are strongly intermixed /3,6/. As a result, the interpretation of avalanche currents from the electron component only, becomes impossible. The analysis of the ion component, however, is not straightforward because many different ion species may be involved.

The choice of the appropriate model can be made on the basis of the observed waveform. We will make a distinction between electron avalanches with or without delaying processes. We will illustrate how the delaying processes can result in "ion-dominated avalanches".

THE AVALANCHE CURRENT WAVEFORM

The method which we used for the avalanche current measurement is the so-called time-resolved swarm method. To ensure a sufficient time resolution, the avalanche is initiated with a N_2 laser pulse of very short duration (0.6 ns), and the measuring electrode is subdivided. The waveform is recorded with a Tektronix 7912 AD digitizer. The time resolution of the whole system is 1.4 ns. A detailed description of the measuring technique and the experimental setup can be found elsewhere /7,8,9/.

For the choice of an appropriate model, we distinguish between avalanches without delaying processes, avalanches with delaying processes, and the "ion-dominated avalanches". Figures 1-3 show typical measured waveforms for each kind of avalanche.

Avalanches without delaying processes

Figure 1 shows a current waveform of an avalanche without delaying processes, measured in N_2 /10/. Such waveforms are characterized by the electron drift velocity and by the ionization and attachment coefficients. At low pressure the waveform may be affected by diffusion. In fact, it requires a good
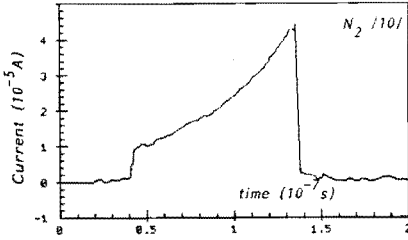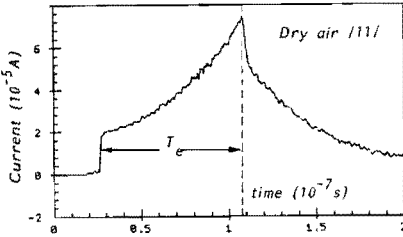
1

Figure 2

Waveform of avalanche with delaying processes.
Electron comp., Dry Air, p = 98.8 kPa (741 Torr),
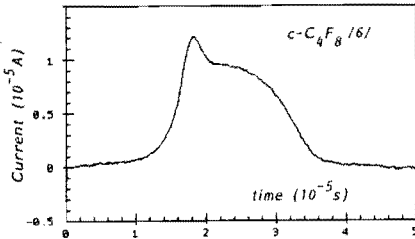E/p = 0.26 V/cm.Pa (34.7 V/cm.Torr), d = 1.0 cm.

Figure 3

Waveform of ion-dominated avalanche.
Total current, $c-C_4F_8$, p = 20 kPa (150 Torr),
E/p = 1.1 V/cm.Pa (146 V/cm.Torr), d = 1.0 cm.

time resolution to distinguish between diffusion and delaying processes such as detachment. Secondary emission may cause second generations.

In avalanches without delaying processes all electrons are contained in the avalanche-head and reach the anode at the same time, aside from the effect of diffusion. This results in a sharp drop of the current after the electron transit time.

Avalanches with delaying processes

Figure 2 shows a current waveform of an avalanche with delaying processes, measured in dry air /11/. This kind of waveform may be characterized by the electron drift velocity and by the swarm coefficients for ionization, attachment, detachment and ion conversion. At low pressure the waveform may again be affected by diffusion.

Avalanches with delaying processes contain electrons not only in the head but also in the tail of the avalanche, which shows up in the electron current as an "aftercurrent" /5/. A sharp drop in the current after one electron transit time is observed only if the avalanche head still contains a number of undelayed electrons. If not, an apparent decrease of drift velocity is observed /2/.

Detachment acts as a "secondary, delayed, ionization process". Ion conversion stabilizes the negative ions formed by attachment, and thereby reduces the probability of detachment /5/.

Ion-dominated avalanches

Figure 3 shows a current waveform of an "ion-dominated avalanche", measured in $c-C_4F_8$ /6/. This kind of waveform deviates from the "normal" waveform of avalanches with delaying processes in two respects. Firstly, at pressures above 1.3 kPa (10 Torr), no distinct electron current is observed. Secondly, the current has been observed to increase during microseconds before decreasing again. Normally, after the electron transit time, the current is a strictly decreasing function of time /12/. Although we call this kind of avalanche "ion-dominated" because of the apparent absence of an electronic contribution, the long production time for ions observed, can only be explained if at least a small electron component is present.

The avalanche currents described can be explained by the combination of a strong attachment process, and a lifetime of the unstable negative ion formed that is large compared to the electron transit time. The ion conversion rate should not be high compared to the electron detachment rate /6/.

AVALANCHE MODEL

For an adequate avalanche model we require that:
1. the number of parameters is limited,
2. the parameters are physically meaningful,
3. the model fully describes the charge distribution and the current waveform of the avalanche, and
4. the set of parameters allows experimental verification.

The last requirement also depends on the kind of experiment used. A pulsed experiment with high time resolution allows the verification of more complex models than, for example, steady state experiments.

A detailed description of the model that we use to analyze avalanche current waveforms is presented elsewhere /5,10/. Secondary emission and diffusion are not considered but can be incorporated /10/. Apart from neutral molecules, four species are involved: electrons, positive ions, unstable negative ions and stable negative ions. In contrast to stable negative ions, the unstable negative ions are able either to release their electrons, or to be converted into stable ones, within the ion's transit time. The processes considered in our model are ionization (coefficient α), attachment (η), detachment (δ), ion conversion (β) and drift.

The model describes, for a parallel-plate gap, the temporal evolution of the density distributions of all species. Integration over the gap provides, for each species, the number of particles contained in the gap as a function of time. The avalanche current is obtained from these numbers and the corresponding drift velocities. With the model one can simulate the current waveform for any given set of swarm parameters, or one can derive the swarm parameters from experiments by fitting the simulated waveform to the measured one.

The interpretation of avalanche current waveforms is primarily based on the electron component of the current, because it involves only one species with one drift velocity. As was shown earlier, from the
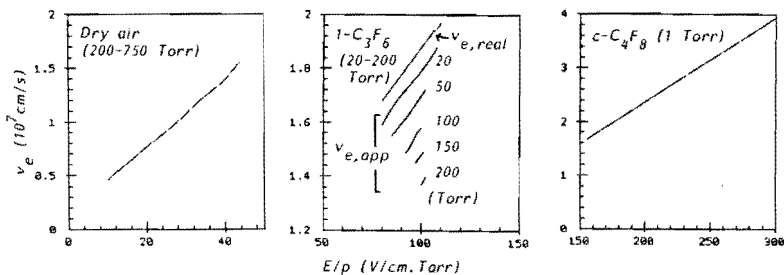
2

Figure 4
Electron drift velocity versus E/p
Left : Dry Air, from transit time (drop in current) /11/
Middle: 1-C$_3$F$_6$, apparent (from transit time), and real value (corrected for electron trapping) /2/
Right : c-C$_4$F$_8$, from transit time (can only be observed at low pressure) /3/

electron current only, the four parameters cannot be derived individually, but only in the combinations /5/:

$$C_1 = \alpha - \eta \qquad C_2 = \delta + \beta \qquad C_3 = \eta.\delta \qquad (1)$$

Here C_1 is the "real" effective ionization coefficient, C_2 describes the loss rate of unstable negative ions and C_3 is a secondary, delayed, ionization parameter.

Application of a "simplified" model, without detachment and ion conversion, to the (electron component of the) avalanche current results in an "apparent" effective ionization parameter for which we have shown earlier /2/ that

$$(\alpha - \eta)_{apparent} = (\alpha - \eta)_{real} + \frac{\eta.\delta}{\delta + \beta} = C_1 + C_3/C_2 \qquad (2)$$

WAVEFORM ANALYSIS

Based on the number of parameters involved we make a distinction between a two parameter model (α and η) and a four parameter model (α, η, δ and β). Before applying the appropriate model to the measured waveform the electron drift velocity should be derived, and the electronic and ionic contributions to the waveform should be separated.

Derivation of the electron contribution

For gases that are not strongly attaching, the electronic component of the current is much larger than the ionic part, and during (a few times) the electron transit time the ionic contribution can be neglected. For strongly attaching gases the ionic component may become considerable and a separation of the waveform into the two contributions becomes essential. For avalanches without delaying processes a technique has been developed for this separation on the basis of the two parameter model /10,13/. Such a technique has not yet been developed for avalanches with delaying processes, and as a result the electronic contribution should be estimated. The uncertainty introduced is limited if a distinct electron component is present. For ion-dominated avalanches, the separation is not possible.

Derivation of the electron drift velocity

The determination of the electron drift velocity is crucial for the analysis of avalanche current waveforms. An incorrect drift velocity results in an incorrect determination of other swarm parameters.

If the avalanche head contains a considerable number (or all) of the undelayed electrons, a sharp drop in the current is observed after one electron transit time, which corresponds to the electron drift velocity. Dry air is given as an example (waveform Fig.2, drift velocity Fig.4, left). If most or all electrons are delayed, the "zero-density" drift velocity should be determined in order to correct for electron trapping /2/. In Fig.4 (middle) the apparent and real drift velocities in 1-C$_3$F$_6$ are given as an example. For ion-dominated avalanches, the electron drift velocity cannot be derived from the observed waveform. As a result the electron drift velocity in c-C$_4$F$_8$ can only be derived at low pressure, where a distinct electron component is still present (Figure 4, right).

Derivation of the swarm parameters

For gases where the two parameter model is applicable (N$_2$, SF$_6$), the effective ionization coefficient is derived directly from the slope of the electron current waveform /8,10,12,13/.

For gases that exhibit detachment and ion conversion processes next to ionization and attachment processes, the three combinations of parameters ($\alpha - \eta, \delta + \beta$ and $\eta.\delta$) are derived from a fit between the measured and calculated waveforms (provided that the waveform is not ion-dominated). Examples are c$_{34}$ (dry or humid) air and 1-C$_3$F$_6$. For dry air the results are given in Figs.5-7. A discussion of these results in terms of the responsible processes and their pressure dependencies is presented elsewhere /11/. A similar analysis has been performed for 1-C$_3$F$_6$ /2,4/.

For ion-dominated avalanches a fitting procedure becomes inaccurate because next to the other swarm parameters, also the drift velocities, are unknown. A simulation of the current waveform, with assumed values for all parameters involved, shows that the kind of waveform observed in c-C$_4$F$_8$ could be explained on the basis of the four parameter model /6/. An example is given in Figure 8.
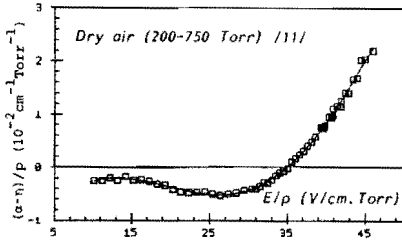
3

Figure 5
Real effective ionization coefficient in dry air
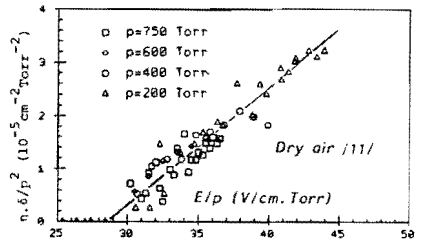
Figure 6
$n.\delta/p^2$ versus E/p in dry air
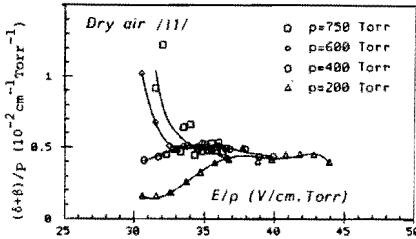
Figure 7
$(\delta+\beta)/p$ versus E/P in dry air
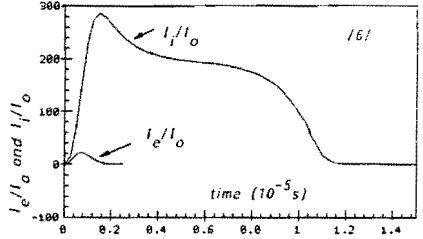
Figure 8
Simulation of ion-dominated avalanche current
Electron (I_e/I_o) and ion (I_i/I_o) current $(I_o$ is the initial electron current) for following parameters: Electron transit time 50 ns; ion transit time 10 µs; $\alpha = 98$, $\eta = 100$, $\delta = 0.05$, $\beta = 0.4$ (unit: cm-1)

CONCLUSIONS

1. From the observation of time-resolved current waveforms, we can distinguish between avalanches without delaying processes (N_2, SF_6), avalanches with delaying processes (dry and humid air, 1-C_3F_6), and "ion-dominated" avalanches (c-C_4F_8).
2. A four parameter model, involving detachment and ion conversion besides ionization and attachment, in principle describes all three kinds of avalanches.
3. Analysis of avalanches with delaying processes, with a model that does not include detachment and ion conversion, results in apparent values for the electron drift velocity and the effective ionization coefficient which do not follow scaling laws.
4. An evaluation of avalanche waveforms with the four parameter model, and with the electron drift velocity corrected for electron trapping, shows that the "real" electron drift velocity, and the "real" effective ionization coefficient in air and in 1-C_3F_6 agree with scaling laws.

AUTHORS ADDRESS

High-Voltage Group
Eindhoven University of Technology
PO Box 513, 5600 MB Eindhoven
THE NETHERLANDS

REFERENCES

/1/ Verhaart,H.F.A., and van der Laan, P.C.T., 4th. Int.Symp.on High Voltage Eng., Athens, Paper 33.12, 1983.

/2/ Wen, C., and Wetzer, J.M., Int.Symp.on Electr. Insulation, Boston, pp. 108-111, 1988.

/3/ Wen, C., and Wetzer, J.M., 9th.Int.Conf.on Gas Disch.and their Appl., Venice, pp. 367-370, 1988.

/4/ Wetzer, J.M., and Wen, C., 5th.Int.Symp.on High Voltage Eng., Braunschweig, Paper 15.06, 1987.

/5/ Wen, C., and Wetzer, J.M., IEEE Trans.on Electr.Insulation, 23, pp. 999-1008, 1988.

/6/ Wen, C., and Wetzer, J.M., IEEE Trans.on Electr.Insulation, 24, pp. 143-149, 1989.

/7/ Wetzer, J.M., and van der Laan, P.C.T., Invited Contribution to Special Europe Issue of IEEE Trans.on Electr.Insulation, to appear in April, 1989.

/8/ Verhaart, H.F.A., and van der Laan, P.C.T., J.Appl.Phys., 53, pp. 1430-1436, 1982.

/9/ Wetzer, J.M., Wen, C., and van der Laan, P.C.T., Int.Conf.on Electr.Insulation, Boston, pp. 355-358, 1988.

/10/ Wen, C., Ph.D. Thesis, Eindhoven University of Technology, the Netherlands, to appear in 1989.

/11/ Wen, C., and Wetzer, J.M., submitted to 19th. Int.Conf.on Phen.in Ionized Gases, Belgrade, 1989.

/12/ Verhaart, H.F.A., Ph.D. Thesis, Eindhoven University of Technology, the Netherlands, 1982.

/13/ Aschwanden, Th., Ph.D. Thesis, ETH Zurich, Switzerland, 1985.

4

5.3 Nitrogen

5.3.1 Introduction

Nitrogen is used as an admixture to SF_6, as an insulating gas in itself, and in various other applications such as UV-lasers.

Extensive studies, both experimental and theoretical, have been undertaken for N_2 in the past decades and a wealth of swarm data is available. In this work N_2 is a typical example of what we call "simple" gases. Our evaluation of the measured avalanche current waveforms in N_2 demonstrates how to derive swarm parameters for "simple" gases. The swarm parameters determined include the electron drift velocity v_e, the ionization coefficient α and the electron (longitudinal) diffusion coefficient D.

The N_2 used in the present work was supplied by Hoekloos (Holland) and has an analyzed volume composition of nitrogen: ≥ 99.999 %, oxygen: <5 ppm, water: <5 ppm, argon: <1 ppm.

Swarm parameters have been studied in the pressure range of 1~750 Torr (20^0C) in order to verify the validity of scaling laws. The E/p_{20} range covered is 11~444 V/cmTorr (E is the electric field and p_{20} is the gas pressure reduced to 20^0C). The results are presented and compared with other investigations in section 5.3.3.

5.3.2 Determination of swarm parameters in N_2

For avalanche current waveforms in N_2 the ion component of the current is negligibly small. The measured waveform then equals the electron current waveform. Typical waveforms in N_2 at high pressure are given in Fig. 5.3.1. Later (in section 5.4.1 for SF_6) we shall discuss the evaluation of waveforms in which the ion contribution cannot be neglected.

Nitrogen is a non-attaching gas. This can be concluded from the observations that the measured electron current waveform never has a negative exponent, and that the ion component is very small in comparison with the electron component. Consequently, no delaying processes can occur in N_2. This corresponds to a steep fall of the electron current waveform at the electron transit time T_e; all electrons reach the anode at the same time. Therefore, next to drift and diffusion, only ionization is involved in the avalanche growth.
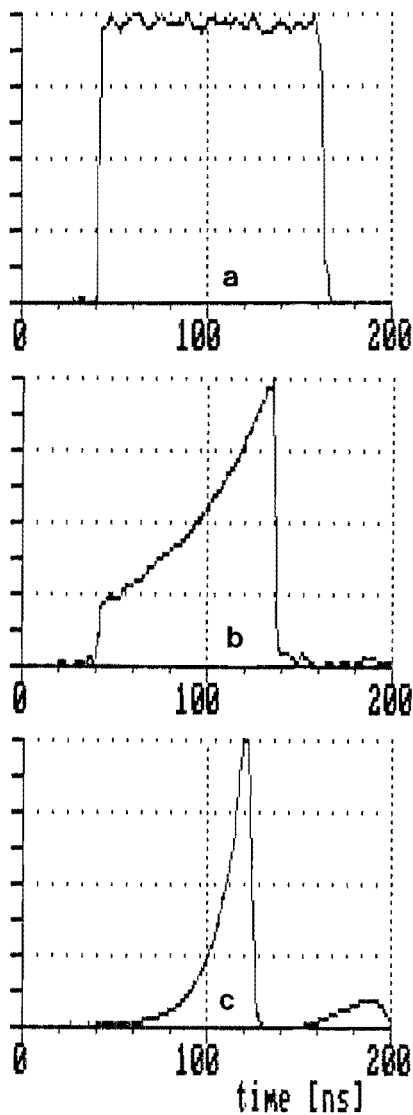
Figure 5.3.1

The electron component of the measured avalanche current waveforms in N_2 at high pressure. Here p_{20}=750 Torr, d=1.0 cm, E/p_{20} (V/cmTorr): (a) 25.3, (b) 33.3, (c) 40.0. The unit at the vertical axis (μA) is: (a) 3.4, (b) 5.5, (d) 72.9.

The waveform in Fig. 5.3.1a corresponds to the situation of a constant number of electrons crossing the gap without ionization. The increase of the current in Figs. 5.3.1b and 5.3.1c is caused by ionization. The second pulse in Fig. 5.3.1c is caused by secondary emission due to photons. Secondary emission due to positive ions reaching the cathode, occurs at a much later stage because of the low ion drift velocity. It is seen that the secondary emission can be clearly distinguished, and therefore separated, from the primary current pulse.

For the evaluation of the waveforms shown in Fig. 5.3.1, the two-parameter model described in chapter 3, section 3.2 is applicable. The attachment coefficient η in this model is considered zero for N_2. The determination of swarm parameters from these waveforms is straightforward. The duration of the (primary) current pulse gives the electron transit time T_e, from which the electron drift velocity $v_e=d/T_e$ is determined. The high time-resolution ensures an accurate determination of the electron drift velocity v_e, which is important for the determination of the other swarm parameters.

The ionization coefficient α can be determined by the ratio: $i_e(T_e)/i_o=\exp(\alpha d)$ (see Verhaart, 1982), where $i_e(T_e)$ is the electron current at T_e, and i_o is the initial current. A more accurate determination of α is obtained from a linear fit to the slope of the logarithmic plot of the electron current, which yields the ionization frequency $R_i=\alpha v_e$.

Because the electron diffusion coefficient is inversely proportional to gas pressure, diffusion is only observed at low pressure. Figure 5.3.2 shows a typical electron component of the measured avalanche current waveform in N_2 at low pressure. Due to electron diffusion, the swarm is spread out (see the simulated electron distributions in chapter 3, Fig. 3.4.1). This results in a spread in the arrival time of the electrons at the anode, which causes a gradual fall of the current.

In this case a direct determination of the electron transit time T_e (and hence the electron drift velocity v_e) is not possible. For that purpose, an equal charge method (Aschwanden, 1985) is employed. This method is based on the two-parameter model and therefore only

applicable to "simple" gases (no detachment or conversion).
Figure 5.3.3 illustrates the method.
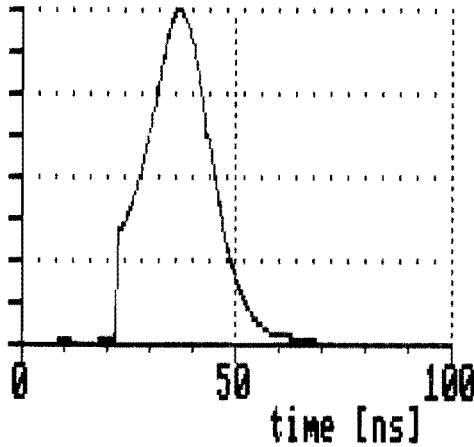
Figure 5.3.2

Electron component of the measured avalanche current waveform
in N_2 at low pressure. Here $p_{20}=1$ Torr, $d=1.0$ cm, $E/p_{20}=181.7$
V/cmTorr. The unit at the vertical axis is 18.5 μA.

This method assumes an "equivalent" electron current waveform
without diffusion but with the same exponential rise and the same
charge as the measured one. The charge of the "equivalent" waveform
is given by:

$$Q_{ec} = \int_0^{T_e} i_o \exp(R_i t)dt = \frac{i_o}{R_i} [\exp(R_i T_e)-1] \qquad \text{for } R_i \neq 0 \quad (5.3.1a)$$

$$= i_o T_e \qquad \text{for } R_i = 0 \quad (5.3.1b)$$

where

$$i_o = \frac{en_o}{T_e} \qquad (5.3.2)$$

$$R_i = \alpha v_e \qquad (5.3.3)$$

$i_e(t)$

"Equivalent"

S_1

$S_1 = S_2$

i_0

"Measured"

S_2

0

T_e

t

The interval for determining R_i and i_0
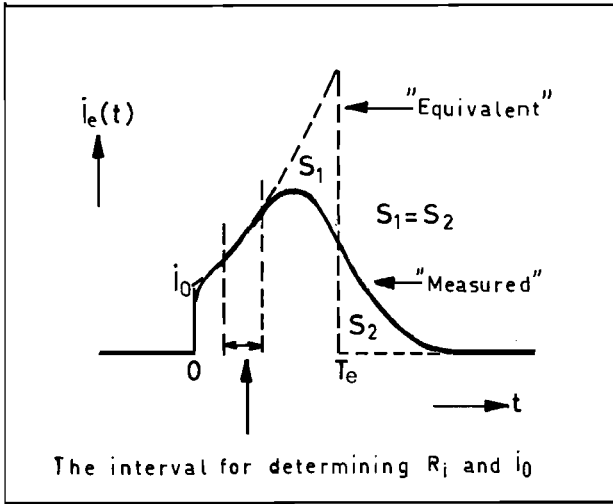
Figure 5.3.3

"Measured" electron current waveform with diffusion
(low pressure), and the "equivalent waveform used to
determine the electron transit time T_e.

The charge of the measured current is obtained from the
integration of the measured electron current:

$$Q_{em} = \int_0^\infty i_{em}(t)dt \qquad\qquad (5.3.4)$$

Note that in practice the upper limit in this integration should be
such that the electron current has completely dropped to zero. This
value is about $2T_e$. We now require that $Q_{ec} = Q_{em}$. As a result we find:

$$T_e = \frac{1}{R_i}\ln(\frac{Q_{em}R_i}{i_o} + 1) \qquad\text{for } R_i \neq 0 \qquad (5.3.5a)$$

$$= \frac{Q_{em}}{i_o} \qquad\qquad\text{for } R_i = 0 \qquad (5.3.5b)$$

83

The ionization frequency R_i and the initial current i_o are found from the slope of the logarithmic plot of the measured electron current:

$$\ln[i_{em}(t)] = \ln(i_o) + R_i t \qquad (5.3.6)$$

An accurate determination of R_i requires a time interval in which both the finite risetime of the setup, and the electron diffusion, have a negligible influence (see Fig. 5.3.3).

With the present evaluation we simultaneously obtain the ionization coefficient from:

$$\alpha = \frac{R_i}{v_e} = \frac{R_i T_e}{d} = \frac{1}{d}\ln(\frac{Q_{em}R_i}{i_o} + 1) \qquad (5.3.7)$$

For the determination of the electron (longitudinal) diffusion coefficient D, the model described in chapter 3, section 3.4 is employed. With v_e, R_i, i_o and α derived as described above, the coefficient D can be determined by fitting the calculated current (Eqs. (3.4.6) and (3.4.10)) to the measured one. An example of such a curve fitting is shown in Fig. 5.3.4.

The above described approach for the determination of swarm parameters from the measured electron current waveforms in N_2 is actually a general one and applicable to any "simple" gas. In the general case, however, the ionization coefficient α and the ionization frequency R_i should be replaced by the effective ionization coefficient $\overline{\alpha} = \alpha - \eta$ and the effective ionization frequency $\overline{R}_i = R_i - R_a$. Here η and R_a are the attachment coefficient and attachment frequency.
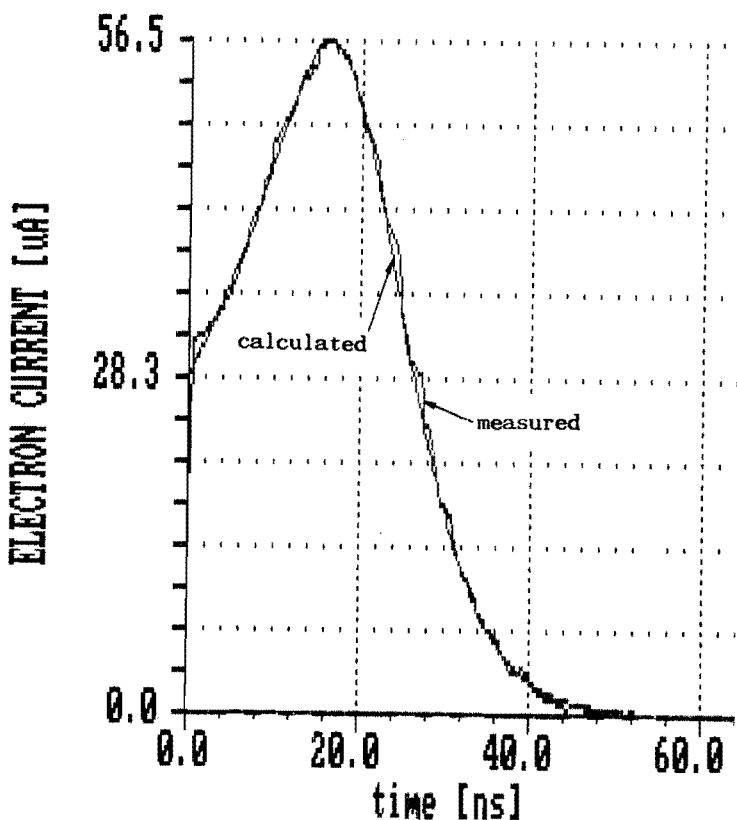
Figure 5.3.4

Measured and calculated electron current waveforms with diffusion in N_2. Here $p_{20}=1$ Torr, $d=1.0$ cm, $E/p_{20}=142.6$ V/cmTorr. The parameters obtained from the curve fit are: $\alpha=1.20$ cm^{-1}, $T_e=24.2$ ns, $i_o=28.5$ μA and $D=1.55$x10^6 cm^2/s.

5.3.3 Swarm parameters in N_2: experimental results

Swarm parameters such as the electron drift velocity v_e, the ionization coefficient α and the electron (longitudinal) diffusion coefficient D for N_2 have been determined. For the electron drift velocity and the ionization coefficient, the pressure p_{20} was varied from 1~750 Torr to cover as wide an E/p_{20} range as possible. Within

the experimental accuracy of ±2% no abnormal pressure dependence has been observed. The electron longitudinal diffusion coefficient has been derived from measurements at 1 Torr. All results are shown in Figs. 5.3.5, 5.3.6 and 5.3.7.

The ratio of the electron (longitudinal) diffusion coefficient D over the electron drift mobility K_e, which is defined as $K_e = v_e/E$, is shown in Fig. 5.3.8.

For comparison, also the results of Verhaart (1982, time-resolved swarm measurement), Aschwanden (1985, time-resolved swarm measurement), Wedding and co-workers (1985, time-of-flight measurement) and Ohmori and co-workers (1988, Boltzmann equation analysis) are shown. It can be seen that the present results are in good agreement with those of these investigators for the E/p_{20} ranges they have covered.
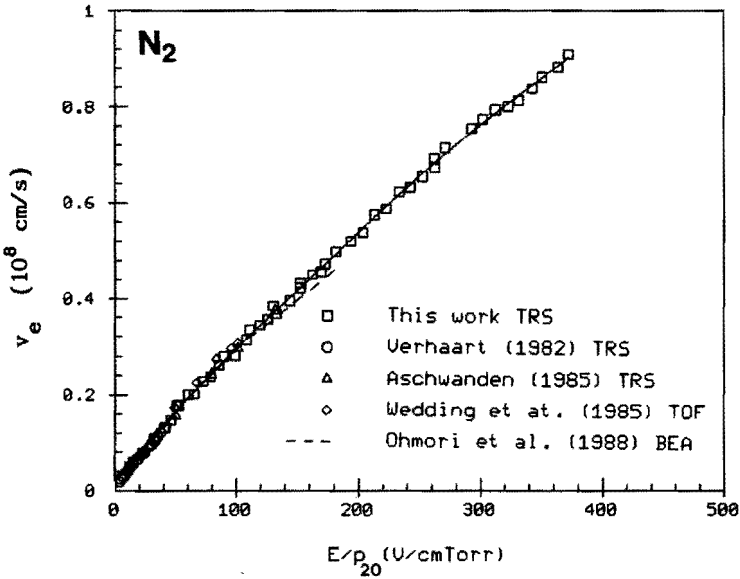
Figure 5.3.5

The electron drift velocity v_e in N_2.
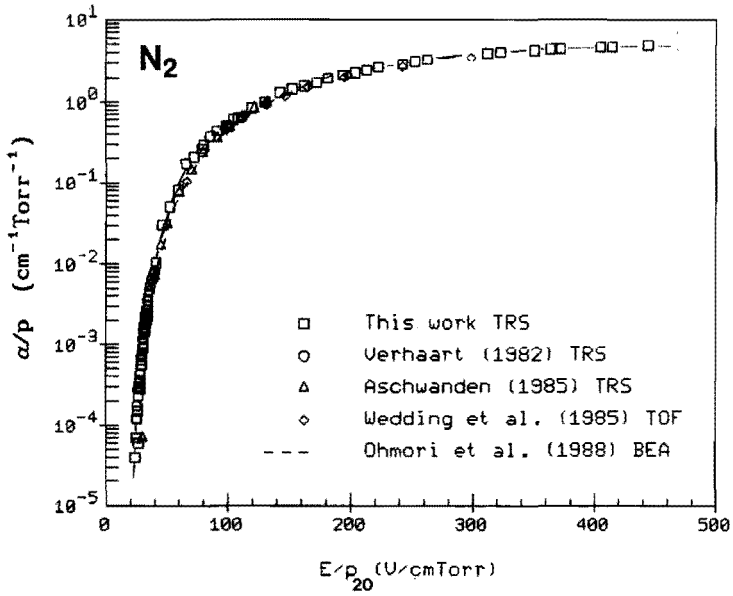
Figure 5.3.6

The pressure-reduced ionization coefficient α/p_{20} in N_2.
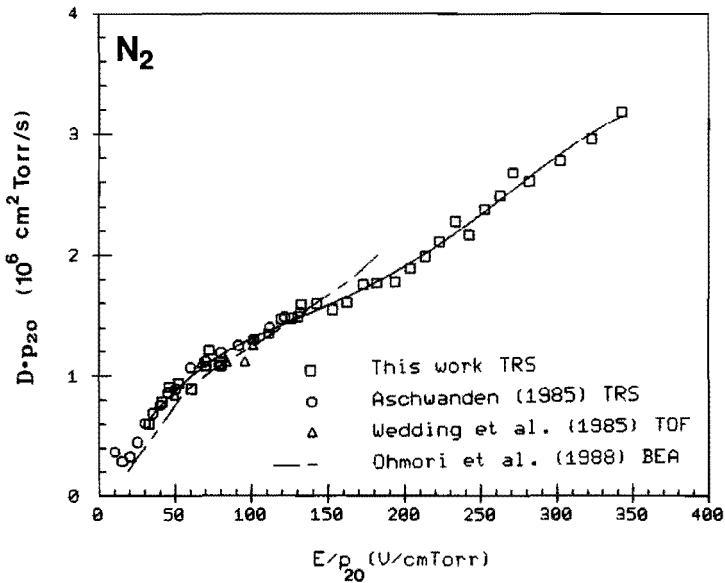
Figure 5.3.7

The electron (longitudinal) diffusion coefficient $D \cdot p_{20}$ in N_2.
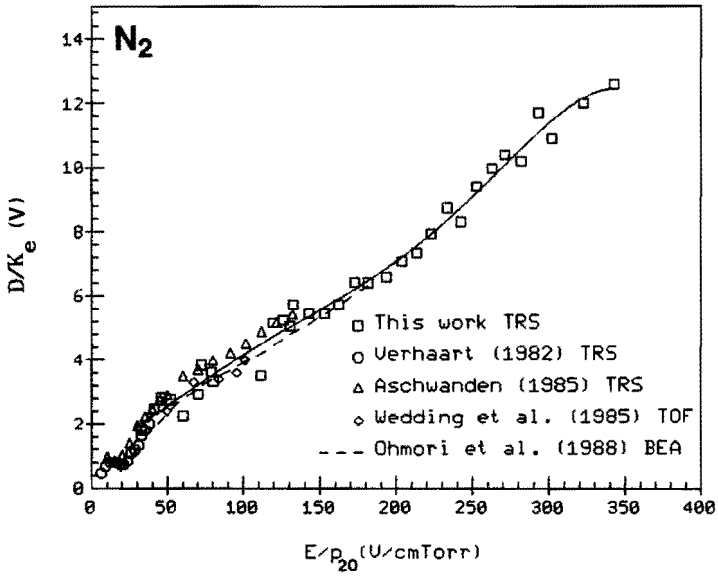
Figure 5.3.8

D/K_e versus E/p_{20} in N_2.

5.4 Sulfur hexafluoride

5.4.1 Introduction

Sulfur hexafluoride (SF_6) has been utilized as an insulating gas in power systems for quite some years because of its high dielectric strength. Extensive studies, both experimental and theoretical, have been carried out to quantify and predict the dielectric behavior of this gas or its mixtures with other gases.

In the present work, we report on fast swarm experiments in SF_6 over a pressure range of 1~49 Torr ($20^{o}C$) and an E/p_{20} range of 110~292 V/cmTorr. The SF_6 used in the present work was supplied by Hoekloos (Holland) and has an analyzed volume composition of SF_6: $\geq 99.8\%$, air: <500 ppm, CF_4: <500 ppm, H_2O: <15 ppm, HF: <1 ppm.

The fast swarm measurements in SF_6, first of all, show a relatively large ion contribution to the current. This indicates that considerable attachment takes place, and that detachment may be important. The measurements do not provide clear evidence of delaying processes in SF_6 because no clear "tail" shows up in the electron current waveform (see Fig. 5.4.3). However, at relatively high pressure where electron diffusion is negligible, the fall of the electron current waveform at the electron transit time T_e is not as steep as that in N_2 (a gas in which no delaying processes occur). This indicates that detachment is significant because almost all electrons are somewhat delayed by trapping (consecutive attachment and detachment). This detachment process is, however, strongly counteracted by stabilization processes, which results in a fall time that is still short. This can be illustrated by the simulation in Fig. 3.3.51 for a moderate detachment coefficient ($\delta=1.03$ cm^{-1}), and by the simulation shown in Fig. 5.4.1 below for a high detachment coefficient ($\delta=7.21$ cm^{-1}). In both simulations the conversion coefficient is chosen high (19.95 and 22.56 cm^{-1} respectively).

Electron detachment and ion conversion processes in SF_6 have been considered in the literature (see, for instance, Hansen and co-workers, 1983; O'Neill and Craggs, 1973b; Teich, 1981; Teich and Branston, 1974; de Urquijo-Carmona, 1983; de Urquijo-Carmona and co-workers, 1986), but the reported data on these delaying processes show large differences, up to a factor of 100 for the electron

detachment coefficient (Morrow, 1986).
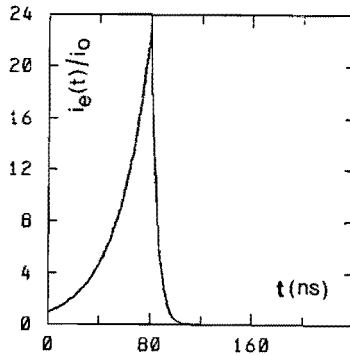
Figure 5.4.1

Electron current waveform calculated with the four-parameter model with a high detachment coefficient (δ=7.21 cm^{-1}) and a high conversion coefficient (β=22.56 cm^{-1}). Here α=9.2 cm^{-1}, η=7.7 cm^{-1} and T_e=80 ns.

Although detachment and conversion processes are likely to occur in SF$_6$, neither the electron drift velocity v_e nor the pressure-reduced effective ionization coefficient $\bar{\alpha}/p$, derived by a two-parameter model for simple gases, possess an abnormal pressure dependence. In conclusion, we may state that detachment does take place in SF$_6$ but is effectively counteracted by conversion (stabilization). We can therefore quite adequately describe the avalanche current waveform in SF$_6$ by the two-parameter model for "simple" gases, and the procedure described for N$_2$ can also be applied to evaluate the electron component of the measured avalanche current waveforms in SF$_6$.

When electron attachment is appreciable and the gas pressure is high, the ion component becomes considerable. Figure 5.4.2 shows an example of a measured avalanche current waveform in SF$_6$ with a considerable ion contribution.

The constant current after the fall (at the electron transit time) is caused by the ionic contribution. From the total current

waveform, the electron component has to be derived for further
evaluation. A procedure to separate the electron and ion
contributions has been developed by Aschwanden (1985) and is briefly
described below.

time [ns]
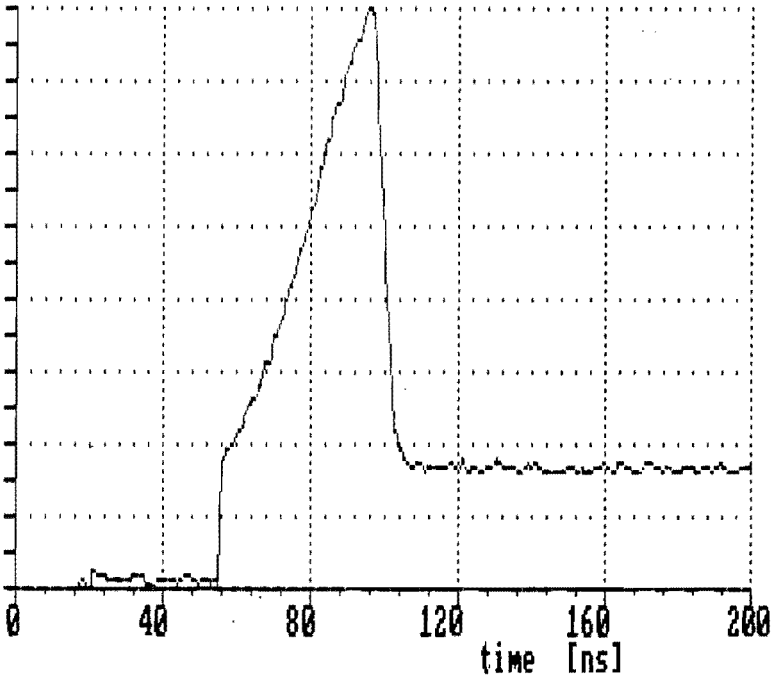
Figure 5.4.2

Measured avalanche current waveform in SF_6 showing a
considerable ion contribution. Here p_{20}=49.2 Torr,
E/p_{20}=121.50 V/cmTorr. The unit at the vertical axis is
4.9 μA. The separated electron and ion components of this
waveform are shown in Fig. 5.4.3.

We consider an avalanche in which only ionization and attachment
processes occur. The total current $i_t(t)$ is composed of an electron
component $i_e(t)$ and two ion components (the positive ion component
$i_p(t)$ and the negative ion component $i_n(t)$):

$$i_t(t) = i_e(t) + i_p(t) + i_n(t) \qquad (5.4.1)$$

91

From the expressions of these currents given in chapter 3 (Eqs. (3.2.16), (3.2.17), (3.2.18), (3.2.22) and (3.2.23)), the following relation is obtained for $t \leq T_e$:

$$i_t(t) = i_e(t) + C\int_0^t i_e(\tau)d\tau \qquad (5.4.2)$$

where

$$C = \alpha v_p + \eta v_n \qquad (5.4.3)$$

Differentiation of Eq. (5.4.2) gives:

$$\frac{di_t(t)}{dt} = \frac{di_e(t)}{dt} + Ci_e(t) \qquad (5.4.4)$$

Since the current is measured in digital form, it is convenient to write Eq. (5.4.4) as:

$$\frac{i_t(t_k) - i_t(t_{k-1})}{\Delta t} = \frac{i_e(t_k) - i_e(t_{k-1})}{\Delta t} + Ci_e(t_k) \qquad (5.4.5)$$

where $\Delta t = t_k - t_{k-1}$ and $k=1, 2, \cdots\cdots$. From Eq. (5.4.5), $i_e(t_k)$ can be written as:

$$i_e(t_k) = \frac{i_t(t_k) - i_t(t_{k-1}) + i_e(t_{k-1})}{1 + C\Delta t} \qquad (5.4.6)$$

Equation (5.4.6) shows how the electron component $i_e(t_k)$ can be calculated from its previous value $i_e(t_{k-1})$ if the constant C is known. This constant C is obtained by an iterative procedure, in which C is varied until the calculated $i_e(t)$ from Eq. (5.4.6) satisfies the following conditions:

$$i_e(0) = i_t(0) \qquad (5.4.7)$$

$$i_e(T_e) = i_t(T_e) - i_i(t>T_e) \qquad (5.4.8)$$

92

Figure 5.4.3 shows an example of such a separation.
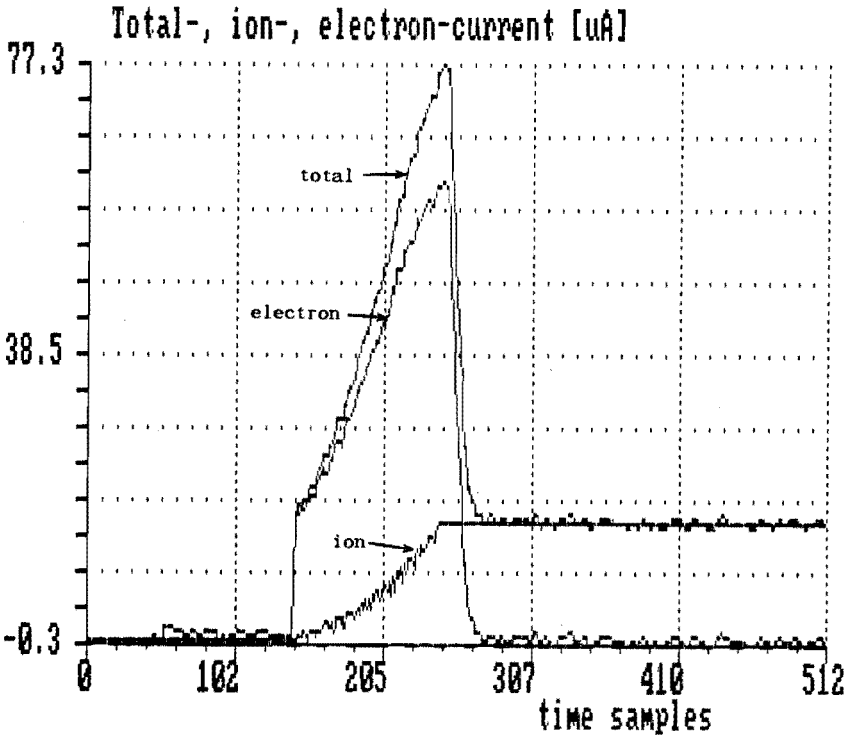
Figure 5.4.3

The measured avalanche current waveform shown in Fig. 5.4.2,
and the electron and ion components derived according to the
separation procedure.

5.4.2 Swarm parameters in SF_6; experimental results

Figure 5.4.4 shows some typical electron component of the
avalanche current waveforms measured in SF_6 at low pressure. The
steep rise of these waveforms demonstrates the time resolution of the
present setup. The slow fall of the waveforms is caused by electron
diffusion. Note the sharp peak observed at the beginning of the
current waveform (see Figs. 5.4.4a and 5.4.4b). This peak may be
explained by excessive attachment in the non-equilibrium region near
the cathode, where the final velocity distribution has not yet been

established (see also chapter 2, section 2.4).
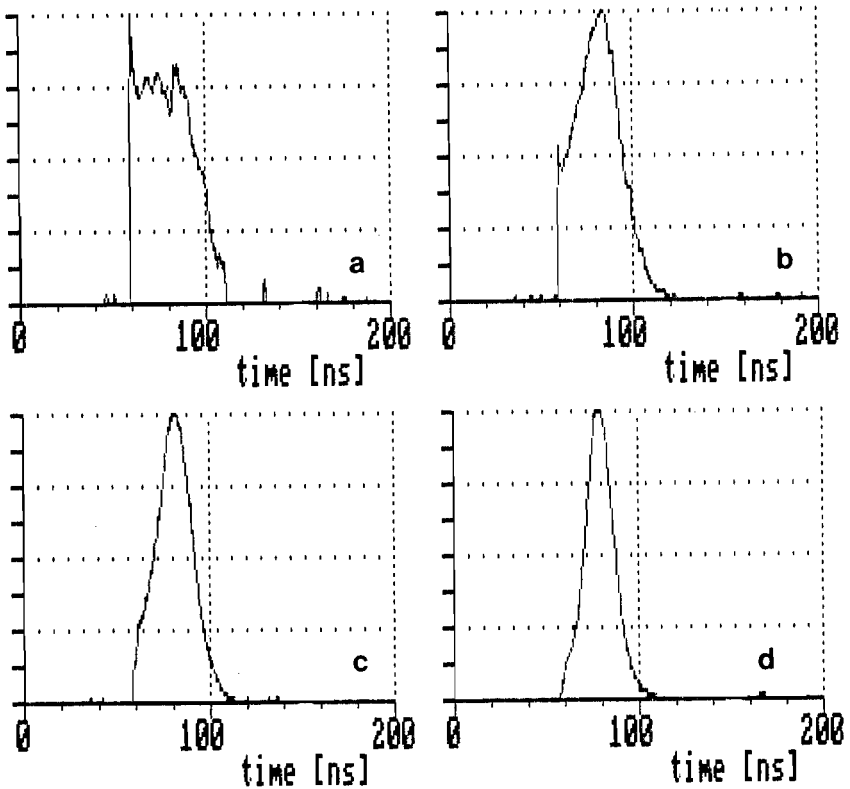
Figure 5.4.4

Examples of the electron component of the avalanche current
waveform measured in SF_6 at low pressure. Here $p_{20}=1$ Torr,
d=1.0 cm, E/p_{20} (V/cmTorr): (a) 118.81, (b) 175.89,
(c) 211.43, (d) 261.27. The unit at the vertical axis (μA) is:
(a) 0.769, (b) 4.24, (c) 13.2, (d) 49.4.

Figure 5.4.5 shows some typical avalanche current waveforms
measured in SF_6 at higher pressure. The fall time after one electron
transit time is relatively short, but too long to be explained by
diffusion. This shows that detachment occurs but is strongly
counteracted by conversion processes. As a result the description of

94

SF$_6$ in terms of a two-parameter model is justified. The constant current after the fall of the current is caused by ions. Since the ion component is considerable here, a separation of the ion component from the total current is essential for the evaluation of the electron component.
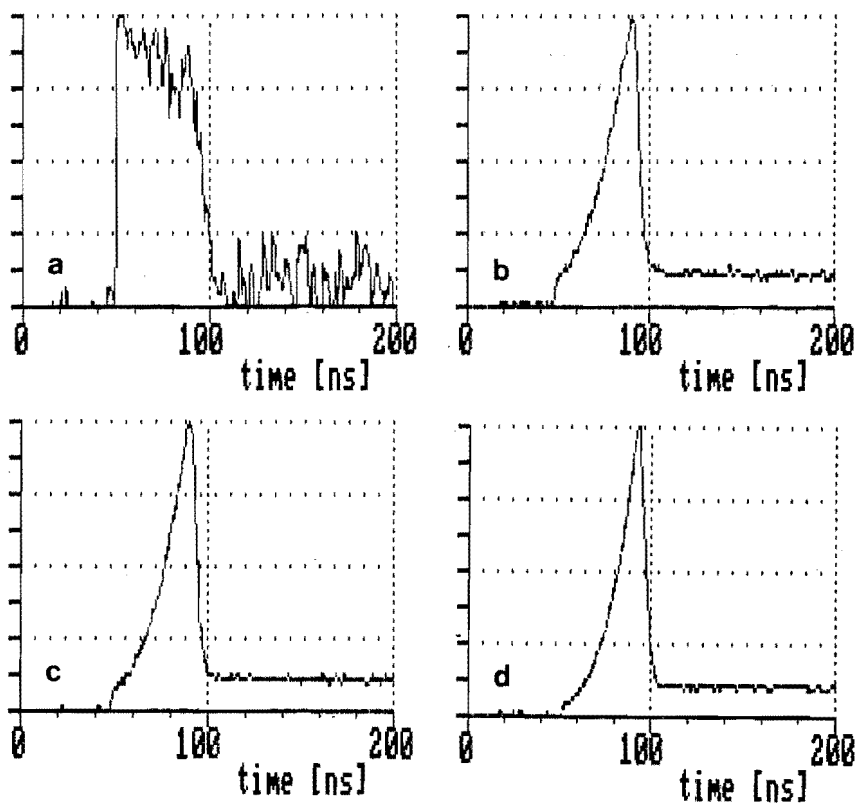
Figure 5.4.5

Typical avalanche current waveforms measured in SF$_6$ at higher pressure. Here p_{20}=30 Torr, d=1.0 cm, E/p_{20} (V/cmTorr): (a) 117.43, (b) 121.47, (c) 122.49, (d) 123.50. The unit at the vertical axis (μA) is: (a) 0.573, (b) 6.74, (c) 9.36, (d) 19.2.

Figures 5.4.6 and 5.4.7 show the electron drift velocity v_e and the pressure-reduced effective ionization coefficient $\overline{\alpha}/p_{20}$. For

comparison, also the results of Verhaart (1982, time-resolved swarm measurement), Aschwanden (1985, time-resolved swarm measurement), Satoh and co-workers (1988, Monte Carlo simulation) and Morrow (1986, best fit to 13 sources up to 1986) are shown in these figures.

The electron drift velocity derived here is about 12% higher than that derived by Aschwanden for $E/p_{20} > 120$ V/cmTorr, but is in excellent agreement with the results of Satoh and co-workers. The present results are also consistent with those of Verhaart, who however covered a smaller E/p_{20} range.

The pressure-reduced effective ionization coefficient $\bar{\alpha}/p_{20}$ is in good agreement with that derived by other investigators for the E/p_{20} range covered. The limiting $(E/p_{20})_{lim}$ value, at which $\bar{\alpha}(E/p_{20})=0$, is 119.6 V/cmTorr, which is consistent with Verhaart (1982, 118 V/cmTorr), Aschwanden (1985, 119.1 V/cmTorr), and Satoh and co-workers (1988, 118.8 V/cmTorr).

It should be noted that, in spite of the presence of detachment and conversion processes, an evaluation based on the two-parameter model does not introduce an abnormal pressure dependence in v_e or $\bar{\alpha}/p$. This can be explained with the help of Fig. 3.3.5. If detachment occurs, but is strongly counteracted by conversion, the measured drift velocity equals the real drift velocity and the measured $\bar{\alpha}$ approaches the real one. Furthermore, even if the measured (apparent) $\bar{\alpha}$ and the real one are different, the measured $\bar{\alpha}$ does not show an abnormal pressure dependence if the detachment process and the conversion process have the same pressure dependence, for example if both processes are two-body collisions.
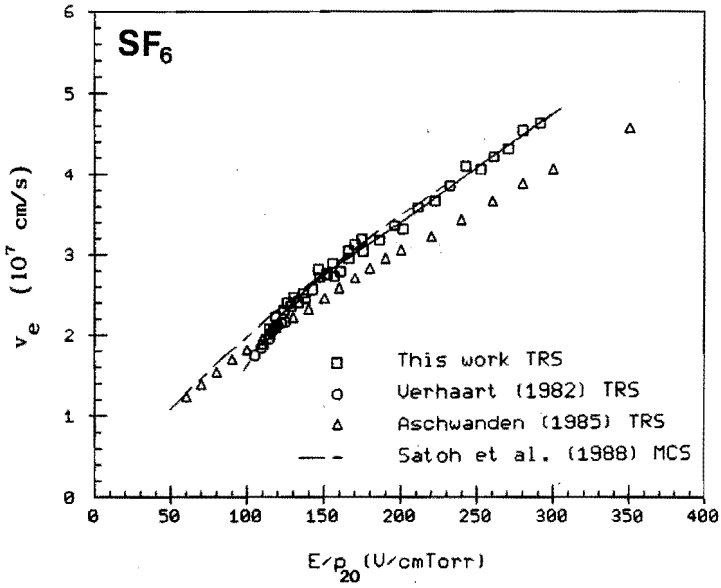
Figure 5.4.6

The electron drift velocity v_e in SF_6.
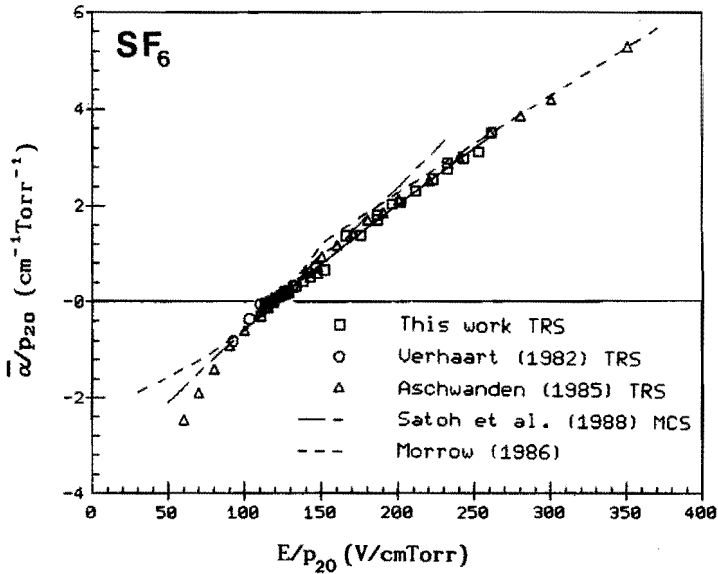
Figure 5.4.7

The pressure-reduced effective ionization

coefficient $\bar{\alpha}/p_{20}$ in SF_6.

5.5 Dry air

5.5.1 Introduction

Fast swarm experiments in dry air have been performed in an E/p_{20} range from 10 to 45 V/cmTorr. The pressure p_{20} was varied from 200 to 750 Torr in order to study the possible pressure dependences of individual processes. The electron component of the measured avalanche current waveform shows a very clear "tail" after one electron transit time. This clearly indicates the presence of electron detachment processes. Therefore the four-parameter model described in chapter 3, section 3.3 is employed for the evaluation of the measured avalanche current waveform in this gas. The ion component in dry air is very small in comparison with the electron component and is therefore neglected in the evaluation.

The results described in section 5.5.2 have been presented as a conference contribution at the XIX Int. Conf. on Phenomena in Ionized Gases, Belgrade, Yogoslavia (10-14 July, 1989).

5.5.2 Determination of swarm parameters in dry air with a fast time-resolved swarm technique

DETERMINATION OF SWARM PARAMETERS IN DRY AIR WITH A FAST TIME-RESOLVED SWARM TECHNIQUE

C. Wen and J.M. Wetzer

High-Voltage Group, Eindhoven University of Technology, Eindhoven, The Netherlands

INTRODUCTION

Air continues to be the subject of investigation because it serves as an insulating medium for open air substations and overhead transmission lines. Recent photodetachment swarm studies in air, O_2 and O_2/N_2 mixtures [1-4] show clearly the need to re-examine the literature on swarm data, especially on electron detachment and ion conversion coefficients, because of the poor agreement among the various literature data and the unsuccessful simulation of measured discharge currents based on such data.

As far as the time-resolved swarm study is concerned, the major difficulties encountered in accurately determining swarm parameters in air were the insufficient time-resolution of the measuring system and the inadequacy of the model used for the evaluation of the measured avalanche current waveform.

In this paper we report on fast time-resolved swarm measurements (time resolution in the order of 1 ns) performed in dry air in the pressure range from 200 to 750 Torr and the E/p (electric field over gas pressure) range from 10 to 45 V/cmTorr. Swarm parameters have been determined from the measured avalanche current waveforms in terms of a model which accounts not only for ionization and attachment but also for detachment and conversion.

EXPERIMENTAL TECHNIQUES

The time-resolved swarm method is used for the avalanche current measurement. The experimental setup is basically the same as the one described in [5] and has been used previously for other studies [6-10]. The avalanche is initiated with a TEA N_2 laser pulse of very short duration (0.6 ns, FWHM), the avalanche current waveform is recorded by a fast 9 bit Tektronix 7912 AD digitizer (with 7A29 and 7B10 plug-in units). The time resolution of the whole measuring system is about 1.4 ns. The vessel is evacuated with a turbomolecular pump down to 10^{-7} Torr before the dry air was admitted in. The dry air, supplied by Hoekloos (Holland), has an analyzed volume composition of nitrogen: 0.78, oxygen: 0.21, argon: 0.0096, carbon dioxide: $<400 \times 10^{-6}$, water: $<25 \times 10^{-6}$, hydrocarbon: $<5 \times 10^{-6}$. The gas pressure was measured by two Pennwalt pressure gauges (ranges from 0 ~ 450 and 400 ~ 800 Torr, respectively). All pressure measurements were carried out at room temperature (around 22°C) and

reduced to 20°C.

RESULTS AND DISCUSSION

Figure 1 shows a typical electron component of the avalanche current waveform measured in dry air with the present setup. The long tail after one electron transit time T_e clearly indicates the occurence of electron detachment. Also shown in Fig.1 is the calculated waveform (smooth curve) using a model described earlier in [6,10]. This model accounts for detachment and conversion as well as ionization and attachment.

From the present observation and the literature studies [1-4,11], the following processes are believed to be dominant in dry air for the pressure and the E/p ranges covered:

ionization α: $\quad e + N_2(O_2) \longrightarrow 2e + N_2^+(O_2^+)$ (1)

attachment η: $\quad e + O_2 \longrightarrow O^{-*} + O$ (2)

detachment δ: $\quad O^{-*} + O_2(N_2) \longrightarrow O + O_2(N_2) + e$ (3)

conversion β: $\quad O^{-*} + O_2 \longrightarrow O_2^- + O \quad$ (2-body) (4)

$\quad O^{-*} + 2O_2 \longrightarrow O_3^- + O_2 \quad$ (3-body) (5)
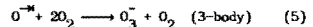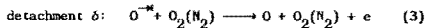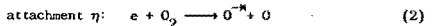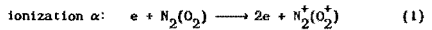
where O^{-*} denotes an unstable negative oxygen ion which can undergo either detachment (Eq.(3)) or conversion (Eqs.(4) and (5)).

In the above reaction scheme, coefficients α and η are defined as usual, while coefficients δ and β are defined as the mean number of detachment and conversion events per unstable negative ion (O^{-*}) in a *time that an electron travels 1 cm in the field direction*.

By fitting the calculated and the measured electron component of the avalanche current waveforms as is shown in Fig.1, swarm parameters such as the electron drift velocity v_e, the "real" effective ionization coefficient $\alpha-\eta$, and the detachment and conversion coefficients in the combinations $\delta+\beta$ and $\eta\delta$ can be determined. These results are shown in Figs.2 to 5 respectively.

Although the coefficients α, η, δ and β cannot be determined separately from the electron component only [6,10], the derived combinations of these parameters as shown in Figs.3 to 5 fully describe the electron current. In Fig.3 $(\alpha-\eta)/p$ shows no pressure dependence over the whole range of E/p covered, implying that both α/p and η/p are pressure

99

independent. This is consistent with reactions (1) and
(2). Similarly the lack of a pressure dependence in
$\eta\delta/p^2$ in Fig.4 (given some scatter) indicates that δ/p
is independent of pressure over the E/p range covered.
This is consistent with reaction (3). In Fig.5 a clear
pressure dependence is observed for $(\delta+\beta)/p$,
especially if E/p is below 38 V/cmTorr. As δ/p is
independent of pressure, this indicates a three-body
conversion process as described by reaction (5). For
lower pressure the pressure dependence becomes less
pronounced, because the two-body conversion process
(reaction (4)) becomes more likely (see also [11]).

ACKNOWLEDGMENT

REFERENCES

[1] Brennan, M.J., and Teich, T.H., 1988,
    Proc. GD88, Venezia, 343-346.
[2] Gallimberti, I., Poli, E., Stangherlin, S., and
    Teich, T.H., 1988,
    Proc. GD88, Venezia, 351-354.
[3] Teich, T.H., and Morris, E.C.A., 1988,
    Proc. XVIII ICPIG, Swansea, 50-51.
[4] Teich, T.H., and Morris, E.C.A., 1987,
    In L.G. Christophorou and Bouldin, D.W. (Eds.),
    Gaseous Dielectrics V, Pergamon Press, 18-26.
[5] Verhaart, H.F.A., and van der Laan, P.C.T., 1982,
    J. Appl. Phys. Vol.53, 1430-1436.
[6] Wetzer, J.M., and Wen, C., 1987,
    Proc. 5th ISH, Braunschweig, paper 15.06.
[7] Wen, C., and Wetzer, J.M., 1988,
    Proc. IEEE Int. Symp. on Elec. Insul., Boston,
    108-111.
[8] Wen, C., and Wetzer, J.M., 1988,
    Proc. GD88, Venezia, 367-370.
[9] Wen, C., and Wetzer, J.M., 1989,
    IEEE Trans. Elec. Insul. (in press).
[10] Wen, C., and Wetzer, J.M., 1988,
    IEEE Trans. Elec. Insul., Vol.23, No.6, 999-1008.
[11] Badaloni, S., and Gallimberti, I., 1972,
    Report UPee-72/05, Universita' di Padova.
[12] Ducos, M., Segur, P., and Yousfi, M., 1982,
    Proc. GD82, London, 335-338.
[13] Sheldrake, R., 1977,
    Ph. D. Thesis, University Manchester.
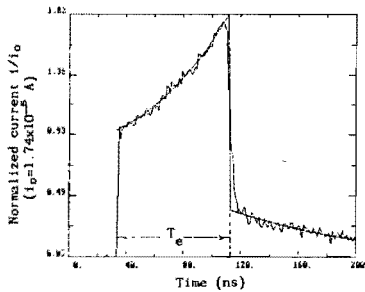
Fig.1 Measured and calculated electron component of
the avalanche current waveforms in dry air,
p=200 Torr, E/p=36.31 V/cmTorr, d=1.0 cm.
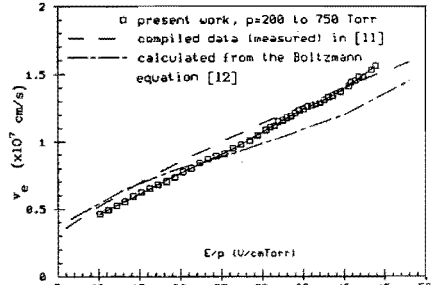
Fig.2 Measured electron drift velocity v_e in dry air.
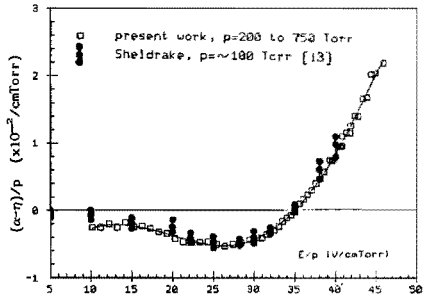
Fig.3 Real effective ionization coefficient in dry air.
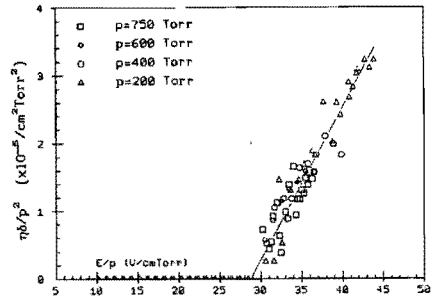
Fig.4 $\eta\delta/p^2$ versus E/p in dry air.
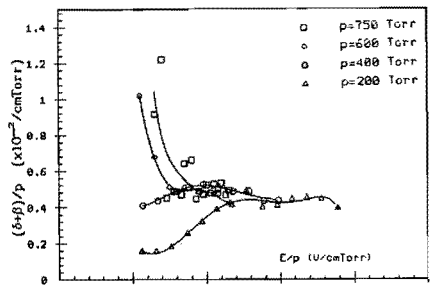
Fig.5 $(\delta+\beta)/p$ versus E/p in dry air.

5.6 Oxygen

5.6.1 Introduction

The avalanche study in oxygen contributes to the understanding of electrical discharges in air or in other gases that contain O_2 molecules. In addition, the understanding of the collisional processes in O_2 is important for the study of ozone production.

Although collisional processes, in particular electron attachment and detachment, in O_2 have been studied by a number of investigators during the past decades (Frommhold, 1963; Gallimberti and co-workers, 1988; O'Neill and Craggs, 1973a; Teich and Morris, 1987a, 1987b; Wagner, 1971), the agreement among the available swarm parameters is still poor, and the basic processes involved in the avalanche growth are not well understood. As far as the time-resolved swarm study is concerned, the previous studies in O_2 suffered the same difficulties as those in air: the time-resolution of the experiments is insufficient and the models used for the evaluation are inadequate.

The present experiments have been performed over a pressure range of 5~750 Torr (20°C) and an E/p_{20} range of 10~120 V/cmTorr. The O_2 used in the present work was supplied by Hoekloos (Holland) and has an analyzed volume composition of O_2: 99.7 %, water: ≤6 ppm and methane: ≤25 ppm.

5.6.2 Fast swarm experiments in O_2

Figure 5.6.1 shows some typical electron current waveforms measured at relatively low pressure. The rise of these waveforms is fast as a result of the high time-resolution of the setup. Note the sharp peak at the beginning of the waveform in Figs. 5.6.1a and 5.6.1b. A similar peak was observed in other attaching gases such as SF_6. An explanation has been given earlier in chapter 2, section 2.4. The slow fall of the waveforms is attributed mainly to the effect of electron diffusion. The effect of delaying processes, such as detachment, on the current waveform can, however, not be excluded.

The fact that the current is not only affected by electron diffusion but also by delaying processes complicates the evaluation. The models described in chapter 3, sections 3.3 and 3.4, neglect either diffusion or delaying processes, whereas no fitting procedure

has been developed yet on the basis of the model presented in section 3.5.
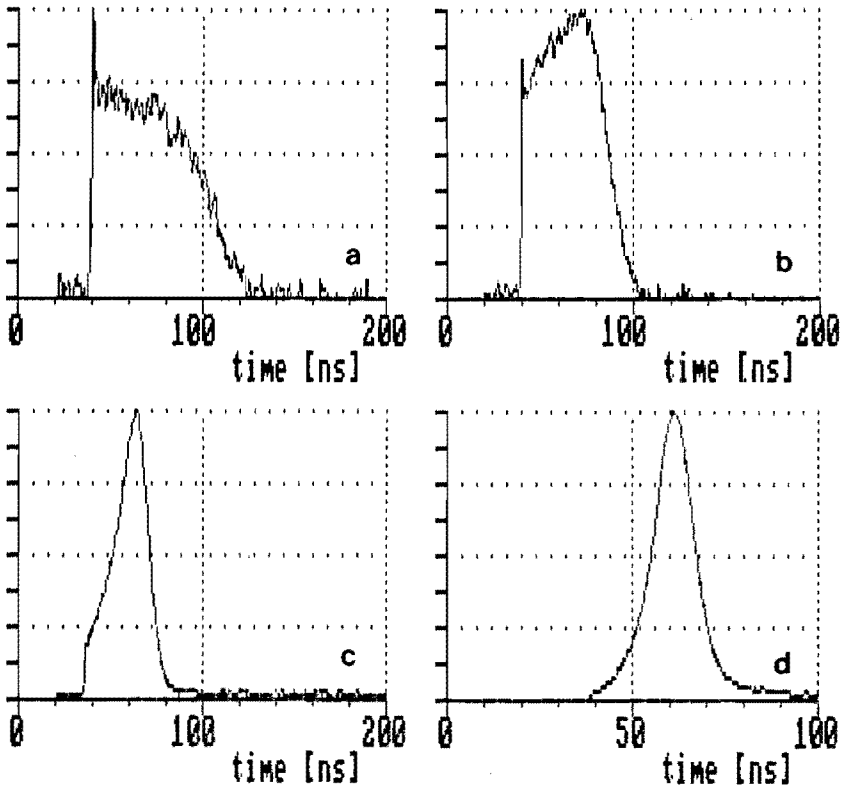
Figure 5.6.1

Typical electron current waveforms measured in O_2 at low pressure. Here p_{20}=5 Torr, d=1.0 cm, E/p_{20} (V/cmTorr): (a) 30.00, (b) 50.00, (c) 80.00, (d) 110.0. The unit at the vertical axis (μA) is: (a) 1.68, (b) 3.31, (c) 11.4, (d) 59.6.

Figure 5.6.2 shows some typical avalanche current waveforms measured in O_2 at relatively high pressure. At such high pressure diffusion does not play a significant role.

102
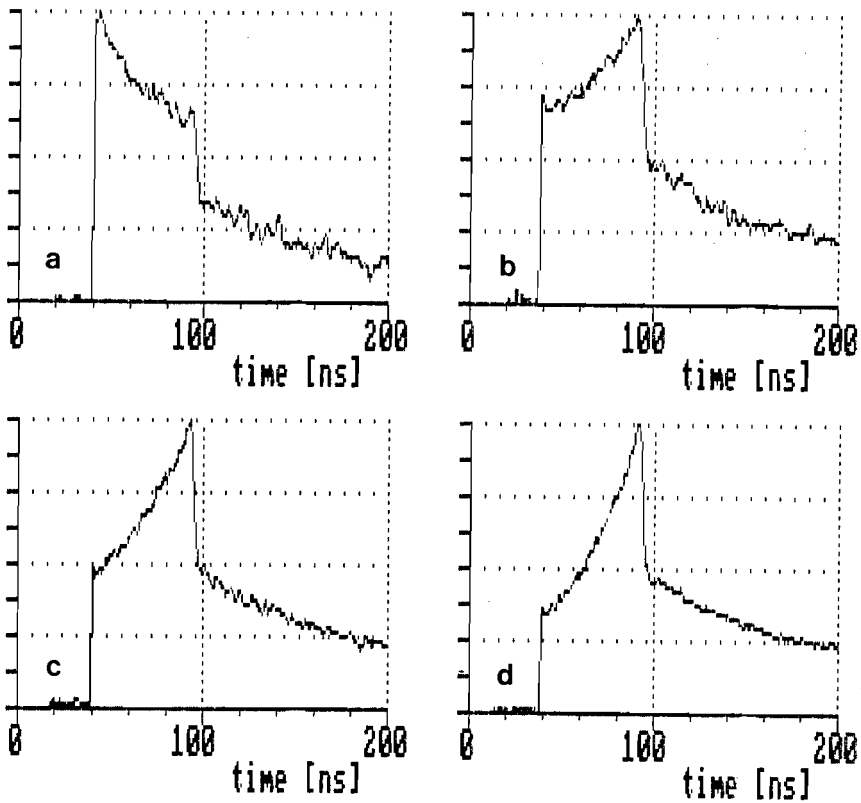
Figure 5.6.2

Typical avalanche current waveforms measured in O_2 at
relatively high pressure. Here p_{2O}=300 Torr, d=1.0 cm,
E/p_{2O} (V/cmTorr): (a) 37.00, (b) 37.50, (c) 37.75,
(d) 38.00. The unit at the vertical axis (μA) is: (a) 2.16,
(b) 2.80, (c) 4.07, (d) 6.90.

The steep drop of the current waveforms indicates that a number
of electrons reaches the anode without having been attached. The
interval between the steep rise and fall gives the electron transit
time T_e. The long "tail" after T_e clearly shows that electron
detachment does take place. As has been discussed in section 5.5 for
dry air, the possible reactions in O_2 under the present conditions

103

are the following:

ionization: $\quad$ e + O_2 $\longrightarrow$ 2e + O_2^+ $\qquad\qquad$ (5.6.1)

attachment: $\quad$ e + O_2 $\longrightarrow$ O^{-*} + O $\qquad\qquad$ (5.6.2)

detachment: $\quad$ O^{-*} + O_2 $\longrightarrow$ 0 + O_2 + e $\qquad\qquad$ (5.6.3)

conversion: $\quad$ O^{-*} + O_2 $\longrightarrow$ O_2^- + O $\quad$ (2-body) $\qquad$ (5.6.4)

$\qquad\qquad\qquad$ O^{-*} + $2O_2$ $\longrightarrow$ O_3^- + O_2 $\quad$ (3-body) $\qquad$ (5.6.5)
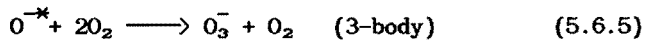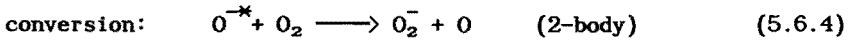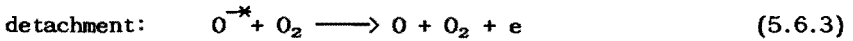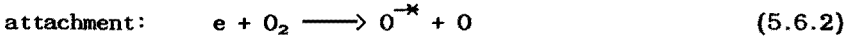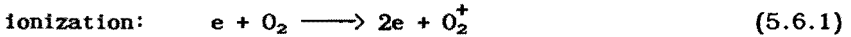
Here O^{-*} denotes an unstable negative ion which can undergo either detachment or conversion.

For pure O_2 at high pressure, also electron attachment and detachment of the negative ion O_2^{-*} are possible processes (Frommhold, 1963; O'Neill and Craggs, 1973a):

attachment: $\quad$ e + O_2 $\longrightarrow$ O_2^{-*} $\qquad\qquad$ (5.6.6)

detachment: $\quad$ O_2^{-*} + O_2 $\longrightarrow$ $2O_2$ + e $\qquad\qquad$ (5.6.7)
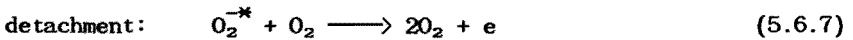
The evaluation of the current waveforms shown in Fig. 5.6.2 with the four-parameter model is impeded by the presence of a large ionic contribution, which calls for a separation of electron and ion components. This separation technique has not yet been developed for "complex" (four-parameter) gases.

In the case of dry air, the ion component is negligible in comparison with the electron component. The ion contribution in O_2 is much larger than that in dry air. In dry air less negative oxygen ions are formed (about one-fifth of the amount formed in O_2), and detachment is more pronounced because of the reaction:

O^{-*} + N_2 $\longrightarrow$ 0 + N_2 + e .
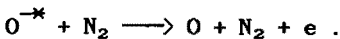
5.7 Hexafluoropropene

5.7.1 A review of the literature study on 1-C_3F_6

There has been a growing interest recently in the possibility of using hexafluoropropene 1-C_3F_6 (abbreviated as C_3F_6 in this section) as a new high voltage insulating gas. A number of unusual properties, however, have been observed for this gas, which are summarized below.

I. Positive synergism

Mixtures of C_3F_6 with SF_6, SO_2 or c-C_4F_8 have a higher breakdown strength than that of either of the constituent gases (Biasiutti and co-workers, 1983; Christophorou and co-workers, 1979; Hunter and co-workers, 1982; James and co-workers, 1980; Tagashira and co-workers, 1985; Wootton and co-workers, 1980). For instance, at a total pressure of 1 bar (=750 Torr), a mixture of 75% C_3F_6 and 25% SF_6 gives a dielectric strength about 1.9 times that of SF_6 and 1.7 times that of C_3F_6 (Biasiutti, 1985). This synergetic effect was studied by breakdown voltage measurements, or by swarm experiments, from which the limiting E/p was derived.

From the observations in C_3F_6/SF_6, C_3F_6/SO_2 or C_3F_6/c-C_4F_8 mixtures, and in some other gas mixtures such as SF_6/SO_2 and SF_6/C_3F_8, Hunter and Christophorou (1984, 1985) summarized the requirements for the occurrence of positive synergism:

(1) at least one of the electronegative constituent gases exhibits an abnormal pressure dependence of the electron attachment coefficient (abnormal means other than $\eta=pf(E/p)$);

(2) one component has a high rate coefficient for the stabilization of unstable negative ions of the other component, which reduces the number of collisional detachment processes; and

(3) over the gas pressure range of interest, an unambiguous identification of positive synergism requires that the breakdown strengths of the constituent gases are not too far apart.

II. Deviation from Paschen's law

The breakdown voltage U_B of most insulating gases in uniform electric fields is, in accordance with Paschen's law, only a function of the product of the gas pressure p and the electrode separation d:

$$U_B = f(pd) \qquad\qquad (5.7.1)$$

At large enough values of pd (i.e., in the region well above the Paschen minimum), the breakdown voltage approaches a linear function of pd:

$$U_B = U_o + pd(E/p)_{lim} \qquad\qquad (5.7.2)$$

Here U_0 is a constant voltage and $(E/p)_{lim}$ is the limiting (E/p) value at which breakdown occurs. At very high gas pressure, U_B can vary more than linearly with increasing p for a fixed d because of the compressibility of the gas.

The reduced breakdown field strength E_B/p or $(E/p)_{lim}$ of C_3F_6 increases substantially with increased gas pressure (Aschwanden and Biasiutti, 1981; Biasiutti and co-workers, 1983; Chen and co-workers, 1982; Hunter and co-workers, 1982; Verhaart and van der Laan, 1983). Above a pressure of 4 bar, Biasiutti and co-workers (1983) showed that this increase may be accounted for by compressibility effect.

Several researchers ascribed the deviation from Paschen's law below 4 bar to the abnormal pressure dependence of the apparent attachment coefficient observed in C_3F_6 (Aschwanden and co-workers, 1982; Aschwanden, 1985; Hunter and co-workers, 1982; Hunter and co-workers, 1983). From measurements of the ionization threshold energy and cross section magnitude by Aschwanden and co-workers (1982), it seems that the ionization coefficient is not likely to be responsible for the observed pressure dependence.

III. Deviation of swarm parameters from scaling laws (similarity laws)

According to scaling laws the pressure-reduced ionization coefficient α/p or the pressure-reduced effective ionization coefficient $\bar{\alpha}/p$, as well as the electron drift velocity v_e depend only on E/p, on the gas temperature, and on the nature of the gas (Francis, 1960).

Contrary to the scaling laws, the measured $\bar{\alpha}/p$ and v_e in C_3F_6 decrease with increasing gas pressure (Aschwanden and co-workers,

1982; Aschwanden, 1985; Verhaart and van der Laan, 1983).

As will be discussed in section 5.7.2 the above mentioned values for v_e and $\bar{\alpha}/p$ are "apparent" values, involving different kinds of collisional processes that scale differently. In case of multi-body attachment, attachment to van der Waals molecules (Aschwanden and co-workers, 1982), or formation and stabilization of negative dimer ions (Hunter and co-workers, 1983), the resulting apparent attachment coefficient η_a/p is very likely to have an abnormal pressure dependence.

Based on previous work by Lifshitz and Grajower (1972), Harland and Thynne (1972) and on their own work, Hunter and co-workers (1983) proposed a reaction scheme for the formation of stable negative ions in C_3F_6 in a buffer gas (N_2 or Ar):

$$C_3F_6 + e \xrightarrow{k_1} C_3F_6^{-*} \begin{cases} \xrightarrow{\nu_2 = 1/\tau_{a1}} C_3F_6 + e & (1) \\ \xrightarrow{\nu_3} C_xF_y^- + C_{3-x}F_{6-y} & (2) \\ \xrightarrow{k_4 M} C_3F_6^- + \text{energy} & (3) \\ \xrightarrow{k_5 M} C_3F_6 + e & (4) \end{cases}$$

$$C_3F_6^{-*} + C_3F_6 \xrightarrow{k_6} (C_3F_6)_2^{-*} \begin{cases} \xrightarrow{\nu_7 = 1/\tau_{a2}} 2C_3F_6 + e & (5) \\ \xrightarrow{k_8 M} (C_3F_6)_2^- + \text{energy} & (6) \\ \xrightarrow{k_9 M} 2C_3F_6 + e & (7) \end{cases}$$
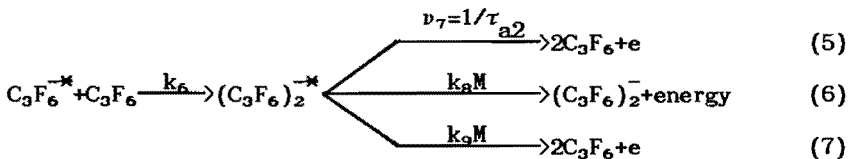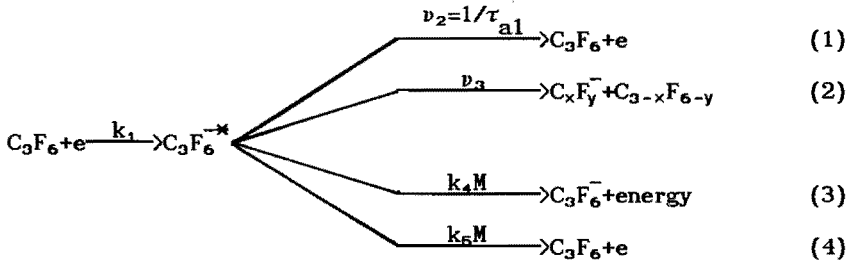
Here $C_3F_6^{-*}$ and $(C_3F_6)_2^{-*}$ denote an unstable negative C_3F_6 ion (with a life time τ_{a1}) and an unstable negative C_3F_6 dimer ion (with a life time τ_{a2}) respectively, M is the number density of the buffer gas and k_i is the relevant reaction rate constant, which is related to the swarm coefficient θ_i by $k_i = \theta_i v_e/N_a$ (N_a is the number density of C_3F_6).

From this reaction scheme, the apparent attachment rate constant

k_a $(=\eta_a v_e / N_a)$ can be expressed as:

$$k_a(N_a, M) = \frac{k_1 k_6 k_8 N_a M}{(\nu_2 + k_5 M + k_6 N_a)(\nu_7 + k_8 M + k_9 M)} \quad (5.7.3)$$

provided that both dissociative attachment (reaction (2)) and parent negative ion formation (reaction (3)) are negligible. From Eq. (5.7.3) it can be seen that k_a in general depends on the C_3F_6 number density as well as on the total gas number density (or pressure).

Aschwanden and co-workers (1982) and Hunter and co-workers (1983) proposed that temporary trapping of electrons, due to formation of unstable negative ions, could account for the reduction in the electron drift velocity v_e in C_3F_6.

To explain the observations of the large decrease in v_e with very high p in H_2 and N_2 by Grünberg (1967, 1968), Frommhold (1968) assumed that the correction of the electron drift velocity v_e at high pressure has the form:

$$v_e = \frac{v_{eo}}{1 + \nu\tau} \quad (5.7.4)$$

Here v_{eo} is the "zero-density" (or low pressure) drift velocity, which is the averaged velocity of an electron between two trapping collisions and is not pressure dependent if E/p and T are constant, ν is the collision frequency for unstable negative ion formation, and τ is the mean lifetime of the unstable negative ion. This relation is applied in section 5.7.2 for the determination of the "real" electron drift velocity in C_3F_6.

5.7.2 Fast swarm experiments in C_3F_6

The present experiments have been performed both in C_3F_6/N_2 mixtures and in pure C_3F_6. The electron component of the measured avalanche current waveform for low pressure C_3F_6 in a high pressure buffer N_2 gas (as given in Fig. 5.7.1) shows a clear "tail" after one electron transit time T_e. This indicates the presence of delaying processes in C_3F_6 (no delaying processes occur in N_2). In pure C_3F_6

this "tail" is not immediately clear, especially at low E/p, due to the increased stabilization of unstable negative ions upon collisions with C_3F_6 molecules. Examples are given in Fig. 5.7.2. Furthermore, under certain experimental conditions, the measured avalanche current waveform in pure C_3F_6 shows a double exponential behavior (see Verhaart and van der Laan, 1983). This double exponential behavior is a clear indication of the occurrence of electron detachment and ion conversion processes (compare also with the simulation shown in Fig. 3.3.6 in chapter 3).
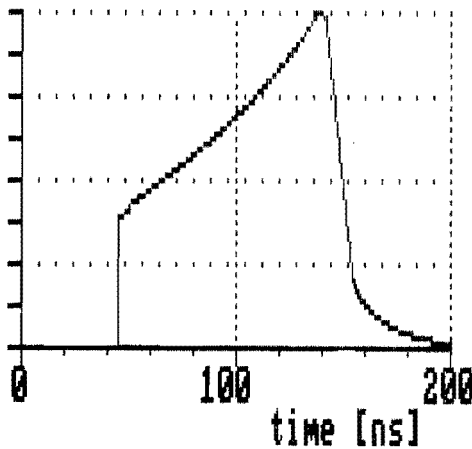
Figure 5.7.1

Typical electron component of the measured avalanche current waveform for low pressure C_3F_6 (4 Torr) in a high pressure buffer gas N_2 (746 Torr). Here d=1.0 cm, E/p_T=30.92 V/cmTorr (p_T is the total pressure of the mixture at $20^\circ C$). The unit at the vertical axis is 44.6 μA.

The two-parameter model cannot adequately describe the electron current waveforms, either in C_3F_6/N_2 or in pure C_3F_6, because the swarm parameters thus derived show abnormal pressure dependences. The four-parameter model should therefore be applied.

The results for C_3F_6 in a buffer gas N_2 have been presented as a conference contribution at the 5th Int. Symp. on High Voltage

Engineering, Braunschweig, Germany (24-28 Aug., 1987). The results
for pure C_3F_6 have been presented at the IEEE Int. Symp. on
Electrical Insulation, Boston, USA (5-8 June, 1988).
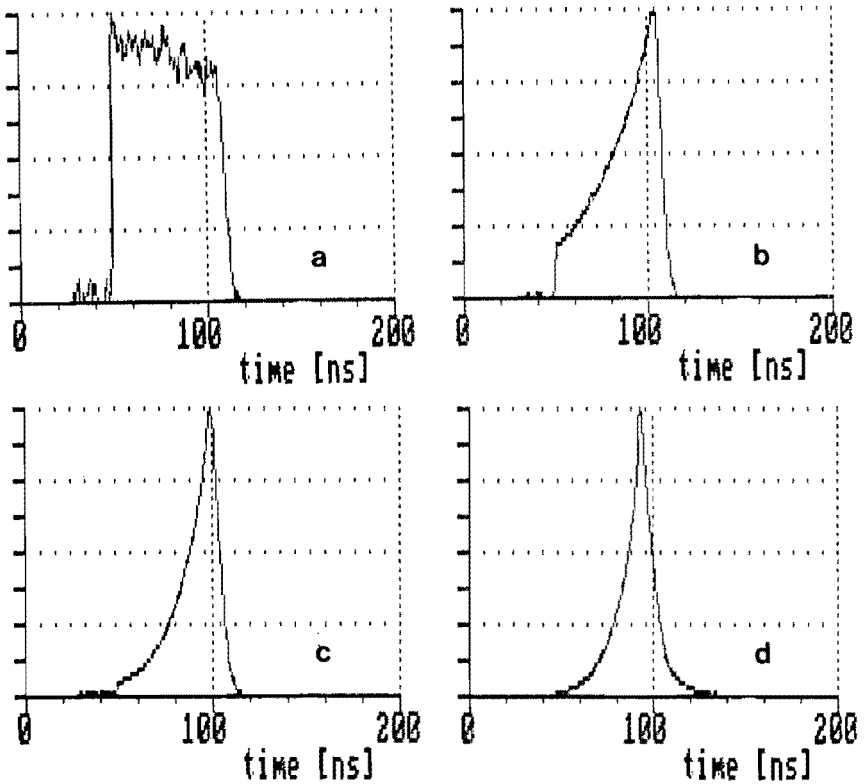
Figure 5.7.2

Examples of the electron component of the avalanche current
waveforms measured in C_3F_6. Here $p_{20}=50$ Torr, $d=1.0$ cm, E/p_{20}
(V/cmTorr): (a) 87.62, (b) 92.62, (c) 97.62, (d) 102.62. The
unit at the vertical axis (μA) is: (a) 2.14, (b) 12.5, (c) 68.3,
(d) 175.0.

I. Detachment and conversion processes in C_3F_6

Analysis and observation from fast swarm experiments

FIFTH INTERNATIONAL SYMPOSIUM
ON HIGH VOLTAGE ENGINEERING

15.06

BRAUNSCHWEIG   24–28 AUGUST 1987   FEDERAL REPUBLIC OF GERMANY

DETACHMENT AND CONVERSION PROCESSES IN C_3F_6

ANALYSIS AND OBSERVATION FROM FAST SWARM EXPERIMENTS

J. M. Wetzer and C. Wen

HIGH-VOLTAGE GROUP
EINDHOVEN UNIVERSITY OF TECHNOLOGY, THE NETHERLANDS

ABSTRACT

A model is presented describing the avalanche growth in gases that exhibit detachment and conversion next to ionization and attachment. The effect of detachment and conversion on the electron distribution and on the current waveform is illustrated. Swarmparameters are derived from measurements in C_3F_6/N_2 mixtures. Within the pressure-range covered the "real" effective ionization coefficient agrees with scaling laws. The obtained detachment and conversion parameters are analysed and discussed.

KEYWORDS: Insulating gases, avalanches, detachment, conversion, hexafluoropropene.

INTRODUCTION

In recent years hexafluoropropene (C_3F_6) has been studied by several investigators as a possible gaseous dielectric for high voltage insulation. The breakdown voltage in C_3F_6, unlike that in many other insulating gases, does not follow Paschen's law: it increases more rapidly with pressure than with electrode separation [1-5]. Below a pressure of four bar this behaviour can not be accounted for by the effect of compressibility [6]. In addition it was found from swarm experiments that neither the pressure reduced effective ionization coefficient $(\alpha-\eta)/p$ nor the electron drift velocity v_e are unique functions of E/p [7]. However, the limiting E/p-values (where $\alpha=\eta$) derived from swarm experiments were found to be consistent with the observed breakdown voltage [1].

These observations suggest that the question: "why does C_3F_6 deviate from Paschen's law" could be rephrased as: "why are v_e and $(\alpha-\eta)/p$ not unique functions of E/p in the case of C_3F_6". Indeed several authors have ascribed the observed breakdown behaviour to a strong pressure dependence of the apparent attachment process [3,7-10].

As to the cause of this pressure dependence, a reaction scheme involving detachment and conversion has been proposed by Hunter et al [8]. Verhaart and van der Laan, who earlier performed a quantitative analysis of humid air [11], proposed the same processes from the observed analogy between time resolved measurements in C_3F_6 and in air [5].

In this paper it is shown how detachment and conversion processes affect the spatial distribution of charge carriers in the avalanche and, as a result, the current waveform. The derivation of swarmparameters from the avalanche current will be discussed. The neglect of detachment and conversion leads to incorrect values for the effective ionization coefficient and, in some cases, even to incorrect values for the electron drift velocity. We therefore distinguish between real and apparent coefficients (see also [5]). The extended model including detachment and conversion is applied to the measurements performed in C_3F_6/N_2 mixtures.

THEORETICAL MODEL

The theoretical model, described earlier by Verhaart et al. [11], incorporates detachment and conversion, next to the commonly used ionization and attachment processes. Secondary emission and diffusion are not considered. Apart from neutral molecules four species are involved: electrons (index e), positive ions (index p), unstable negative ions (index nu) and stable negative ions (index ns). The unstable ions have a relatively short lifetime and are able to release their electron within the ion's transit time. Unstable negative ions can be converted into stable ones that do not release their electron within the transit time.

Ionization and attachment processes are denoted by the coefficients α and η, defined as the mean number of ionizing or attaching collisions of one electron traveling 1 cm in the field direction. The coefficients δ and β describe detachment and conversion, and are defined as the mean number of detachment or conversion events per unstable negative ion in the time that an electron travels 1 cm in the field direction. Hence all coefficients relate to the same time scale governed by the electron drift velocity. This choice is more convenient for the study of avalanche growth than the conventional definitions [12,13] that relate δ and β to the ion drift velocity.

The above mentioned definitions and conditions result in a set of linear first order differential equations for the temporal evolution of the four components. For times not exceeding one electron transit time ($T_e=d/v_e$) an analytical solution was presented earlier [11]. For the electrons, for example (assuming that n_0 primary electrons are released from the cathode in an infinitely short time interval), it was found that:

$$n_e(t) = \frac{n_0}{A_1 - A_2} \cdot \left[\left[A_1 + \delta + \beta\right] \cdot \exp(A_1 v_e t) - \left[A_2 + \delta + \beta\right] \cdot \exp(A_2 v_e t) \right] \quad (1)$$

in which:

$$A_{1,2} = \frac{1}{2}\left[\alpha - \eta - \delta - \beta \pm \left[(\alpha - \eta - \delta - \beta)^2 - 4 \cdot (\beta\eta - \alpha\beta - \alpha\delta)\right]^{\frac{1}{2}}\right] \quad (2)$$

For times exceeding T_e one should account for the loss of charged particles at the electrodes. This involves not only the number of particles $n_j(t)$ (integrated over the gap), but also their density distribution $\rho_j(x,t)$ (unit: cm^{-1}). With the definitions and conditions mentioned above these densities can be described by the partial differential equations (3)-(6).

In order to solve this set of equations Verhaart et al. [11] developed a numerical model. Swarm coefficients were determined from experiments by a (time-consuming) comparison between measured and simulated waveforms.

$$\frac{\partial \rho_e(x,t)}{\partial t} + v_e \frac{\partial \rho_e(x,t)}{\partial x} = (\alpha - \eta)v_e\rho_e(x,t) + \delta v_e\rho_{nu}(x,t) \tag{3}$$

$$\frac{\partial \rho_p(x,t)}{\partial t} - v_p \frac{\partial \rho_p(x,t)}{\partial x} = \alpha v_e\rho_e(x,t) \tag{4}$$

$$\frac{\partial \rho_{nu}(x,t)}{\partial t} + v_{nu} \frac{\partial \rho_{nu}(x,t)}{\partial x} = \eta v_e\rho_e(x,t) - (\delta + \beta)v_e\rho_{nu}(x,t) \tag{5}$$

$$\frac{\partial \rho_{ns}(x,t)}{\partial t} + v_{ns} \frac{\partial \rho_{ns}(x,t)}{\partial x} = \beta v_e\rho_{nu}(x,t) \tag{6}$$

In this paper we present an analytical solution valid also for $t > T_e$. The method of solving the set of the equations was published earlier by Llewellyn-Jones [12] and Meek and Craggs [13], however with somewhat different definitions of the coefficients used. In this method delayed and undelayed electrons are treated separately. Application to our set of equations yields for the delayed part [14]:

$$\rho_e^{del}(x,t) = \frac{n_0 y \cdot e^f}{2(v_e t - x)} \cdot I_1(y) \tag{7}$$

$$\rho_{nu}(x,t) = \frac{n_0 \eta v_e e^f}{v_e - v_{nu}} \cdot I_0(y) \tag{8}$$

in which:

$$y = 2 \cdot \frac{v_e}{v_e - v_{nu}} \left[\eta\delta(v_e t - x)(x - v_{nu}t) \right]^{\frac{1}{2}} \tag{9}$$

$$f = \frac{v_e}{v_e - v_{nu}} \left[(\alpha - \eta)(x - v_{nu}t) - (\delta + \beta)(v_e t - x) \right] \tag{10}$$

$I_j(y)$ is the jth order modified Bessel function:

$$I_j(y) = \left[\frac{y}{2} \right]^j \sum_{k=0}^{\infty} \left[\frac{1}{k!(k+j)!} \cdot \left[\frac{y}{2} \right]^{2k} \right] \tag{11}$$

The solution is valid for $v_{nu}t \leq x \leq v_e t$ if $v_e t \leq d$
and for $v_{nu}t \leq x \leq d$ if $v_e t > d$

The densities of positive ions and stable negative ions can easily be derived from the expressions for electrons and unstable negative ions, with the appropriate boundary conditions.

The undelayed part of the solution (for electrons) is given by:

$$\rho_e^{und}(x,t) = n_0 D(x - v_e t) \cdot \exp[(\alpha - \eta)v_e t] \quad (v_e t \leq d) \tag{12}$$
$$\rho_e^{und}(x,t) = 0 \quad (v_e t > d)$$

Here D stands for the Dirac-function. The distribution of ions left behind by the undelayed electrons serves as an initial condition for the solution of the delayed particle equations [14].

The electron and ion components of the current are finally obtained from:

$$i_e(t) = \frac{e \cdot n_e(t) \cdot v_e}{d} = \frac{e \cdot n_e(t)}{T_e} \tag{13}$$

$$i_i(t) = \frac{e}{d} \sum_j n_j(t) v_j = e \cdot \sum_j \frac{n_j(t)}{T_j} \quad (j = p, nu, ns) \tag{14}$$

where $n_j(t) = \int_0^d \rho_j(x,t)dx \quad (j = e, p, nu, ns) \tag{15}$

IMPLICATIONS OF DETACHMENT AND CONVERSION

1. The avalanche electron distribution

In the "classical" description of swarms, with ionizing and attaching collisions only, it is assumed that all electrons are contained in the avalanche head. Due to detachment however swarms may have a distinct tail of electrons. An example is given in Figure 1.

Fig.1 Example of avalanche electron distribution in humid air (see also [11]). Undelayed part is reduced for clarity.

When breakdown is governed by the Townsend mechanism any experiment or model that results in the correct number of electrons (integrated over the gap) will be consistent with the breakdown field strength. In case of streamer breakdown however the breakdown field strength depends on the field distortion due to the swarm, and thereby on the spatial distribution of electrons. In that case detachment and conversion processes should be taken into account.

2. The current waveform

The model presented illustrates the effects of detachment and conversion processes. In Figure 2, δ and β values are varied at constant values of α (11 cm^{-1}) and η (12 cm^{-1}). In all examples the electron current is shown, and the "apparent" effective ionization coefficient $\overline{\alpha}_A$ is compared to the "real" value $(\alpha - \eta)_R$, where the apparent $\overline{\alpha}_A$ is derived from:

$$\overline{\alpha}_A = \frac{1}{d} \ln \left[i_e(T_e)/i_e(0) \right] \tag{16}$$

In Figures 2a-2c, δ is varied at a high value of β (22 cm^{-1}). Detachment acts as a secondary ionization mechanism that strongly affects the slope of the current waveform ($\overline{\alpha}_A > \overline{\alpha}_R$). Figures 2d-2f ($\delta = 1$ cm^{-1}) and 2g-2i ($\delta = 7$ cm^{-1}) clearly demonstrate that conversion reduces the growth. Further it is shown that detachment may affect the apparent transit time (defined as the time at which the current reaches its maximum value).

The increase of the apparent transit time (or decrease of the apparent drift velocity) occurs at high values of the product $\eta\delta$ because of consecutive attachment and detachment processes: the actual drift velocity does not change, but the electrons are immobilized during some time. This effect is counteracted by conversion processes, since conversion reduces the number of unstable negative ions, and as a consequence the number of detached (i.e. delayed) electrons.

2

112

In many cases the effect of detachment and conversion is not easily recognized from the current waveform. The neglect of such processes results in apparent values for the effective ionization coefficient ($> \alpha_R$) and the electron drift velocity ($< v_{e,R}$). This may obscure physical interpretation and seemingly violate known scaling laws. When examining such processes experimentally, a good time resolution ($\lesssim 1$ ns or better) is of paramount importance.
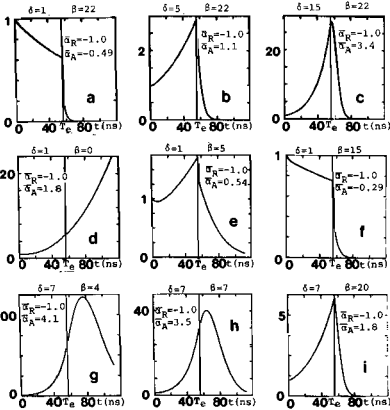

Fig.2 Electron current waveform at various δ and β values (unit: cm^{-1}, $\alpha=11\ cm^{-1}$, $\eta=12\ cm^{-1}$, $T_e=56$ ns). For comparison real and apparent effective ionization coefficients are given.

3. Swarm coefficients from measured waveforms

Swarmparameters are obtained from the measured electron current by means of a fitting program. Evaluation of the electron current expressions, however, reveals that the parameters occur in three combinations, viz:

$$C_1 = \alpha - \eta \quad ; \quad C_2 = \delta + \beta \quad ; \quad C_3 = \eta \delta$$

Hence, a unique identification of the individual parameters is not possible from the electron current only. Nevertheless these three quantities fully describe the electron avalanche growth. A physical interpretation would therefore be useful.

$C_1 : \alpha - \eta$ is easily identified as the (real or primary) effective ionization coefficient, which differs from the "apparent" value obtained from a model including only ionization and attachment. $C_2 : \delta + \beta$ describes the loss rate of unstable negative ions (the primary result of attachment), and is inversely proportional to their lifetime. $C_3 : \eta \delta$ may be interpreted as a secondary, delayed, ionization parameter describing the number of attached electrons which are still being released.

Relating the avalanche growth to collisional processes requires a separation of the three quantities into the individual parameters. This can be accomplished by extending the analysis to the ion current. This ion component of the current involves different positive and negative ions, each having their own driftvelocity, which complicates the analysis. Assuming all ion driftvelocities equal, one can derive the individual parameters quite easily from C_1, C_2 and C_3 by regarding the ratio of measured electron- and ion-current components at $t:T_e$: $i_e(T_e)/i_i(T_e)$ [14].
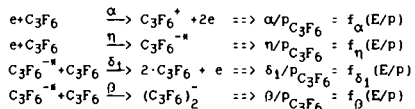
The setup used does not differ substantially from the one described earlier [15]. The most important feature is the timeresolution of 1.4 ns, which results from: 1) an N_2-laser with an 0.6 ns puls duration (FWHM), 2) a subdivided measuring electrode (reduction of stray capacitance), 3) a careful layout of the connection between measuring electrode and cable, and 4) a fast 9 bit transient digitizer (Tektronix 7912 AD).

The choice of experimental conditions, such as to allow verification of our model, is restricted: at high C_3F_6 pressure the electron drift velocity may not directly be derived from the current waveform. Further the electronic current component will be small, and the ionic component high. At low C_3F_6 pressure diffusion may no longer be neglected. The present experiments have been performed at a low partial C_3F_6 pressures (4÷10 Torr) in a high pressure buffer gas (N_2, around 750 Torr). N_2 is chosen because it is a non-attaching gas that has extensively been studied before.

Figure 3 shows the measured electron drift velocity: it is affected even by the small addition of C_3F_6 (0.5÷1.3%). This is ascribed to the large collision cross section of C_3F_6 as compared to N_2.

From the measured electron waveforms the three combinations $C_1 : \alpha - \eta$, $C_2 : \delta + \beta$ and $C_3 : \eta \delta$ are derived. Since C_1 also contains a nitrogen contribution it is first corrected using α-data for N_2 readily available from literature and from our experiments. All C_3F_6 quantities are plotted versus E/p_{total}, where p_{total} is corrected for ambient temperature variations. We hereby implicitly assume that the drift velocity depends only on E/p_{total}. At high C_3F_6 pressure this assumption is no longer valid (Figure 3.)

The following reactions are assumed to be responsible for ionization, attachment, detachment and conversion:

$$e + C_3F_6 \xrightarrow{\alpha} C_3F_6^+ + 2e \implies \alpha/p_{C_3F_6} = f_\alpha(E/p)$$
$$e + C_3F_6 \xrightarrow{\eta} C_3F_6^{-*} \implies \eta/p_{C_3F_6} = f_\eta(E/p)$$
$$C_3F_6^{-*} + C_3F_6 \xrightarrow{\delta_1} 2 \cdot C_3F_6 + e \implies \delta_1/p_{C_3F_6} = f_{\delta_1}(E/p)$$
$$C_3F_6^{-*} + C_3F_6 \xrightarrow{\beta} (C_3F_6)_2^- \implies \beta/p_{C_3F_6} = f_\beta(E/p)$$

Here $C_3F_6^{-*}$ stands for the excited negative ion. The pressure dependencies follow from evalution of the reaction rates and from the definitions of α, η, δ and β. The reaction schemes for conversion and detachment are proposed by Hunter et al. [8] who suggest that a short-living dimer-ion is formed that either detaches its electron or can be converted to a stable negative dimer ion. Of both two-stage processes only the initial and final products are given above.

With these dependencies in mind, pressure reduced coefficients have been plotted in Figures 4-6. From Figure 4 it is seen that, given some scatter, the "real" $(\alpha - \eta)/p_{C_3F_6}$ does not depend on the partial C_3F_6 pressure, in contrast to the "apparent" effective ionization coefficient. In Figure 5 $(\delta + \beta)/p_{C_3F_6}$, and in Figure 6 $\eta \delta/p^2_{C_3F_6}$, turn out to be independent on the partial C_3F_6 pressure above 6 torr. This is consistent with the reaction schemes mentioned above and indicates that at relatively high partial pressure (above 6 torr) detachment involves collisions with C_3F_6 molecules ($\delta : \delta_1$).

The pressure dependence observed at lower C_3F_6 pressure suggests a detachment mechanism without interference of a C_3F_6 molecule (autodetachment, or upon collision with a N_2 molecule. In that case we find (at constant nitrogen pressure):
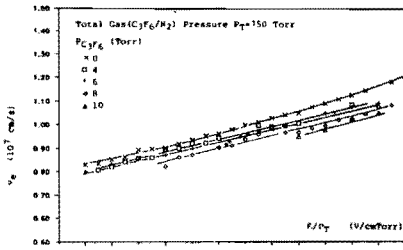
$$\delta_2 = f_{\delta_2}(E/p)$$

3

113
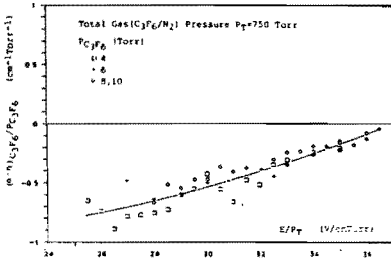
Fig.3 Measured electron drift velocity v_e
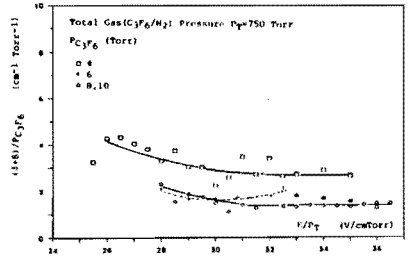
Fig.5 Unstable negative ion loss coefficient $(\delta+\beta)$

Fig.4 Real effective ionization coefficient $(\alpha-\eta)$
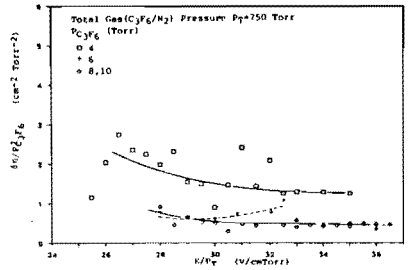

Fig.6 Secondary, delayed, ionization coefficient $\eta\delta$

The large scatter found at low partial C_3F_6 pressures is ascribed to the inaccuracy in the mixing ratio.

CONCLUSIONS

1. Detachment and conversion processes affect the electron distribution in the avalanche and may thereby influence the streamer breakdown threshold.
2. The neglect of these processes in the analysis of swarm experiments results in "apparent" values for the effective ionization coefficient and the electron drift velocity that may substantially differ from the "real" values. This obscures physical interpretation and seemingly violates known scaling laws.
3. Experimental observation of detachment and conversion processes from swarm experiments requires a time resolution in the order of 1 ns or better.
4. The "real" pressure reduced effective ionization coefficient in C_3F_6, $(\alpha-\eta)_{C_3F_6}/P_{C_3F_6}$, is a unique function of E/P_{total} in the pressure range covered. This is not true for the "apparent" values.
5. The present observations of the detachment process can be explained by the dominating effect of collisions with C_3F_6 molecules above a critical C_3F_6 pressure of about 6 Torr.

ACKNOWLEDGEMENT

REFERENCES

[1] Aschwanden, Th. and Biasiutti, G.,
   J. Phys. D: Appl. Phys., 14(1981) L189-192.
[2] Biasiutti, G., Gaseous Dielectrics III, Pergamon Press, New York, 1982, pp. 174-182.
[3] Hunter, S. R., et al, Gaseous Dielectrics III, Pergamon Press, New York, 1982, pp. 7-22.
[4] Chen, C. L., et al, IEE 7th Int. Conf. on Gas Discharges, London 1982, pp. 321-324.
[5] Verhaart, H. F. A. and van der Laan, P. C. T., 4th Int. Symp. on High Voltage Engineering, Athens, 1983, paper 33.12.
[6] Biasiutti, G., et al, 4th Int. Symp. on High Voltage Engineering, Athens, 1983, paper 33.02.
[7] Aschwanden, Th., et al, Gaseous Dielectrics III, Pergamon Press, New York, 1982, pp. 23-33.
[8] Hunter, S. R., et al, J. Phys. D: Appl. Phys., 16(1983) pp. 573-580.
[9] Hunter, S. R. and Christophorou, L. G., Gaseous Dielectrics IV, Pergamon Press, New York, 1984, pp. 115-127.
[10] Hunter, S. R. and Christophorou, L. G., J. Appl. Phys. 57(9), 1985, pp. 4377-4385.
[11] Verhaart, H. F. A. and van der Laan, P. C. T., J. Appl. Phys. 55(9), 1984, pp. 3286-3292.
[12] Llewellyn-Jones, F., Ionization avalanches & Breakdown, Science Paperbacks, 1967, Ch. 2.6.
[13] Meek, J. M. and Craggs, J. D., Electrical breakdown in Gases, Wiley, New York, 1978, Ch. 3.3.
[14] Wen, C. and Wetzer, J. M., to be published.
[15] Verhaart, H. F. A. and van der Laan, P. C. T., J. Appl. Phys., 53(3), 1982, pp. 1430-1436.

AUTHORS ADRESS: High-Voltage Group
   Eindhoven University of Technology
   P. O. Box 513, 5600 MB Eindhoven
   THE NETHERLANDS

4

II. Swarm parameters in hexafluoropropene $1-C_3F_6$

SWARM PARAMETERS IN HEXAFLUOROPROPENE 1-C3F6

C. Wen and J. M. Wetzer

High-Voltage Group, Dept. of Electrical Engineering,
Eindhoven University of Technology, Eindhoven, the Netherlands.

ABSTRACT—Fast swarm measurements have been performed in Hexafluoropropene, 1-C3F6 (hereafter abbreviated as C3F6), with pressures p ranging from 20 to 200 Torr and E/p values from 80 to 110 V/cmTorr. The "apparent" swarm parameters, derived from a simple model (ionization and attachment only), confirm the pressure dependences reported in the literature. The existence of detachment has been clearly identified from the observed time resolved avalanche current waveforms. A model that includes detachment and conversion in addition to ionization and attachment processes has been applied to derive the "real" swarm parameters in C3F6. The present work indicates that two-body collisional detachment and three-body stabilization of the transient anion C3F6^{-*} are responsible for the observed pressure dependence of the dielectric strength of C3F6.

1. INTRODUCTION

Much effort has been spent on the search for new gases or gas mixtures with insulating characteristics superior to SF6. Among the gases that have been investigated so far, C3F6, as a possible new high voltage insulant, is interesting because its inherent dielectric strength $(E/p)_{lim}$ (the limiting value of electric field strength E over gas pressure p) increases considerably with increasing gas pressure, and because it shows a positive synergism when mixed with SF6, or with several other gases (see Ref.[1] and the Refs. therein).

Literature[2,3] shows unexpected pressure dependences of the measured electron drift velocity and the pressure-reduced effective ionization coefficient in this gas. The explanations of these pressure dependences are still incomplete, though several authors have ascribed these pressure dependences to "electron trapping" and to the observed strongly pressure dependent apparent attachment process in this gas[1-4]. We feel that a further quantitative identification of the various processes, such as detachment and conversion processes, associated with the apparent attachment in this gas will contribute to the understanding of the above-mentioned pressure dependences. In our previous work[5], we have reported on the analysis of fast swarm measurements performed with low pressure C3F6 in a high pressure N2 buffer gas. We there used a four parameter model including ionization, attachment, detachment and conversion (stabilization/charge transfer). The thus derived real effective ionization coefficient $\bar{\alpha}/p$ for C3F6 has been shown to be pressure independent in the pressure range covered (4~10 Torr). This is consistent with scaling laws. In the present paper, our previous work is extended to the case of pure C3F6 at higher pressures. Fast swarm measurements have been performed and analysed. The derived swarm parameters are presented and discussed.

2. EXPERIMENTAL TECHNIQUES

The experimental setup has been presented elsewhere[5,6]. It is a slightly modified version of the setup described earlier by Verhaart and van der Laan[7] and features an overall time resolution of about 1.4 ns. The vessel is evacuated with a turbomolecular pump down to 10^{-7} Torr before filling in

high purity (99%) C3F6 gas (supplied by Ventron, West Germany). All pressure measurements were performed at room temperature (around 22°C) and reduced to 20°C.

3. RESULTS AND DISCUSSIONS

3.1. Electron drift velocity

The apparent electron drift velocity at various C3F6 pressures has been determined from the measured electron current waveforms, and is shown in Fig.1. Also shown in this figure are the results of Aschwanden[3] and the results that we derived from the measurements performed earlier by Verhaart and van der Laan[8]. These three sets of results show a very good agreement.
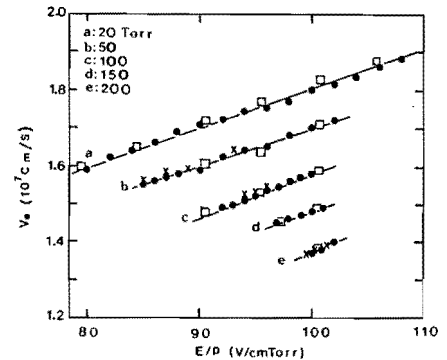

Fig.1. The apparent electron drift velocity v_e versus E/p in C3F6.
● This work, x derived from [8], □ [3].

Temporary trapping of the electrons, due to formation of unstable negative ion complexes, has been proposed[1-3] to account for the reduction of the electron drift velocity in this gas. Earlier, when analysing the reported decrease of v_e with p in H2 and N2 at very high pressures, Frommhold[9] assumed that the apparent electron drift velocity v_e is related to the so-called "zero-density" drift velocity v_{eo} (the averaged velocity in between two trapping collisions) by:

$$v_e^{-1} = v_{eo}^{-1} (1+kp) \qquad (1)$$

where k is a proportionality factor (unit: Torr^{-1}). For a specific gas v_{eo} depends only on E/p and on the gas temperature. From our measurements in C3F6 at various pressures, this linear relation (Eq.(1)) has indeed been observed as shown in Fig.2. When we multiply v_e^{-1} by $\sqrt{E/p}$, as also shown in Fig.2, we obtain a unique, and linear, relationship. This indicates that the "zero density" drift velocity v_{eo} indeed depends only on $\sqrt{E/p}$. From an extrapolation of the curve $v_e^{-1}\sqrt{E/p}$ versus

p to the "zero pressure", we derive:

$$v_{eo} = 1.88 \times 10^6 \sqrt{E/p} \qquad (2)$$

in the range $80 \lesssim E/p \lesssim 110$ V/cmTorr and $p \lesssim 200$ Torr. Equation (2) is consistent with the apparent electron drift velocity at very low pressures (0.5 and 1 Torr) reported by Aschwanden[3] in the range $80 \lesssim E/p \lesssim 110$ V/cmTorr. At very low pressure, the probability for electron trapping is significantly reduced, and therefore the apparent electron drift velocity approaches the real value. This "zero-density" electron drift velocity v_{eo} is, in our opinion, the real drift velocity in C_3F_6 and should be used in the derivation of the other swarm parameters.
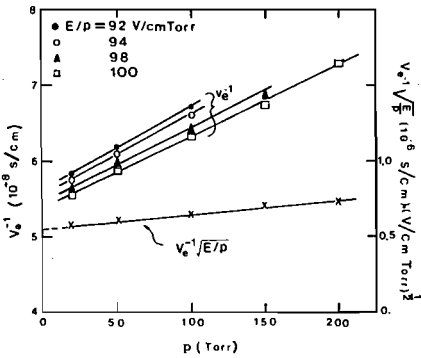

Fig.2. v_e^{-1} or $v_e^{-1}\sqrt{E/p}$ versus p in C_3F_6.

3.2. Effective ionization coefficient

From our measurements apparent values of the effective ionization coefficient $\bar{\alpha}_a/p$ have been derived by a simple model that includes only ionization and attachment (see e.g. Ref.[3] or [7]). The results are shown in Fig.3. Also shown in this figure are the
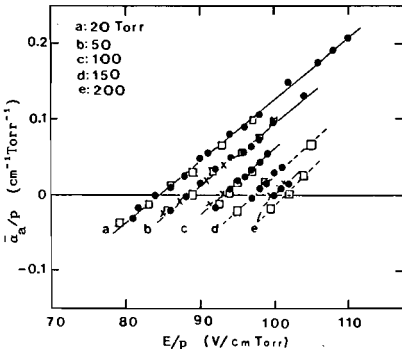

Fig.3 The apparent effective ionization coefficient $\bar{\alpha}_a/p$ versus E/p in C_3F_6.
● This work. x derived from [6]. □ [3].

results of Aschwanden[3] and the results that we derived from the measurements of Verhaart and van der Laan[8]. The three sets of measurements show an excellent agreement except at p=200 Torr, where our values are larger than those of Aschwanden.

The real effective ionization coefficient has been obtained with the four parameter model presented earlier[5,10] and is shown in Fig.4 (right side). Also shown in this figure are the results that we derived previously for low pressure C_3F_6 in a N_2 buffer gas[5] (left side). From the present measurements in pure C_3F_6 only those with pressures $\gtrsim 50$ Torr have been analysed, in order to allow the neglect of diffusion in our four parameter model.
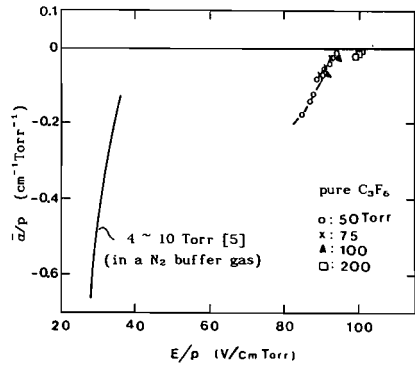

Fig.4 The real effective ionization coefficient $\bar{\alpha}/p$ versus E/p in C_3F_6.

In the present evaluation, for pressures up to 100 Torr, the real drift velocity as derived from Eq.(2) has been used in the curving fitting procedure. The results show a unique dependence on E/p, as was expected from scaling laws. The values derived at 200 Torr seem to disagree with these laws. The 200 Torr results, however, have been determined with a drift velocity derived from the time interval needed for the electron current waveform to reach its maximum value. This was done because the real drift velocity v_{eo} failed to give an accurate fitting between measured and calculated waveforms.

Also the previously performed experiments[5] at low C_3F_6 pressures (below 10 Torr) in a N_2 buffer gas give a real effective ionization coefficient that depends only on E/p (left side in Fig.4). These measurements were performed at E/p values up to 36 V/cmTorr, whereas the present ones cover the range from 80 to 110 V/cmTorr. The intermediate range is not yet covered. The left and the right side of Fig.4 do not necessarily relate to one unique curve since, for low pressure C_3F_6 in a N_2 buffer gas, the velocity distribution might be different from the one in a pure C_3F_6 environment.

3.3 Detachment and conversion coefficients

As described earlier[5,10] the four parameters α, η, δ and β can only be derived from the electron current component in their combinations $\alpha-\eta$, $\delta+\beta$ and $\eta\delta$. The results for $\delta+\beta$ and $\eta\delta$ are shown in Figs.5 and 6 respectively (right side). Also shown are the results that we derived previously for low pressure C_3F_6 in a N_2 buffer gas[5] (left side).
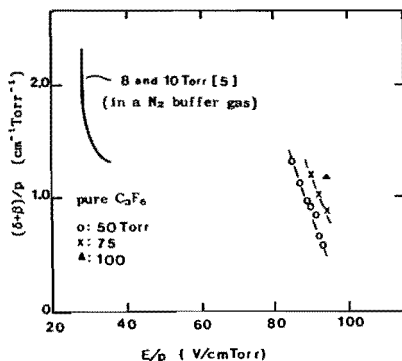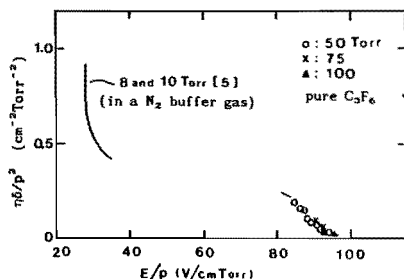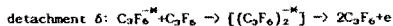
109
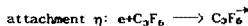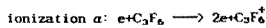
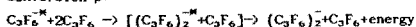Fig.5 $(\delta+\beta)/p$ versus E/p in C_3F_6.

Fig.6 $\eta\delta/p^2$ versus E/p in C_3F_6.

No pressure dependence occurs in Fig.6. This indicates that both η/p and δ/p depend only on E/p and relate to two-body collisions. The pressure dependence in Fig.5 for E/p exceeding 80 V/cmTorr then implies that β/p in pure C_3F_6 depends not only on E/p but also on p. This indicates that a three-body collision is involved in the conversion process. Whether this three body collision is the only contributing process, can only be decided when the three combinations of the coefficients are further split into the four individual coefficients. From the study of Hunter et al.[1] it is assumed, however, that the three-body collisional process is the most likely mechanism to provide a stable negative ion.

The above discussion is consistent with the following simplified reaction scheme for C_3F_6:

ionization α: $e+C_3F_6 \longrightarrow 2e+C_3F_6^+$

attachment η: $e+C_3F_6 \longrightarrow C_3F_6^{-*}$

detachment δ: $C_3F_6^{-*}+C_3F_6 \rightarrow [(C_3F_6)_2^{-*}] \rightarrow 2C_3F_6+e$

conversion β:

$C_3F_6^{-*}+2C_3F_6 \rightarrow [(C_3F_6)_2^{-*}+C_3F_6] \rightarrow (C_3F_6)_2^- + C_3F_6 + energy$

This reaction scheme is sufficient to explain the observed pressure dependences. Furthermore a more complicated and refined reaction scheme can not be verified by the techniques employed in the present work.

In the above reaction scheme an electron is assumed to attach to a C_3F_6 molecule to form an unstable negative ion $C_3F_6^{-*}$. This unstable negative ion can either lose its electron by collisional detachment (possibly via subsequent dimer ion $(C_3F_6)_2^{-*}$ formation and autodetachment) or it can be stabilized by three-body conversion (possibly via dimer ion $(C_3F_6)_2^{-*}$ formation and a subsequent collision with a C_3F_6 gas molecule).

The comparison of the present results (right side in Figs.5 and 6) in pure C_3F_6 with those derived earlier[5] for low pressure C_3F_6 in a N_2 buffer gas (left side) is, again, not straightforward. The possibly different velocity distribution has been mentioned before. Further at pressures below 10 Torr the three-body conversion process in the above-reaction scheme is not likely, and has not been observed. A three-body conversion process involving a N_2 molecule may play a role but this will not show up as a dependence on the C_3F_6 pressure. Also for low pressure C_3F_6 in a N_2 buffer gas, collisional detachment involving a N_2 molecule may play a role, however only at C_3F_6 pressures below 6 Torr[5]. The study of the region between 36 and 80 V/cmTorr would require a model that incorporates diffusion, next to the four coefficients α, η, δ and β. Such a model is not available at present. Further, the low signal to noise ratio encountered at low E/p in pure C_3F_6 makes an accurate analysis difficult.

From the above reaction scheme, the apparent attachment coefficient η_a can be related to the real coefficients η, δ and β as follows:

$$\eta_a = \frac{\eta\beta}{\delta+\beta} \qquad (3)$$

When we assume that the real and the apparent ionization coefficients α and α_a are identical, i.e., when α/p depends only on E/p, the apparent effective ionization coefficient $\bar{\alpha}_a$ can be written as:

$$\bar{\alpha}_a = \bar{\alpha} + \frac{\eta\delta}{\delta+\beta} \qquad (4)$$

Equation (4) has been checked, for all measurements performed, by applying both the two parameter model and the four parameter model. Excellent agreement has been found.

Since the analysis on attachment η, detachment δ and conversion β indicates that both attachment and detachment are two-body processes and that a three-body collision is involved in the conversion process, a simple analysis on Eqs.(3) and (4) shows that the pressure-reduced apparent attachment coefficient η_a/p increases, and the pressure-reduced apparent effective ionization coefficient $\bar{\alpha}_a/p$ decreases with increasing pressure p.

The above reaction scheme is similar to the one proposed by Hunter et al.[1] but only accounts for the most dominant processes involved, and can explain the observations in the present work.

110

118

CONCLUSIONS

1. Fast swarm experiments have been performed for pure C_3F_6 in the pressure range of $20 \sim 200$ Torr and the E/p range of $80 \sim 110$ V/cmTorr in a uniform gap. The apparent values for the electron drift velocity and the effective ionization coefficient, derived from a two parameter model (α and η_a only), confirm the pressure dependences of the swarm parameters reported in the literature.

2. The real electron drift velocity v_{e0} in pure C_3F_6 has been extrapolated from the measured apparent velocity by taking into account electron trapping.

3. A four parameter model that includes detachment(δ) and conversion(β) besides ionization(α) and attachment(η) has been applied to derive the real coefficients in their combinations $\alpha-\eta$, $\delta+\beta$ and $\eta\delta$. Up to 100 Torr both $(\alpha-\eta)/p$ (the real effective ionization coefficient) and $\eta\delta/p^2$ depend only on E/p. However $(\delta+\beta)/p$ increases with pressure.

4. The apparent attachment process is influenced by the counteracting detachment and conversion processes. Their different pressure dependences (two-body detachment versus three-body stabilization of the unstable negative ion $C_3F_6^{-*}$) can explain how the apparent η_a/p increases, and how the apparent $\bar{\alpha}_a/p$ decreases with pressure.

ACKNOWLEDGMENT

REFERENCES

[1] Hunter, S. R., et al. "Anomalous electron atachment properties of perfluoropropylene ($1-C_3F_6$) and their effect on the breakdown strength of this gas", J. Phys. D: Appl. Phys., Vol. 16, pp.573-580, 1983.

[2] Aschwanden, Th., et al. "Mobility and recombination of ions and effective ionization coefficient in hexafluoropropylene(C_3F_6)", in Gaseous Dielectrics III(Christophorou, L. G., Ed.), Pergamon Press, New York, pp.23-33, 1982.

[3] Aschwanden, Th., Dissertation ETH-Zurich, Nr. 7931, 1985.

[4] Hunter, S. R., et al. "Pressure-dependent electron attachment rates in perfluoroalkanes and perfluoropropylene ($1-C_3F_6$) and their effect on the breakdown strength of these gases", in Gaseous Dielectrics III (Christophorou, L. G., Ed.), Pergamon Press, New York, pp.7-22, 1982.

[5] Wetzer, J. M. and Wen, C., "Detachment and conversion processes in C_3F_6. Analysis and observation from fast swarm experiments", Proc. 5th Int. Symp. on High Voltage Engineering(ISH), Braunschweig, Paper 15.06, 1987.

[6] Wetzer, J. M., Wen, C. and van der Laan, P. C. T., "Bandwidth limitations of gap current measurements", submitted to this conference, 1988.

[7] Verhaart, H. F. A. and van der Laan, P. C. T., "Fast current measurements for avalanche studies", J. Appl. Phys., 53(3), pp.1430-1436, 1982.

[8] Verhaart, H. F. A. and van der Laan, P. C. T., "Fast avalanches measurements in C_3F_6", Proc. 4th Int. Symp. on High Voltage Engineering(ISH), Athens, Paper 33.12, 1983.

[9] Frommhold, L., "Resonance scattering and the drift motion of electrons through gases", Phys. Rev., 172, pp.118-123, 1968.

[10] Wen, C. and Wetzer, J. M., "Electron avalanches influenced by detachment and conversion processes", submitted to IEEE Trans. on Electrical Insulation, 1988.

111

119

5.8 Octafluorocyclobutane

5.8.1 Introduction

Octafluorocyclobutane $(c\text{-}C_4F_8)$ has several unusual properties:

(a) it has a high dielectric strength (Berril and co-workers, 1987; Christophorou and co-workers, 1987);

(b) it shows unexpectedly large values for the figure of merit M (which is inversely proportional to the sensitivity of the gas to the electrode surface-roughness) at relatively high pressure (Berril and co-workers, 1987);

(c) it shows a positive synergism when mixed with $1\text{-}C_3F_6$ (James and co-workers, 1980); and

(d) it has an abnormal pressure dependence of both the breakdown voltage and the pressure-reduced effective ionization coefficient (Berril and co-workers, 1987; Tagashira and co-workers, 1987).

To understand these observations, fast swarm experiments have been performed in $c\text{-}C_4F_8$ both at low and at relatively high pressures. The results at low pressures (1~5 Torr) have been contained in a conference contribution presented at the IX Int. Conf. on Gas Discharges and Their Applications, Venezia, Italy (19-23 Sept., 1988). The observations at higher pressures (5~200 Torr) have been published in IEEE Trans. on Electrical Insulation, Vol. 24, No. 1, 1989, pp.143-149. Both contributions are included in section 5.8.2.

5.8.2 Fast swarm experiments in $c\text{-}C_4F_8$

I. Swarm parameters in octafluorocyclobutane $(c\text{-}C_4F_8)$ and its mixtures with N_2

SWARM PARAMETERS IN OCTAFLUOROCYCLOBUTANE (c-C$_4$F$_8$) AND ITS MIXTURES WITH N$_2$

C. Wen and J.M. Wetzer

High-Voltage Group, Dept. of Electrical Engineering, Eindhoven University of Technology, P.O.BOX 513, 5600 MB Eindhoven, The Netherlands.

ABSTRACT

Fast swarm experiments have been performed in Octafluorocyclobutane (c-C$_4$F$_8$) and its mixtures with N$_2$ at low pressures (below 10 Torr). Swarm parameters, such as the electron drift velocity and the apparent effective ionization coefficient, together with (E/p)lim have been determined. The results are presented and discussed with reference to other investigations.

INTRODUCTION

Much effort has been spent on the search for new gases or gas mixtures with insulating characteristics superior to SF$_6$. In this context, several fluorocarbon gases have been found to have higher dielectric strengths than that of SF$_6$ (James and co-workers, 1978; James and co-workers, 1980) and, due to the non-toxicity and thermal stability of several of these gases (Bouldin and co-workers, 1984), they are clearly of interest as possible high voltage insulants.

c-C$_4$F$_8$, amongst the fluorocarbon gases that have been investigated so far, is interesting because of the following reasons. Firstly, its inherent dielectric strength (E/p)lim (defined as the value of E/p (electric field strength E over gas pressure p) at which breakdown occurs at high values of pd (pressure times gap distance d)) is high (about 1.22 times that of SF$_6$ (Berril and co-workers, 1987; Christophorou and co-workers, 1987)). Secondly, contrary to most strongly electronegative gases, the reported values of the figure of merit M are unexpectedly large at relatively high pressures (Berril and co-workers, 1987). The figure of merit M is a measure of the sensitivity of the gas to the surface roughness of the electrodes, a large M-value corresponds to a low sensitivity. Thirdly, c-C$_4$F$_8$, when mixed with l-C$_3$F$_6$, exhibits a positive synergism, i.e., the breakdown strength of the mixture is higher than that of either one of the constituents (James and co-workers, 1980). All of these observations make c-C$_4$F$_8$ particularly suitable for high voltage insulation applications.

The pressure dependence in the Paschen curve recently found by Berril and co-workers (1987) and Tagashira and co-workers (1987), and the pressure dependence of the pressure-reduced effective ionization coefficient observed by Tagashira and co-workers (1987) in pure c-C$_4$F$_8$ are, however, not yet understood in terms of the basic physical processes involved, and merit further study.

In this paper, we report on fast swarm experiments performed both in c-C$_4$F$_8$ and in c-C$_4$F$_8$/N$_2$ mixtures at low pressures (below 10 Torr). The swarm parameters, such as the electron drift velocity and the apparent effective ionization coefficient, have been determined. The inherent dielectric strength (E/p)lim of this gas and its mixtures with N$_2$ has been deduced from the apparent effective ionization coefficient. The results are presented and discussed with reference to other investigations.

EXPERIMENTAL TECHNIQUES

The method which we used for the avalanche current

measurement is the so called Time-Resolved-Townsend method; the avalanche is initiated with a N$_2$ laser pulse of short duration (0.6 ns). The experimental setup has been presented elsewhere (Wen and Wetzer, 1988a; Wetzer and Wen, 1987; Wetzer and co-workers, 1988). It is a slightly modified version of the setup described earlier by Verhaart and van der Laan (1982) and features an overall time resolution of about 1.4 ns. The vessel is evacuated with a turbomolecular pump down to 10^{-7} Torr before filling in high purity c-C$_4$F$_8$ (99.9%) and N$_2$ (99.999%) (supplied by Hoekloos, Holland). The gas pressure was measured by a Pennwalt pressure gauge (0 ~ 50 Torr) with a stated accuracy of 0.3%. All pressure measurements were performed at room temperature (around 22°C) and reduced to 20°C.

RESULTS AND DISCUSSIONS

Like in our previous work (Wen and Wetzer, 1988a 1988b; Wetzer and Wen, 1987) we distinguish between apparent and real swarm parameters. The apparent parameters are derived from models including only ionization and attachment processes; the real parameters are derived from models that also account for detachment and conversion processes.

Results in pure c-C$_4$F$_8$

The present experiments in pure c-C$_4$F$_8$ have been performed only at low pressures (below 10 Torr). Above 10 Torr, we were not able to clearly observe the electron component of the avalanche current waveform during the electron transit time (which is in the order of several tens of nanoseconds) even at electric fields close to breakdown. This may be ascribed to a very dominant attachment process, and/or to the interaction of c-C$_4$F$_8$ molecules with the cathode surface, which hinders the release of sufficient primary electrons. Even below 10 Torr, the ion current contribution to the measured avalanche current has been observed to be very large. Figure 1 shows, for instance, the measured avalanche current waveforms at a pressure of 3 Torr. Such a high ion current contribution supports the idea of a very dominant attachment process, whereas the increasing ion current in Fig. 1b is an indication of detachment processes.

The models that we use to evaluate the avalanche current require that we separate the waveform into an electron contribution and an ion contribution. For waveforms such as shown in Fig. 1b this separation is not straightforward, and requires a priori knowledge of the processes involved. So far, we have therefore only analysed the experiments performed at 1 Torr. Here the ion contribution is small and can be corrected for. At such a low pressure, diffusion of the electrons cannot be neglected and should be taken into account when we derive the electron drift velocity from the measured electron current waveform. This has been achieved by deriving an equivalent electron current waveform which has no diffusion but has the same e-folding time and the same charge as the measured current waveform (Aschwanden, 1985; Brambring, 1964). An example of this approach is shown in Fig. 2.

The electron drift velocity in pure c-C$_4$F$_8$ at 1 Torr is shown in Fig. 3. Also shown in this figure are the

results measured by Naidu and co-workers (1972) with the Time-of-Flight method and those calculated from the Boltzmann equation by Novak and Fréchétte (1984). Our results are about 10% lower than those of Naidu and co-workers at low E/p (<200 V/cmTorr) but seem to be consistent with the tendency of their results at high E/p values (>225 V/cmTorr). Our results are also compatible, when extrapolated to low E/p (<125 V/cmTorr), with those calculated by Novak and Fréchette.

Due to electron diffusion, the identification of the possible processes responsible for the formation of negative ions in pure c-C_4F_8 from the presently measured electron current waveforms is not straightforward. At these low pressures, any sign of, for instance, delaying processes (if there are any) on the current waveform will be masked by the large effect of the electron diffusion. Further, basic knowledge about the detailed processes in pure c-C_4F_8 cannot be found in the literature. We have therefore in the

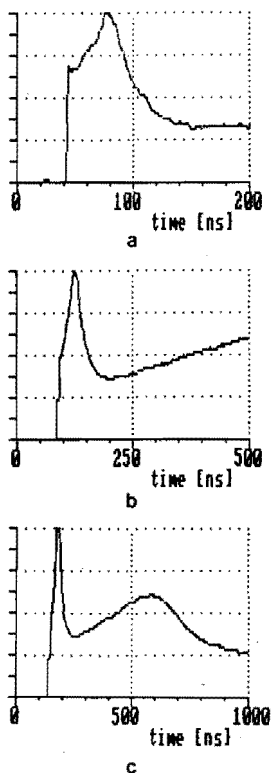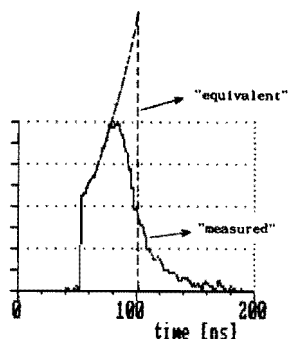Fig. 2. An example of measured electron current waveform, and equivalent waveform used for the derivation of the electron transit time T_e and the electron drift velocity v_e (=d/T_e). p=1 Torr (c-C_4F_8). d=1.0 cm. E/p=176.4 V/cmTorr, Vert: 3.8 µA/div.

Fig. 1. Measured avalanche current waveforms in c-C_4F_8 at a pressure of 3 Torr; d=1.0 cm.
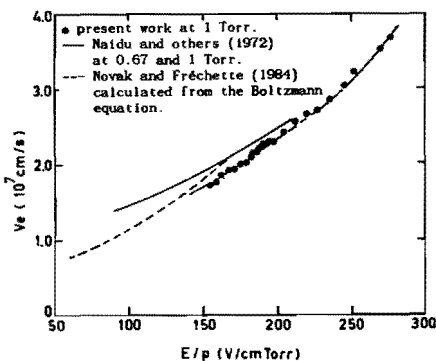(a) E/p=176.2 V/cmTorr. Vert: 5.2 µA/div;
(b), (c) E/p=183.8 V/cmTorr. Vert: 8.4 µA/div.

Fig. 3. v_e versus E/p in c-C_4F_8.

present work only derived the apparent effective ionization coefficient $\bar{\alpha}_a$/p for c-C_4F_8 which is shown in Fig. 4. Also shown in Fig. 4 are the results reported by Naidu and co-workers (1972) (derived from their individual values of α_a/p and η_a/p. Also their results should be regarded as apparent values since no processes other than ionization and attachment are considered). Again our values are smaller than those of Naidu and co-workers at low E/p (<200 V/cmTorr) but are closer to the tendency of their values at higher E/p values (>200 V/cmTorr). The (E/p)lim-value derived from the present curve $\bar{\alpha}_a$/p ~ E/p (defined as the E/p value at which $\bar{\alpha}_a$/p=0) is 143.1 V/cmTorr. From the measured curve $\bar{\alpha}_a$/p ~ E/p by Naidu and co-workers (1972) the (E/p)lim is found to be 118.3 V/cmTorr. Our value is, however, in a good agreement with the values of 142.7-144 V/cmTorr derived from precision breakdown measurements (uniform-field) by Berril and co-workers (1987) at much higher pressures (75 ~ 450 Torr). A value of 144.7 V/cmTorr found by Christophorou and

co-workers (1987) with uniform-field breakdown measurements at 522.8 Torr is also compatible with the presently derived (E/p)lim value.

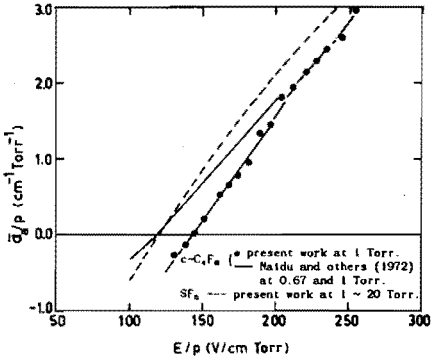Fig. 4. $\bar{\alpha}_a/p$ versus E/p in c-C_4F_8. For comparison also the SF$_6$ curve is shown.

For comparison, the effective ionization coefficient in SF$_6$ measured by us at pressures between 1 and 20 Torr is also shown in Fig. 4 by the dotted line. It is observed that the slopes k of the curves $\bar{\alpha}_a/p \sim$ E/p in the neighbourhood of (E/p)lim in SF$_6$ and in low pressure (1 Torr) c-C_4F_8 are approximately the same. Since this slope is inversely proportional to the figure of merit M, it is a measure of the sensitivity of the gas to the electrode surface roughness. The low sensitivity of c-C_4F_8 at relatively high pressures (>75 Torr) as follows from the large values of the figure of merit M measured by Berril and co-workers (1987) is not observed in the present low pressure swarm experiments.

The apparent effective ionization coefficient does not necessarily obey scaling laws and may, as in the case of 1-C_3F_6 (Wen and Wetzer, 1988b; Wetzer and Wen, 1987), strongly depend on gas pressure. The fact that the breakdown voltage increases with the c-C_4F_8 gas pressure at a fixed pd as observed by Berril and co-workers (1987) and Tagashira and co-workers (1987) indicates that the apparent effective ionization coefficient (pressured-reduced) decreases with increasing pressure. This has indeed been observed in recent measurements of $\bar{\alpha}_a/p$ in c-C_4F_8 by Tagashira and co-workers (1987) (Steady-State-Townsend method). They also found that both the (apparent) ionization coefficient α_a/p and the (apparent) attachment coefficient η_a/p decrease strongly with the c-C_4F_8 gas pressure. When we take into account that the measured (E/p)lim value in c-C_4F_8 is almost constant over the pressure range 75 ~ 450 Torr (Berril and co-workers, 1987) and that we have derived the same (E/p)lim at 1 Torr, we believe that the apparent $\bar{\alpha}_a/p$ versus E/p in c-C_4F_8 near (E/p)lim for different pressures follows the behaviour as indicated in Fig. 5. When the c-C_4F_8 gas pressure increases, (E/p)lim does not change substantially, while the slope k of the curve $\bar{\alpha}_a/p \sim$ E/p decreases. This is consistent with the observations by Berril and co-workers (1987) that the figure of merit M increases with c-C_4F_8 gas pressure. The three different E/p values measured by Tagashira and co-workers (1987), as also shown in Fig. 5, supports the above suggestion. Their (E/p)lim value is, however, about 120 V/cmTorr. What processes are responsible for this pressure dependence in c-C_4F_8 is not clear at present and merits further investigation.
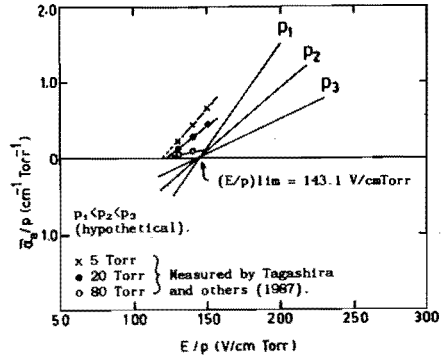

Fig. 5. Hypothetical $\bar{\alpha}_a/p$ versus E/p in c-C_4F_8. Also the measured $\bar{\alpha}_a/p$ by Tagashira and co-workers (1987) is shown in this figure.

Results in c-C_4F_8/N_2 Mixtures

The apparent effective ionization coefficient has also been determined for c-C_4F_8/N_2 mixtures with a total pressure of 1 Torr. The results are shown in Fig. 6. The limiting E/p values derived from the curves $\bar{\alpha}_a/p \sim$ E/p in Fig. 6 are shown in Fig. 7. Also shown in Fig. 7 are the uniform-field breakdown measurements by James and co-workers (1978) and those calculated by Novak and Fréchette (1984) from the Boltzmann equation. The agreement among the three different approaches is good.
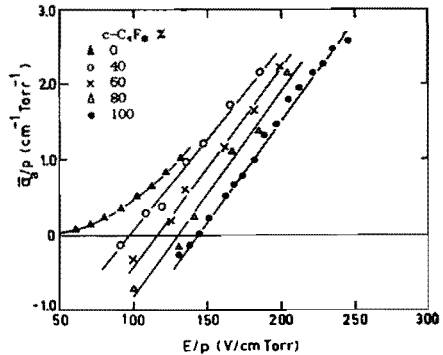

Fig. 6. $\bar{\alpha}_a/p$ versus E/p in c-C_4F_8/N_2 mixtures at a total pressure of 1 Torr.

Electrode erosion by corona discharges in c-C_4F_8

During the experiments, sudden rises of the DC current in the high voltage lead have been observed occasionally. This may be ascribed to corona discharges initiated from protrusions on the aluminum electrodes since complete breakdowns were not observed. Inspection of the electrode surface with an optical microscope indicated that the electrode surface was eroded by the corona discharges. This surface erosion affects the primary electron emission but not the avalanche current waveform. This waveform is governed by processes that occur while the swarm moves through
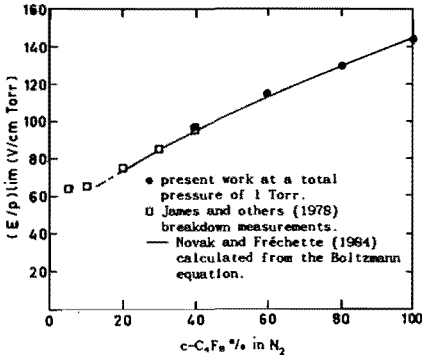
Fig. 7. (E/p)lim versus c-C_4F_8 % in N_2 at a total pressure of 1 Torr.

the gap. The reach of field distortions caused by the eroded surface is limited to a few μm's, which is short compared to the gap distance. The surface erosion may be the result of c-C_4F_8 decomposition products formed in corona discharges. This puts forward the question of stability of c-C_4F_8. It was further observed that the erosion reduces the number of primary electrons which can be released from the cathode by UV illumination. Moreover, the local field enhancements caused by the eroded surface may influence the breakdown voltage.

CONCLUSIONS

1. Swarm experiments in c-C_4F_8 at pressures above 10 Torr are hindered by the absence of a clearly distinguishable electron contribution to the avalanche current, which indicates a very dominant attachment process.

2. At lower pressures (below 10 Torr) the identification of the possible individual (attachment, detachment and conversion) processes that may contribute to the negative ion formation in c-C_4F_8 is impeded by electron diffusion.

3. The electron drift velocity, the apparent effective ionization coefficient, and (E/p)lim have been determined from time resolved Townsend experiments for c-C_4F_8 and c-C_4F_8/N_2 mixtures at a (total) pressure of 1 Torr. Our results are in reasonable agreement with the observations by others.

4. The (E/p)lim observed in c-C_4F_8 at low pressure (1 Torr) is consistent with the uniform-field breakdown measurements by Berril and co-workers (1987) at much higher pressures (75 ~ 450 Torr). This indicates that (E/p)lim does not depend on pressure over a wide pressure range.

5. The large values of the figure of merit M, observed by Berril and co-workers (1987) at relatively high pressures (75 ~ 450 Torr) are not reproduced in our low pressure, swarm experiments. This confirms that the figure of merit M exhibits a strong pressure dependence in c-C_4F_8.

6. Corona discharges in c-C_4F_8 cause surface erosion of the aluminum electrodes, which hinders the release of sufficient primary electrons (from the cathode) in the swarm experiment. This surface erosion does not affect the avalanche current waveform, but may influence the breakdown voltage.

REFERENCES

Aschwanden, Th. (1985). Ph.D Thesis, Swiss Federal Institute of Technology (ETH), Zurich, Diss. ETH No. 7931.
Berril, J., J.M. Christensen, and I.W. McAllister (1987). Measurement of the figure of merit M for several perfluorocarbon gases. In L.G. Christophorou, and D.W. Bouldin (Ed.), Gaseous Dielectrics V. Pergamon Press, New York. pp.304-310.
Bouldin, D.W., D.R. James, M.O. Pace, and L.G. Christophorou (1984). A current assessment of the potential of dielectric gas mixtures for industrial appalications. In L.G. Christophorou, and M.O. Pace (Ed.), Gaseous Dielectrics IV. Pergamon Press, New York. pp.204-212.
Brambring, J. (1964). Der Stromverlauf einer Elektronenlawine mit Diffusion. Zeitschrift für Physik, 179, 532-538.
Christophorou, L.G, R.A. Mathis, S.R. Hunter, and J.G. Carter (1987). Effect of temperature on the uniform field breakdown strength of electronegative gases. In L.G. Christophorou, and D.W. Bouldin (Ed.), Gaseous Dielectrics V. Pergamon Press, New York. pp.88-95.
James, D.R., L.G. Christophorou, R.Y. Pai, M.O. Pace, R.A. Mathis, I. Sauers, and C.C, Chan (1978). Dielectrics strengths of new gases and gas mixtures. Proc. Int. Symp. on Gaseous Dielectrics. Knoxille, Tennessee, March 6-8, 1978. 224-251.
James, D.R., L.G Christophorou, and R.A. Mathis (1980). New unitary and multicomponent gaseous dielectrics. In L.G. Christophorou (Ed.), Gaseous Dielectrics II. Pergamon Press, New York. pp.115-125.
Naidu, A.N., A.N. Prasad, and J.D. Craggs (1972). Electron transport, attachment and ionization in c-C_4F_8 and iso-C_4F_8. J. Phys. D: Appl. Phys., 5, 741-746.
Novak, J.P., and M.F. Fréchette (1984). Calculation of transport properties of N_2, SF_6, CCl_2F_2 and c-C_4F_8 and their respective mixtures. In L.G. Christophorou, and M. O. Pace (Ed.), Gaseous Dielectrics IV. Pergamon Press, New York. pp. 34-41.
Tagashira, H., Y. Miyamoto, and M. Shimozuma (1987). Pressure dependence of electrical breakdown voltage in c-C_4F_8. Proc. XVIII Int. Conf. on Phen. in Ionized Gases. Swansea, July 13-17, 1987. 680-681.
Verhaart, H.F.A., and P.C.T. van der Laan (1982). Fast current measurements for avalanche studies. J. Appl. Phys., 53(3), 1430-1436.
Wen, C., and J.M. Wetzer (1988a). Electron avalanches influenced by detachment and conversion processes. submitted to IEEE Trans. on Electrical Insulation. Jan., 1988.
Wen, C., and J.M. Wetzer (1988b). Swarm parameters in Hexafluoropropene 1-C_3F_6. 1988 IEEE Int. Symp. on Electrical Insulation, Boston, U.S.A, June 5-8. 1988. paper C-11.
Wetzer, J.M. and C. Wen (1987). Detachment and conversion processes in C_3F_6, analysis and observation from fast swarm experiments. Proc. 5th Int. Symp. on High Voltage Engineering (ISH). Braunschweig, West Germany, August 24-28, 1987. Paper 15.06.
Wetzer, J.M., C. Wen, and P.C.T. van der Laan (1988). Bandwidth limitations of gap current measurements. 1988 IEEE Int. Symp. on Electrical Insulation. Boston, U.S.A. June 5-8, 1988. paper I-3.

II. Time-resolved avalanche current waveforms in octafluorocyclobutane

COMMUNICATION

Time-resolved Avalanche Current Waveforms in Octafluorocyclobutane

C. Wen and J. M. Wetzer

High-Voltage Group,
Eindhoven University of Technology,
The Netherlands.

ABSTRACT

Avalanche currents have been measured by means of a time-resolved swarm method in c-C_4F_8 at pressures between 0.7 and 27 kPa. The recorded avalanche current waveforms are, in comparison with those of most insulating gases, unusual. Whereas in most gases avalanche current waveforms are characterized by a clear distinction between the electron contribution (high amplitude, short duration) and the ion contribution (low amplitude, long duration), the waveform in c-C_4F_8 is significantly different. During the first electron transit time an electron component can only be observed at low pressure (below 1.3 kPa) and even then is strongly intermixed with the ion contribution. Above ~ 1.3 kPa the waveform seems completely ion-dominated.

INTRODUCTION

THERE has been recent interest in the use of octafluorocyclobutane (c-C_4F_8) as a high-voltage insulant, primarily in view of its high dielectric strength [1–5].

Several observations related to the breakdown characteristics of this gas have been reported earlier [2,3,6] and can be summarized as follows. The uniform-field breakdown voltage in c-C_4F_8 at constant pd (pressure times gap distance) values has been found to increase with gas pressure [2,3]. In agreement with this, the measured pressure-reduced (apparent) effective ionization coefficient decreases with gas pressure [3]. Moreover, the measured value of the figure of merit M in c-C_4F_8 increases with p and is unexpectedly large at relatively high pressure [2].

To understand these observations in c-C_4F_8, more fundamental and direct information about the possible physical processes involved is obviously required. As an extension of our previous work [6], we present here fast time-resolved swarm experiments in c-C_4F_8 at pressures

between 0.7 and 27 kPa. The recorded avalanche current waveforms show an unusual behavior in comparison with those commonly encountered in insulating gases such as N_2, SF_6, dry air, and 1-C_3F_6.

EXPERIMENTAL TECHNIQUES

THE method which we used for the avalanche current measurement is the so-called time-resolved swarm method, which is based upon the detection of the total displacement current due to the drifting electrons and ions across a parallel-plate discharge gap under the influence of the applied electric field. To ensure a sufficient time resolution of the whole measuring system, the avalanche is initiated with an N_2 laser pulse of very short duration (0.6 ns), and the measuring cathode is subdivided. Furthermore, a Tektronix 7912 AD digitizer (with 7A29 and 7B10 units) is employed for recording the current waveforms. The time resolution of the whole system is about 1.4 ns. A detailed description of the present setup can be found elsewhere [7–10].

The vessel is evacuated with a turbomolecular pump down to 1.3×10^{-5} kPa before filling in high purity (99.9%) c-C_4F_8 gas (supplied by Hoekloos, Holland). The gas pressure was measured by two Pennwalt pressure gauges (0 ~ 6.7 kPa and 0 ~ 53 kPa). All pressure measurements were performed at room temperature (~ 22°C) and reduced to 20°C.

OBSERVATIONS

WITH fast time-resolved avalanche current measurements, one may identify delaying processes (if any), such as electron detachment and ion conversion, in addition to the more commonly recognised ionisation and attachment processes. This often requires a careful analysis of the electron component of the avalanche current at relatively high pressure. Figure 1 shows, for instance, the recorded electron component of the avalanche current waveform in dry air at 98.82 kPa. From such a waveform, the occurrence of delaying processes can be identified clearly since the current peak at one electron transit time T_e does not drop to zero (as would be the case without delaying processes) but is followed by a so-called 'aftercurrent'. At low pressure, this kind of identification is usually difficult due to electron diffusion which also results in an 'aftercurrent' (see Figure 2).

The ionic component of the avalanche current waveform is not only more difficult to interpret (because different ions with different drift velocities are involved), but also often provides little information on delaying
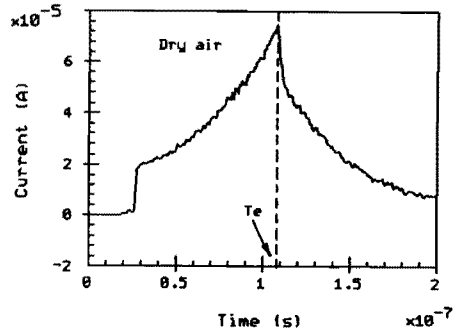

Figure 1.

Measured electron component of the avalanche current in dry air at high pressure. $p = 98.82$ kPa, $d = 1.0$ cm. $E = 25.94$ kV/cm.
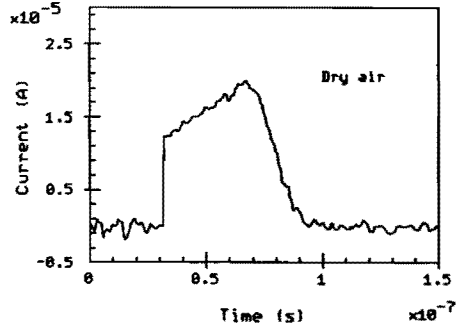

Figure 2.

Measured electron component of the avalanche current in dry air at low pressure. $p = 0.65$ kPa, $d = 1.0$ cm, $E = 324.4$ V/cm.

processes. Figures 3a and 3b show, for example, recorded ion currents in dry air, which is known to exhibit detachment and conversion processes as well as ionisation and attachment processes, and in N_2, which is known to exhibit only ionisation processes. It is clear that these two significantly different gases exhibit more or less similar ion current waveforms.

For avalanches in which only ionisation and attachment processes take place it was shown earlier [11] that
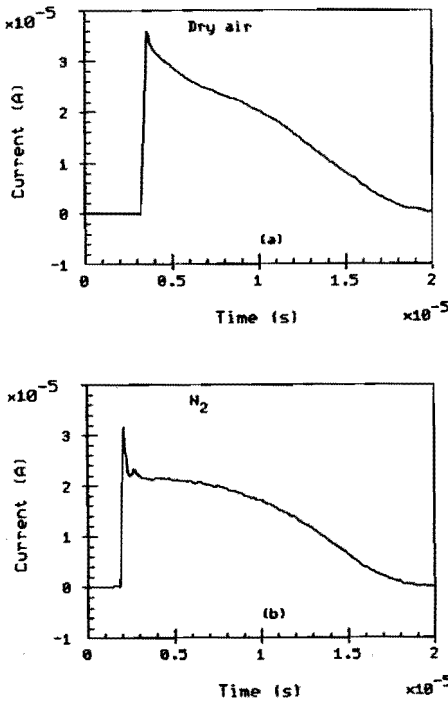
127

Figure 3.

Measured ion component of the avalanche currents in dry air and in N_2, which show little difference. $p = 98.74$ kPa $d = 1.0$ cm, $E = 27.0$ kV/cm,

the ion current is a strictly decreasing function of time after the first electron transit time. The electron and ion components of the avalanche current can usually be easily separated due to the quite different drift velocities of electrons and ions, and because the electron transit time usually can be identified from the current waveform.

The recorded avalanche current waveforms in c-C_4F_8 deviate, however, from the 'normal' waveforms described above. Firstly, at relatively high pressures (above ~ 1.3 kPa), no distinct electron current could be observed during the first electron transit time (which is usually in the order of several tens of ns). After this period, the current has been observed to increase gradu-

ally and then decrease. Some typical current waveforms of this type are shown in Figure 4. The increasing part of the current lasts for μs and should therefore be interpreted as a large ion contribution superimposed on a relatively small electron component. Although the electron component cannot be clearly distinguished from the ion component of the current, the long production time for ions can only be explained if a small electron component is present.

Secondly, at low pressures (below 1.3 kPa), although the electron current could be observed during the first electron transit time, the 'aftercurrent' is not 'normal'. It increases to a certain value, which may even be higher than the electron peak, and then decreases. Figure 5 shows some typical current waveforms of this type. Both types of current waveform, as shown in Figures 4 and 5, demonstrate the presence of delaying processes in c-C_4F_8. As will be shown, such delaying processes could be electron detachment and ion conversion as is the case in air and in 1-C_3F_6.

DISCUSSION

THE observations above strongly indicate ion production processes after the first electron transit time. Similar delayed production processes have also been observed in other gases, such as air [8,11], 1-C_3F_6 [7,9] or even SF_6 [12,13], but usually extend for only a few times the electron transit time. The very pronounced presence of delayed ion production, combined with the apparent absence of an electronic contribution in c-C_4F_8 at pressure above ~ 1.3 kPa can be explained by a combination of a strong attachment process (almost no free electrons during the first electron transit time) and a lifetime of the unstable negative ion formed that is large compared to the electron transit time. As a result, electrons are continuously produced from unstable negative ions even long after the first electron transit time. The drift and the production of these delayed electrons may result in an increasing after-current provided that the ion conversion/stabilization rate is not very high compared with the electron detachment rate. This increasing after-current will finally decrease due to, (a) the neutralization at the anode of those unstable negative ions which have not yet lost their electrons and, (b) the ion conversion/stabilization effect. This interpretation is consistent with the observed current waveforms as shown in Figure 5.

Moreover, the delayed electrons may again produce ions. The production of these delayed ions may last for several μs if the lifetime of the unstable negative ion is
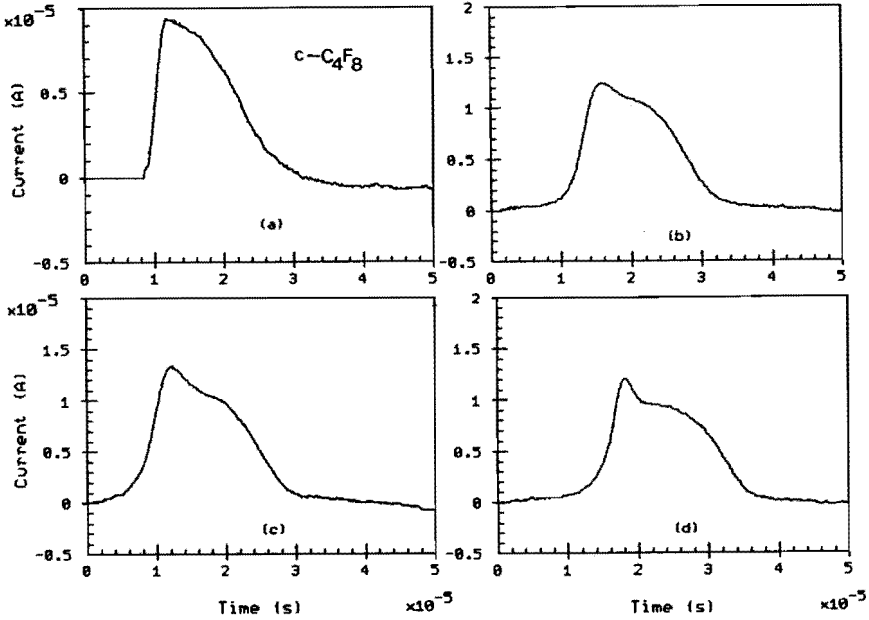
Figure 4.

Measured avalanche currents in c-C_4F_8 at relatively high pressures. $d = 1.0$ cm, (a) $p = 1.3$ kPa, $E = 1.50$ kV/cm; (b) $p = 6.7$ kPa, $E = 7.30$ kV/cm; (c) $p = 10.7$ kPa, $E = 11.70$ kV/cm; (d) $p = 20.0$ kPa, $E = 21.90$ kV/cm.

much longer than the electron transit time. This may explain why in Figure 4 the current continues to increase during a time in the order of 1 to 10 μs.

It is obvious that one cannot simulate the current waveforms as shown in Figures 4 and 5 by the conventional two-parameter model which includes only ionization and attachment (see for example [11]). Also in these circumstances the ionization and attachment coefficients obtained from a steady-state Townsend method [3] are apparent parameters and certainly not real ones at all.

WAVEFORM SIMULATION

To understand the avalanche waveforms presently measured in c-C_4F_8, we have performed some preliminary simulations of both electron and ion currents using a model which includes detachment and conversion in addition to ionization and attachment processes.

The model has been described earlier [7,8,11] and is summarized below.

Apart from neutral molecules, four species are considered: electrons (index e), positive ions (index p), unstable negative ions (index nu) and stable negative ions (index ns). For simplicity, it is assumed that all negative ions formed via electron attachment processes are unstable ions, which can either release their electron (via electron detachment), or can be converted into stable ones (via ion conversion). Furthermore, secondary emission from the cathode and diffusion of both electrons and ions in the gas are excluded. Experimental conditions often can be chosen such that these assumptions are justified.

Ionization (α) and attachment (η) coefficients are defined as usual, while detachment (δ) and conversion
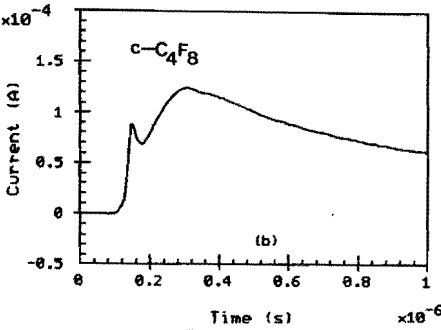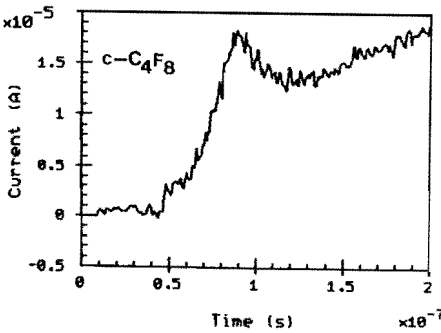
129

Figure 5.

Measured avalanche currents in c-C$_4$F$_8$ at low pressure. $p = 0.67$ kPa, $d = 1.0$ cm. (a) $E = 950.0$ V/cm: (b) $E = 1.00$ kV/cm. Note the difference in time scale.

$$\frac{\partial \rho_e(x,t)}{\partial t} + v_e \frac{\partial \rho_e(x,t)}{\partial x} = (\alpha - \eta) v_e \rho_e(x,t) + \delta v_e \rho_{nu}(x,t)$$
(1)

$$\frac{\partial \rho_p(x,t)}{\partial t} - v_p \frac{\partial \rho_p(x,t)}{\partial x} = \alpha v_e \rho_e(x,t)$$
(2)

$$\frac{\partial \rho_{nu}(x,t)}{\partial t} + v_{nu} \frac{\partial \rho_{nu}(x,t)}{\partial x} =$$

$$\eta v_e \rho_e(x,t) - (\delta + \beta) v_e \rho_{nu}(x,t)$$
(3)

$$\frac{\partial \rho_{ns}(x,t)}{\partial t} + v_{ns} \frac{\partial \rho_{ns}(x,t)}{\partial x} = \beta v_e \rho_{nu}(x,t)$$
(4)

where $\rho_j(x,t)$ is the density distribution across the gap (unit: cm^{-1}) and v_j is the drift velocity of species j ($j = e, p, nu, ns$). From these equations, and the appropriate initial and boundary conditions, the density distributions of the different species can be calculated as a function of position and time. In a recent article [8] we have presented a general analytical solution.

The electron and ion components of the avalanche current in the external circuit can be written as [8]

$$i_e(t) = \frac{e n_e(t)}{T_e} = \frac{e}{T_e} \int_0^d \rho_e(x,t) dx$$
(5)

$$i_i(t) = \sum_j \frac{e n_j(t)}{T_j}$$

$$= \sum_j \frac{e}{T_j} \int_0^d \rho_j(x,t) dx \quad j = p, nu, ns$$
(6)

where e is the elementary charge and $T_j = d/v_j$ is the transit time of species j ($j = e, p, nu, ns$).

The model presented above can be used to simulate avalanche current waveform for a given set of swarm parameters ($\alpha, \eta, \delta, \beta, v_e, v_p, n_{nu}$ and v_{ns}) and the gap separation d. Furthermore, the model has also been used in a curve fitting procedure in order to derive swarm parameters from measured avalanche current waveforms [7-9]. The model described is in principle applicable to all electronegative gases which exhibit detachment and conversion processes in addition to ionization and attachment processes. The interpretation of the swarm parameters depends however on the processes involved. If for example more than one process is responsible for detachment and conversion (multi-stage or simultaneous processes), the coefficients δ and β should be interpreted as 'apparent' values for the resulting overall process.

To our knowledge, a detailed reaction scheme, especially for the formation and destruction of negative ions, is not available for c-C$_4$F$_8$. As a first approximation, we assume that all negative ions formed in c-C$_4$F$_8$

(β) coefficients are defined as the mean number of detachment or conversion events per unstable negative ion in the time that an electron travels unit length in the field direction. These definitions for δ and β are more convenient for the study of avalanche growth than the conventional definitions [14] which relate δ and β to the ion drift velocity.

For a parallel-plate gap of separation d (cathode at $x = 0$, anode at $x = d$), the mentioned above definitions and conditions then result in the following set of partial differential equations for the densities of electrons and ions [8]

are unstable ions that can undergo either detachment or conversion during their drift towards the anode. For simplicity we also assume that all ions (positive, unstable and stable negative ions) have the same drift velocity $v_i = d/T_i$, where T_i is the transit time of ions.

Two typical simulations denoted 'high pressure' and 'low pressure' respectively are shown in Figure 6. In both cases the electron transit time is chosen to be 50 ns and the ion transit time is 10 μs at a gap separation of 1 cm. Hence E/p values are the same for both simulations. The coefficients α, η, δ and β are chosen such as to obtain waveforms similar to the observed waveforms shown in Figures 4 and 5. The similarities between the simulated current waveforms and the observed current waveforms seem to support the idea that electron detachment and ion conversion processes do take place in c-C_4F_8. Further analysis using this four-parameter model is in progress.

CONCLUSION

THE avalanche current waveforms recorded in c-C_4F_8 are unusual in comparison with those in most insulating gases. At low pressures (below ~ 1.3 kPa) the electron component of the current is followed by a large and increasing 'aftercurrent'. At higher pressures (above ~ 1.3 kPa), however, the electron component of the current could not be observed during the first electron transit time while the ionic component of the current is comparatively large. Both types of current waveform indicate that electron detachment and ion conversion processes do take place in c-C_4F_8, in addition to ionization and a very strong attachment process. This is further supported by the preliminary simulations of both electron and ion currents using a model which includes detachment and conversion as well as ionization and attachment processes.

ACKNOWLEDGMENT

REFERENCES

[1] G. Biasiutti, *Neue Isoliergase für gekapselte Hochspannungsanlagen*, Diss. ETH Nr. 7683, Zürich, 1985.

[2] J. Berril, J. M. Christensen and I. W. McAllister, "Measurement of the figure of merit M for several

perfluorocarbon gases", in L. G. Christophorou and D. W. Bouldin (Eds.), *Gaseous Dielectrics V*, Pergamon Press. New York, pp. 304–310, 1987.
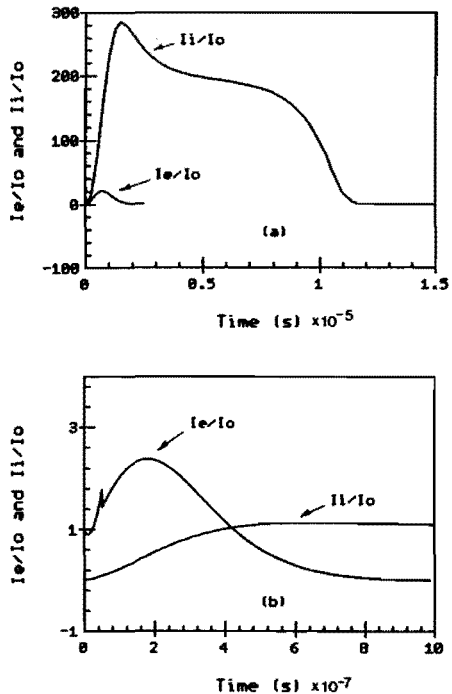
[3] H. Tagashira, Y. Miyamoto and M. Shimozuma, "Pres-

Figure 6.

Simulated electron (I_e/I_0), and ion (I_i/I_0) components of avalanche current waveforms in c-C_4F_8 using a four-parameter model which includes detachment (δ) and conversion (β) in addition to ionization (α) and attachment (η) processes. $d = 1$ cm, $T_e = 50$ ns, $T_i = 10\mu$s (I_0 is the initial electron current at time $t = 0$, T_e and T_i are electron and ion transit times respectively), (a) Simulations of the type of waveform as in Figure 4 (high pressure): $\alpha = 98$/cm, $\eta = 100$/cm, $\delta = 0.05$/cm, $\beta = 0.4$/cm; (b) Simulations of the type of waveform as in Figure 5 (low pressure); $\alpha = 9$/cm, $\eta = 10$/cm, $\delta = 0.5$/cm, $\beta = 0.4$/cm.

sure dependence of electrical breakdown voltage in c-C_4F_8", Proc. XVIII, Int. Conf. on Phen. in Ionized Gases (ICPIG), Swansea, pp. 680-681, July 1987.

[4] L. G. Christophorou, R. A. Mathis, S. R. Hunter and J. G. Carter, "Effect of temperature on the uniform field breakdown strength of electronegative gases", in L. G. Christophorou and D. W. Bouldin (Eds.), *Gaseous Dielectrics V*, Pergamon Press, New York, pp. 88-95, 1987.

[5] W. W. Bysewski and J. Veale, "Diffusion discharges in high-pressure mixtures of c-C_4F_8 and He", in L. G. Christophorou and D. W. Bouldin (Eds.), *Gaseous Dielectrics V*, Pergamon Press, New York, pp. 412-418, 1987.

[6] C. Wen and J. M. Wetzer, "Swarm parameters in Octafluorocyclobutane (c-C_4F_8) and its mixtures with N_2", Proc. 9th Int. Conf. on Gas Discharges and Their Applications (GD88), Venice, Sept. 19-23, pp. 367-370, 1988.

[7] J. M. Wetzer and C. Wen, "Detachment and conversion processes in C_3F_6 - Analysis and observation from fast swarm experiments", Proc. 5th Int. Symp. on High Voltage Engineering (ISH), Braunschweig, August 24-28, paper 15.06, 1987.

[8] C. Wen and J. M. Wetzer, "Electron avalanches influenced by detachment and conversion processes", IEEE Trans. Electr. Insul., Vol. 23, pp. 999-1008, 1988.

[9] C. Wen and J. M. Wetzer, "Swarm parameters in Hexafluoropropene 1-C_3F_6", Proc. Int. Conf. on Electrical Insulation, Boston, pp. 108-111, June 1988.

[10] J. M. Wetzer, C. Wen and P. C. T. van der Laan, "Bandwidth limitations of gap current measurement", Proc. Int. Conf. on Electrical Insulation, Boston, pp. 355-358, June 1988.

[11] H. F. A. Verhaart, *Avalanches in insulating gases*, Ph. D thesis, Eindhoven University of Technology, The Netherlands, 1982.

[12] T. H. Teich and D. W. Branston, "Time resolved observation of ionization and electron detachment in SF_6", Proc. 3rd Int. Conf. on Gas Discharges, London, IEE Conf. Publ. No. 118, pp. 109-113, 1974.

[13] T. H. Teich, M. A. A. Jabbar and D. W. Branston, "Observation and simulation of discharge development in electronegative gases", Proc. 2nd Int. Symp.

on High Voltage Engineering (ISH), Zürich, pp. 390-394, Sept. 1975.

[14] F. Llewellyn-Jones, *Ionisation Avalanches and Breakdown*, Science Paperbacks. Ch. 2.6, 1967.

5.9 Dichlorodifluoromethane

5.9.1 Introduction

Dichlorodifluoromethane (CCl_2F_2) has a slightly higher dielectric strength than SF_6, and is much cheaper (less than 1/7 of the cost of SF_6 (Cookson, 1980)). In the present work, fast swarm experiments have been performed in CCl_2F_2 over a pressure range of 50~198 Torr ($20^{\circ}C$) and an E/p_{20} range of 117~124 V/cmTorr.

5.9.2 Swarm parameters in CCl_2F_2: preliminary results

The experiments have been performed at relatively high pressure in order to observe whether or not delaying processes such as electron detachment occur in CCl_2F_2. Figure 5.9.1 shows some typical avalanche current waveforms measured in CCl_2F_2.

As was the case for SF_6, the measurements do not provide clear evidence of delaying processes: no tail shows up in the electron current waveform. The fall of the electron current waveform after one electron transit time, however, is too long to be explained by diffusion. This again indicates significant detachment, strongly counteracted by stabilization processes.

In spite of the presence of delaying processes, the electron component in SF_6 could well be described by a two-parameter model. Because of the strong resemblance between the waveforms measured in SF_6 and in CCl_2F_2, we again, as a first approximation, apply this two-parameter model to the present measurements. If this two-parameter model is applicable, the technique presented earlier for the separation of the electron and ion component of the current waveform is valid. Figure 5.9.2 shows the resulting electron component corresponding to the waveform in Fig. 5.9.1d.

The obtained electron drift velocity v_e and the effective ionization coefficient $\bar{\alpha}$ are shown in Figs. 5.9.3 and 5.9.4 respectively.

In contrast to the results obtained for SF_6, both the electron drift velocity v_e and the pressure-reduced effective ionization coefficient $\bar{\alpha}/p_{20}$ show a marked decrease with increasing pressure, which tends to saturate at high pressure. At pressures above

133

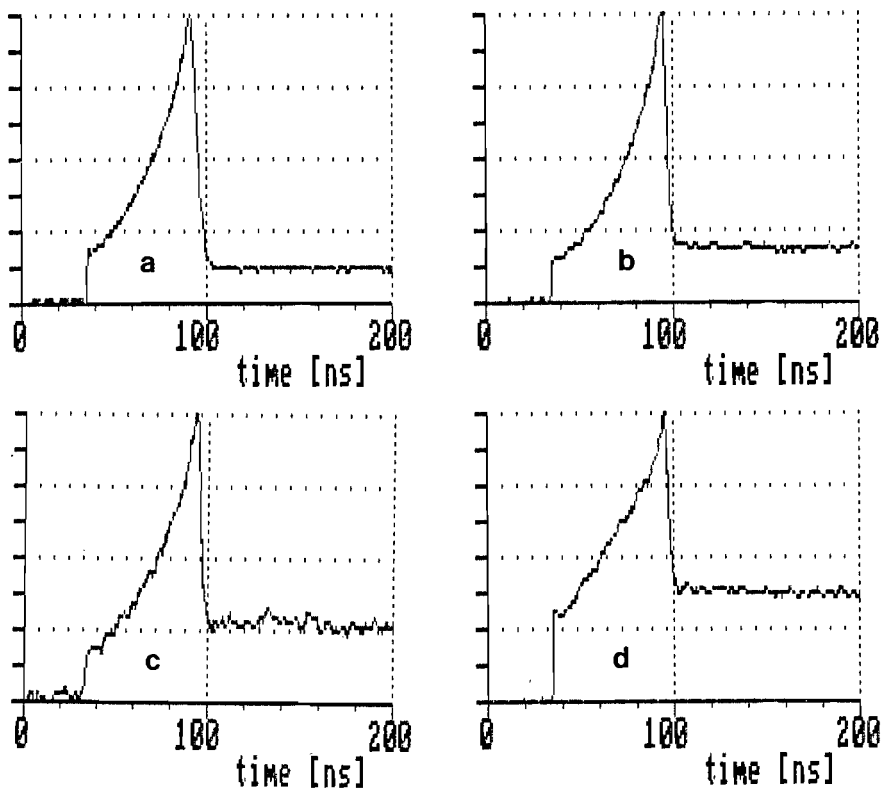150 Torr, the pressure dependence is no longer observed.

Figure 5.9.1

Avalanche current waveforms measured in CCl_2F_2 at relatively high pressure. Here p_{20} (Torr): (a) 49.9, (b) 99.4, (c) 148.9, (d) 197.9. E/p_{20} (V/cmTorr): (a) 121.25, (b) 123.13, (c) 123.45, (d) 123.04. The unit at the vertical axis (μA) is: (a) 11.4, (b) 8.33, (c) 3.73, (d) 5.94, d=1.0 cm. The electron component of the waveform in Fig. 5.9.1d is shown in Fig. 5.9.2.

To the author's knowledge, such a strong pressure dependence in CCl_2F_2 at pressures below 150 Torr has not been reported before, although Boyd and co-workers (1970) also reported a slight decrease in $\overline{\alpha}/p_{20}$ with increasing p_{20}.
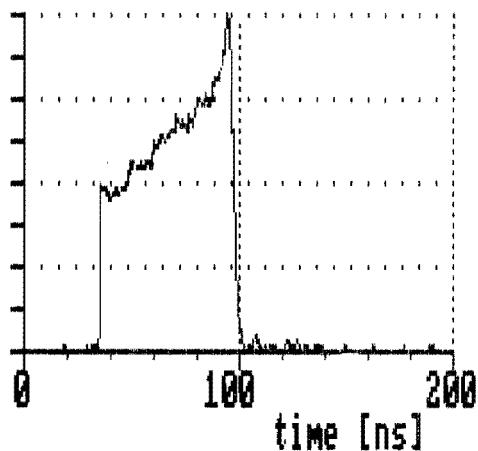
Figure 5.9.2

Electron component of the avalanche current waveform shown in Fig. 5.9.1d. The unit at the vertical axis is 3.75 μA.
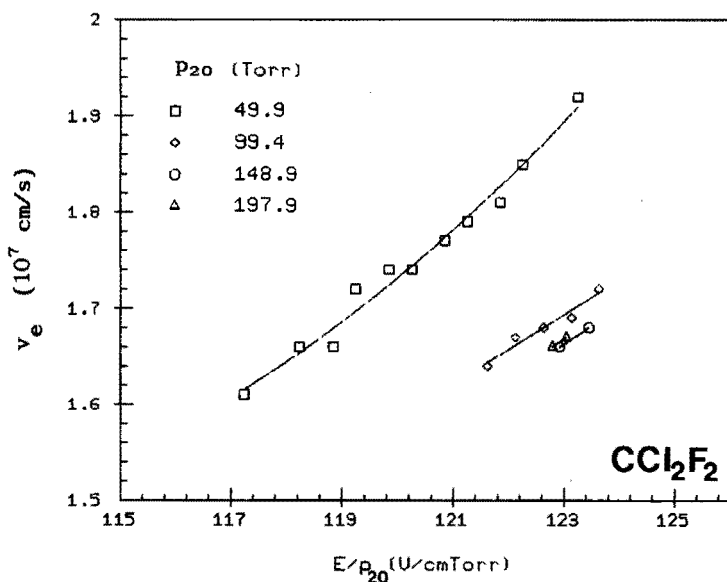

Figure 5.9.3

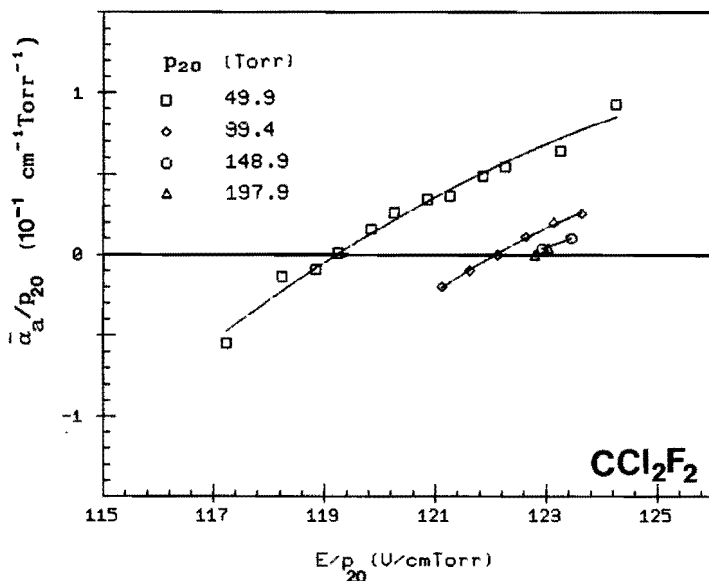The apparent electron drift velocity v_e in CCl_2F_2.

Figure 5.9.4

The apparent pressured-reduced effective

ionization coefficient $\bar{\alpha}/p_{20}$ in CCl_2F_2.

With respect to the observed pressure dependences, CCl_2F_2 resembles $1-C_3F_6$. In $1-C_3F_6$, however, clear evidence of delaying processes was found for low pressure $1-C_3F_6$ in a high pressure buffer gas N_2 (to avoid diffusion). Similar measurements in a CCl_2F_2/N_2 mixture did not reveal such evidence.

A possible explanation for the observed behavior in CCl_2F_2 is that the detachment and stabilization processes active in CCl_2F_2 introduce an abnormal pressure dependence as a result of the different pressure dependences of the individual processes. At sufficiently high pressure, ion conversion becomes so dominant that detachment processes no longer produce delayed electrons to a significant amount.

The four-parameter model should be applied to obtain more detailed information on these processes. This calls, first of all, for a separation of the total current waveform into an electron- and an ion- component. The separation technique applied to SF_6, however,

is based on the two-parameter model. As stated earlier (in the case of O_2) this technique has not yet been developed for "complex" (four-parameter) gases. Note that in $1-C_3F_6$ the ion current is low and separation of the waveform into an electron- and an ion-component is not required.

Further study is required to, first of all, derive the electron component of the current waveforms in "complex" gases, and secondly to obtain more detailed information on the delaying processes in CCl_2F_2.

5.10 Overview of avalanche types

From the results and discussions in the previous sections, we can summarize the types of avalanches encountered in this investigation.

Firstly, avalanches can be subdivided into two significantly different categories, namely electron-dominated avalanches and ion-dominated avalanches. Electron-dominated avalanches show a clear electron component in the avalanche current waveform. This electron component has a much higher amplitude and a much shorter duration than the ion component. This type of avalanche has been observed in all gases studied in this thesis except in $c-C_4F_8$. In $c-C_4F_8$ at low pressure the electron and ion components are strongly intermixed, and above about 10 Torr, the electron component can no longer be recognized and the waveform is completely ion-dominated.

Secondly, in the category of electron-dominated avalanches, we distinguish between avalanches with and without delaying processes. For avalanches in which no attachment processes occur (i.e., where no negative ions are formed), all electrons reach the anode at the same time (no electrons are delayed). This corresponds to a steep fall in the electron component. This type of avalanche has been observed in N_2, and in principle shoud be observed in all non-attaching gases. For avalanches in which attachment processes occur, not all electrons arrive at the anode at the same time if the negative ions formed undergo subsequent detachment processes. This type of avalanche has been observed in all attaching gases studied in this thesis.

Thirdly, for electron-dominated avalanches with delaying processes, we can distinguish between situations with a low and a high conversion rate. If the conversion rate (or conversion coefficient) is low, delayed electrons can be clearly observed from the electron current waveform. At a low or moderate detachment rate the electron current shows a steep drop after one electron transit time, followed by an aftercurrent. Examples are air, O_2 and a mixture of low pressure $1-C_3F_6$ in a high pressure buffer gas N_2. At high detachment rate the steep drop after one electron transit time can no longer be recognized and an apparent decrease in drift velocity is observed. If the conversion rate is high, the detachment process is strongly counteracted, which results in a decrease in the number of delayed electrons. The waveform then resembles that of a gas without

delaying processes, but usually shows a fall time, around the electron transit time, that is too long to be explained by diffusion only. In spite of the presence of delaying processes, the electron current waveform may, in some cases, still be correctly described with a "simple" model that does not include delaying processes. An example is SF_6. For other gases, however, the "simple" model results in abnormal pressure dependences of the coefficients obtained ($1-C_3F_6$ and CCl_2F_2)

CHAPTER 6

CONCLUSIONS

1. Swarm studies provide information on the processes responsible for the avalanche growth, and on the resulting charge distribution of the avalanche, and are thereby an important tool for the understanding of breakdown in insulating gases.

2. Compared to the steady-state Townsend method, the time-resolved swarm method provides more detailed information on processes in avalanches, and their effect on the avalanche growth, and thereby allow the verification of more complex models. The difference is especially important for the understanding of streamer breakdown where the charge distribution is crucial.

3. Electron detachment and ion conversion often play an important role in the avalanche growth because they affect the charge distribution, and may introduce an abnormal pressure dependence in the "apparent" drift velocity, and in the "apparent" attachment coefficient.

4. The observation of the development of an avalanche during its transit, and in particular the observation of electron detachment, ion conversion and electron diffusion, requires a time-resolution in the order of 1 ns or better. Such a time-resolution can be achieved by the use of a pulsed laser with a short pulse width, by a subdivided measuring electrode, by taking into account the effects of stray capacitance and inductance, and by a careful selection of the measuring equipment.

5. The evaluation of time-resolved avalanche current waveforms requires the application of an adequate model that takes into account all relevant processes. The use of too simple models results in "apparent" values for the swarm parameters that may substantially differ from the "real" values. This obscures physical interpretation and seemingly violates known scaling laws.

6. With the coefficients for ionization (α), attachment (η), detachment (δ) and conversion (β) as defined in this work, the

140

electron current waveform can be fully described by the following three sets of swarm coefficients: $\alpha-\eta$ (the "real" effective ionization coefficient), $\delta+\beta$ (which describes the loss rate of unstable negative ions), and $\eta\delta$ (a secondary, delayed, ionization parameter).

7. When applying a two-parameter model to a gas that exhibits all four processes mentioned above, the derived "apparent" coefficient $(\alpha-\eta)$ is related to the "real" coefficients as: $(\alpha-\eta)_{apparent}=(\alpha-\eta)_{real}+\eta\delta/(\delta+\beta)$.

8. If the observation of the electron transit time is obscured by electron trapping, the low pressure ("zero-density") drift velocity should be derived, and used in the determination of the other swarm parameters.

9. Clear evidence of delaying processes was found for dry air, O_2, $1-C_3F_6$ and $c-C_4F_8$. Swarm parameters have been determined for dry air and $1-C_3F_6$, as well as for a mixture of low pressure $1-C_3F_6$ in a high pressure N_2 background with a four-parameter model. These swarm parameters have been interpreted in terms of the responsible collisional processes. An explanation is given for the abnormal pressure dependence of the "apparent" drift velocity and the "apparent" effective ionization coefficient in $1-C_3F_6$. It is found that the corresponding "real" values show no abnormal pressure dependence up to a pressure of 100 Torr.

10. An indication of delaying processes was found in SF_6 and CCl_2F_2. For SF_6 the electron current can, nevertheless, be described by the two-parameter model (ionization and attachment only). For CCl_2F_2 such an approach results in an abnormal pressure dependence in both the electron drift velocity and the "apparent" effective ionization coefficient, for pressures below 150 Torr.

11. Of the gases studied, N_2 is the only gas in which no indication of delaying processes was found. Nitrogen is also the only non-attaching gas studied in this work.

12. Of the gases studied, only N_2 and SF_6 can be adequately described by a two-parameter model. The swarm parameters derived on the basis of this "simple" model are in good agreement with those reported in the literature.

141

13. In c–C_4F_8 delaying processes dominate the avalanche current waveforms. At low pressure (up to 10 Torr) the electron component of the current is strongly intermixed with the ion component. At higher pressure no distinct electron component can be observed. This behavior can be explained by a very strong attachment process, and a lifetime of the unstable negative ion formed that is large compared to the electron transit time.

DERIVATION OF THE ELECTRON DENSITY DISTRIBUTION OF AN AVALANCHE IN WHICH IONIZATION, ATTACHMENT, DETACHMENT, CONVERSION AND ELECTRON DIFFUSION PROCESSES OCCUR

To solve Eqs. (3.5.2a) and (3.5.2b) in chapter 3 (section 3.5), we employ the Laplace and Fourier transform techniques. The definitions of these two transforms for a function $f(t)$ $(t \geq 0)$ are:

Laplace:
$$L[f(t)] = \overline{f(s)} = \int_0^{+\infty} \exp(-st)f(t)dt \qquad (A.1a)$$

Inverse Laplace:
$$L^{-1}[\overline{f(s)}] = f(t) = \frac{1}{2\pi i} \int_{c-i\infty}^{c+i\infty} \exp(st)\overline{f(s)}ds \qquad (A.1b)$$

Fourier:
$$F[f(t)] = \overline{f(\omega)} = \int_{-\infty}^{+\infty} \exp(-i\omega t)f(t)dt \qquad (A.1c)$$

Inverse Fourier:
$$F^{-1}[\overline{f(\omega)}] = f(t) = \frac{1}{2\pi} \int_{-\infty}^{+\infty} \exp(i\omega t)\overline{f(\omega)}d\omega \qquad (A.1d)$$

The following approach for solving Eqs. (3.5.2a) and (3.5.2b) is based on the method used by Ritchie and Turner (1967). Their model, however, is extended here to include also ionization and conversion processes.

Applying the Laplace transform to both Eqs. (3.5.2a) and (3.5.2b) with respect to t, we find:

$$s\overline{\rho_e(x,s)} - \rho_e(x,0) + W_r\frac{\partial\overline{\rho_e(x,s)}}{\partial x} = \overline{\alpha}v_e\overline{\rho_e(x,s)} + \delta v_e\overline{\rho_{nu}(x,s)}$$
$$+ D\frac{\partial^2\overline{\rho_e(x,s)}}{\partial x^2} \qquad (A.2a)$$

$$s\overline{\rho_{nu}(x,s)} - \rho_{nu}(x,0) = \eta v_e\overline{\rho_e(x,s)} - (\delta+\beta)v_e\overline{\rho_{nu}(x,s)} \qquad \text{(A.2b)}$$

If we assume that no unstable negative ions are present at t=0, i.e., $\rho_{nu}(x,0)=0$, then from Eq. (A.2b) we obtain:

$$\overline{\rho_{nu}(x,s)} = \frac{\eta v_e}{s + (\delta+\beta)v_e}\overline{\rho_e(x,s)} \qquad \text{(A.3)}$$

Substitution of Eq. (A.3) and the initial condition $\rho_e(x,0)=n_oD(x)$, where $D(x)$ is the Dirac function (unit: cm^{-1}), into Eq. (A.2a) yields:

$$D\frac{\partial^2\overline{\rho_e(x,s)}}{\partial x^2} - W_r\frac{\partial\overline{\rho_e(x,s)}}{\partial x} - \Gamma\overline{\rho_e(x,s)} = -n_oD(x) \qquad \text{(A.4)}$$

where

$$\Gamma = s - \bar{\alpha}v_e - \frac{\eta\delta v_e^2}{s + (\delta+\beta)v_e} \qquad \text{(A.5)}$$

Applying the Fourier transform to Eq. (A.4) with respect to x, we obtain:

$$-\omega^2D\overline{\overline{\rho_e(\omega,s)}} - i\omega W_r\overline{\overline{\rho_e(\omega,s)}} - \Gamma\overline{\overline{\rho_e(\omega,s)}} = -n_o$$

or

$$\overline{\overline{\rho_e(\omega,s)}} = \frac{n_o}{D\omega^2 + iW_r\omega + \Gamma} \qquad \text{(A.6)}$$

Here $\overline{\overline{\rho_e(\omega,s)}}$ denotes the Fourier transform of function $\overline{\rho_e(x,s)}$ according to Eq. (A.1c). The inverse Fourier transform of $\overline{\overline{\rho_e(\omega,s)}}$ will yield $\overline{\rho_e(x,s)}$:

$$\overline{\rho_e(x,s)} = \frac{1}{2\pi} \int\limits_{-\infty}^{+\infty} \exp(i\omega x)\overline{\overline{\rho_e(\omega,s)}}\,d\omega$$

$$= \frac{n_0}{2\pi D} \int\limits_{-\infty}^{+\infty} \frac{\exp(i\omega x)}{\omega^2 + i\dfrac{W_r}{D}\omega + \dfrac{\Gamma}{D}}\,d\omega$$

$$= \frac{n_0}{2\pi D} \int\limits_{-\infty}^{+\infty} \frac{\exp(i\omega x)}{(\omega - \omega_1)(\omega - \omega_2)}\,d\omega \qquad (A.7)$$

Here

$$\omega_{1,2} = i\left(-\frac{W_r}{2D} \pm \sqrt{\frac{W_r^2}{4D^2} + \frac{\Gamma}{D}}\,\right) \qquad (A.8)$$

and ω_1 takes the positive sign.

The complex integration in Eq. (A.7) is performed by the choice of an integration contour that consists of an infinite semi-circle enclosing the upper half of the complex ω-plane and the root ω_1. Application of the residue theorem (see, for example, Saff and Snider, 1976) gives:

$$\overline{\rho_e(x,s)} = \frac{n_0}{2\pi D}\cdot 2\pi i\cdot\frac{\exp(i\omega_1 x)}{(\omega_1 - \omega_2)} \qquad (A.9)$$

Substitution of $\omega_{1,2}$ into Eq. (A.9) gives:

$$\overline{\rho_e(x,s)} = \frac{n_0\exp(\dfrac{W_r x}{2D})}{2\sqrt{D}}\cdot\frac{\exp\left(-\dfrac{x}{\sqrt{D}}\sqrt{\dfrac{W_r^2}{4D} + \Gamma}\,\right)}{\sqrt{\dfrac{W_r^2}{4D} + \Gamma}} \qquad (A.10)$$

Finally from the inverse Laplace of $\overline{\rho_e(x,s)}$, we can write $\rho_e(x,t)$ as:

$$\rho_e(x,t) = \frac{1}{2\pi i} \int\limits_{c-i\infty}^{c+i\infty} \exp(st)\overline{\rho_e(x,s)}\ ds$$

$$= \frac{n_0 \exp(\frac{W_r x}{2D})}{4\pi i \sqrt{D}} \int\limits_{c-i\infty}^{c+i\infty} \frac{\exp(st - \frac{x}{\sqrt{D}}\sqrt{\frac{W_r^2}{4D} + \Gamma})}{\sqrt{\frac{W_r^2}{4D} + \Gamma}}\ ds \qquad (A.11)$$

Equation (A.11), in a complex integral form, gives the electron number-density distribution at any position x ($0{\le}x{\le}d$) and at any time t ($\underset{\sim}{\le}2T_e$).

To check the validity of Eq. (A.11), we consider the following two situations. Firstly we consider a situation without electron detachment, i.e., $\delta{=}0$. From Eq. (A.5) we obtain $\Gamma{=}s{-}\overline{\alpha}v_e$, and Eq. (A.11) can be written as:

$$\rho_e(x,t) = A\frac{1}{2\pi i} \int\limits_{c-i\infty}^{c+i\infty} \exp(st) \cdot \frac{\exp(-a\sqrt{s+b})}{\sqrt{s+b}}\,ds$$

$$= AL^{-1}\left[\frac{\exp(-a\sqrt{s+b})}{\sqrt{s+b}}\right] \qquad (A.12)$$

where

$$A = \frac{n_0\exp(\frac{W_r x}{2D})}{2\sqrt{D}} \quad ; \qquad a = \frac{x}{\sqrt{D}} \quad ; \qquad b = \frac{W_r^2}{4D} - \overline{\alpha}v_e \qquad (A.13)$$

When we apply the Laplace transform property:

$$L^{-1}[\overline{f(s+c)}] = \exp(-ct)L^{-1}[\overline{f(s)}] \qquad (A.14)$$

where c is a constant, and if we further apply the Laplace transform (Spiegel, 1968):

146

$$L^{-1}[\frac{\exp(-a\sqrt{s})}{\sqrt{s}}] = \frac{\exp(-\frac{a^2}{4t})}{\sqrt{\pi t}} \tag{A.15}$$

Equation (A.12) (and hence Eq. (A.11)) becomes:

$$\rho_e(x,t) = A\exp(-bt)L^{-1}[\frac{\exp(-a\sqrt{s})}{\sqrt{s}}]$$

$$= A\exp(-bt)\frac{\exp(-\frac{a^2}{4t})}{\sqrt{\pi t}} \tag{A.16}$$

Substitution of A, a and b from Eq. (A.13) into Eq. (A.16) gives:

$$\rho_e(x,t) = \frac{n_0\exp(\bar{\alpha}v_e t)}{\sqrt{4\pi Dt}}\exp[-\frac{(x-W_r t)^2}{4Dt}] \tag{A.17}$$

This solution is identical to Eq. (3.4.5) derived in section 3.4 where only ionization, attachment and electron diffusion are considered.

For a second check we consider the situation without electron diffusion (D=0). Equation (A.11) should now yield the same solution that was derived in section 3.3.

Since D=0, and thereby $W_r = v_e + \bar{\alpha}D = v_e$, Eq. (A.6) becomes:

$$\overline{\overline{\rho_e(\omega,s)}} = \frac{n_0}{iv_e\omega + \Gamma} \tag{A.18}$$

Equation (A.7) can then be written as:

$$\overline{\rho_e(x,s)} = \frac{1}{2\pi}\int_{-\infty}^{+\infty}\frac{n_0\exp(i\omega x)}{iv_e\omega + \Gamma}d\omega = \frac{n_0}{2\pi iv_e}\int_{-\infty}^{+\infty}\frac{\exp(i\omega x)}{\omega - \frac{i\Gamma}{v_e}}d\omega \tag{A.19}$$

Complex integration results in:

$$\overline{\rho_e(x,s)} = \frac{n_0}{v_e}\exp(-\frac{\Gamma}{v_e}x) \qquad (A.20)$$

Substitution of Γ from Eq. (A.5) into Eq. (A.20) gives:

$$\overline{\rho_e(x,s)} = \frac{n_0}{v_e}\exp(c_1 x)\exp[(\frac{c_3 v_e^2}{s + c_2 v_e} - s)\frac{x}{v_e}] \qquad (A.21)$$

where

$$c_1 = \alpha - \eta \ ; \quad c_2 = \delta + \beta \ ; \quad c_3 = \eta\delta \qquad (A.22)$$

The electron number density $\rho_e(x,t)$ is obtained by taking the inverse Laplace transform of $\overline{\rho_e(x,s)}$ (Eq. (A.11)):

$$\rho_e(x,t) = L^{-1}[\overline{\rho_e(x,s)}]$$

$$= \frac{n_0}{v_e}\exp(c_1 x)L^{-1}\{\exp[\frac{c_3 v_e^2}{s + c_2 v_e} - (s + c_2 v_e) + c_2 v_e]\frac{x}{v_e}\}$$

$$= \frac{n_0}{v_e}\exp(c_1 x + c_2 x)L^{-1}\{\exp[\frac{c_3 v_e x}{s + c_2 v_e} - (s + c_2 v_e)\frac{x}{v_e}]\} \qquad (A.23)$$

Applying Eq. (A.14), we can write Eq. (A.23) as:

$$\rho_e(x,t) = \frac{n_0}{v_e}\exp[c_1 x - c_2(v_e t - x)]L^{-1}[\exp(\frac{c_3 v_e x}{s} - s\frac{x}{v_e})] \qquad (A.24)$$

For $\overline{f(s)} = \exp(\frac{c_3 v_e x}{s})$ and $\overline{h(s)} = \frac{1}{s}\overline{f(s)}$, we can write (Spiegel, 1968):

$$L^{-1}[\overline{h(s)}] = h(t) = I_0(\sqrt{4c_3 v_e xt}) \qquad (A.25)$$

where $I_0(y)$ is the zero order modified Bessel function (see Eq. (3.3.17)). Since $h(0) = 1$ (Eq. (A.25)), we obtain:

148

$$f(t) = L^{-1}[\overline{f(s)}] = L^{-1}[\exp(\frac{c_3 v_e x}{s})]$$

$$= L^{-1}[s\overline{h(s)}] = L^{-1}[s\overline{h(s)} - h(0) + h(0)]$$

$$= L^{-1}[s\overline{h(s)} - h(0)] + L^{-1}[h(0)]$$

$$= \frac{dh(t)}{dt} + D(t)$$

$$= \sqrt{\frac{c_3 v_e x}{t}} \; I_1(\sqrt{4c_3 v_e xt}) + D(t) \qquad (A.26)$$

where $I_1(y)$ is the first order modifed Bessel function (defined in Eq. (3.3.17)) and $D(t)$ is the Dirac function.

We now apply the theorem that, if $\overline{f(s)}=L[f(t)]$, then:

$$L^{-1}[\exp(-t_0 s)\overline{f(s)}] = p(t) \qquad (A.27)$$

where

$$p(t) = 0 \qquad \text{for } 0 < t < t_0 \qquad (A.28)$$

and

$$p(t) = f(t-t_0) \qquad \text{for } t \geq t_0 \qquad (A.29)$$

From Eqs. (A.24) and (A.26), we then obtain for $0 < t < \frac{x}{v_e}$ (i.e. $x > v_e t > 0$) that:

$$\rho_e(x,t) = 0 \qquad (A.30)$$

and for $t \geq \frac{x}{v_e}$ (i.e., $x \leq v_e t$) that:

$$\rho_e(x,t) = \frac{n_0}{v_e}\exp[c_1 x - c_2(v_e t - x)]f(t - \frac{x}{v_e})$$

$$= \frac{n_0 y_0 \exp(f_0)}{2(v_e t - x)}I_1(y_0) + \frac{n_0}{v_e}D(t - \frac{x}{v_e})\exp(c_1 x) \qquad (A.31)$$

where

$$y_0 = 2\sqrt{c_3(v_e t - x)x} \qquad (A.32)$$

$$f_0 = c_1 x - c_2(v_e t - x) \qquad (A.33)$$

This solution is identical to the summation of Eqs. (3.3.13) (for the delayed component) and (3.3.10a) (for the undelayed component), if we assume that $v_{nu} = 0$.

REFERENCES

Aschwanden, Th. (1985). Die Ermittlung physikalischer Entladungs-parameter in Isoliergasen und Isoliergasgemischen mit einer verbesserten Swarm-Methode. Ph.D Thesis, Swiss Federal Institute of Technology (ETH), Zürich, Diss. ETH, No. 7931.

Aschwanden, Th., and G. Biasiutti (1981). Dielectric strength of hexafluoropropylene (C_3F_6). J. Phys. D: Appl. Phys., Vol. 14, L189-192.

Aschwanden, Th., H. Böttcher, D. Hansen, H. Jungblut, and W.F. Schmidt (1982). Mobility and recombination of ions and effective ionization coefficient in hexafluoropropylene (C_3F_6). In L.G. Christophorou (Ed.), Gaseous Dielectrics III, Pergamon Press, New York, pp.23-33.

Berril, J., J.M. Christensen, and I.W. McAllister (1987). Measurement of the figure of merit M for several perfluorocarbon gases. In L.G. Christophorou, and D.W. Bouldin (Eds.), Gaseous Dielectrics V, Pergamon Press, New York, pp.304-310.

Biasiutti, G. (1985). Neue Isoliergase für gekapselte Hochspannurgs-anlagen. Ph. D Thesis, Swiss Federal Institute of Technology (ETH), Zürich, Diss. ETH, No. 7683.

Biasiutti, G., C. Amman, E. Engler, and W.S. Zaengl (1983). Electric strength of hexafluoropropylene (C_3F_6) and its mixtures with SF_6 at practical pressures. Proc. 4th Int. Symp. on High Voltage Engineering (ISH), Athens, Sept. 5-9, Paper 33.02.

Blevin, H.A. (1985). Spatially dependent energy distribution in swarm experiments. Proc. 17th Int. Conf. on Phen. in Ionized Gases (ICPIG), Budapest, July 8-12, Invited Papers, pp.308-319.

Borghesani, A.F., L. Bruschi, M. Santini. and G. Torzo (1986). The influence of the cell geometry on the signal shape in electron drift velocity measurements. Z. für Naturforschung, Vol. 41a, pp.912-920.

Boyd, H.A., G.C. Crichton, and T. Munk Nielsen (1970). Determination of ionization and attachment coefficients in CCl_2F_2. Proc. 1st Int. Conf. on Gas Discharges, London, Sept. 15-18, IEE Conf. Publ. No. 70, pp.426-430.

Brambring, J. (1964). Der Stromverlauf einer Elektronenlawine mit

Diffusion. Z. für Physik, Vol. 179, pp.532-538.

Brennan, M.J., and T.H. Teich (1988). Swarm parameters in N_2-O_2 mixtures using the photon flux technique. Proc. 9th Int. Conf. on Gas Discharges and Their Applications, Venezia, Sept. 19-23, pp.343-346.

Bronshtein, I.N., and K.A. Semendyayev (1985). Handbook of Mathematics (English translation, edited by K.A. Hirsch). Verlag Harri Deutsch, Thun and Frankfurt/Main, pp.258-259.

Bruce, F.M. (1947). Calibration of uniform-field spark-gaps high-voltage measurement at power frequencies. J. IEE, Vol. 94, Part II, pp.138-149.

Chen, C.L., R.E. Wootton, and P.J. Chantry (1982). Measured attachment and ionization cross sections and dielectric strength of CF_3SF_5 and C_3F_6. Proc. 7th Int. Conf. on Gas Discharges and Their Applications, London, Aug. 31~Sept. 3, Peter Peregrinus, London, pp.321-324.

Christophorou, L.G. (Ed.) (1984). Electron-Molecule Interactions and Their Applications. Vols.1 & 2, Academic Press, New York.

Christophorou, L.G., and S.R. Hunter (1984). From basic research to application. In L.G. Christophorou (Ed.), Electron-Molecule Interactions and Their Applications, Vol.2, Academic Press, New York, pp.318-412.

Christophorou, L.G., D.R. James, R.Y. Pai, R.A. Mathis, I. Sauers, L. Frees, M.O. Pace, D.W. Bouldin, C.C. Chan, and E.J. Kent (1979). High voltage research (breakdown strengths of gaseous and liquid insulators) and environmental effects of dielectric gases. Oak Ridge National Laboratory Report, Oak Ridge, Tennessee, ORNL/TM-6902.

Christophorou, L.G., D.R. James, I. Sauers, M.O. Pace, R.Y. Pai, and A. Fatheddin (1982). Ternary gas dielectrics. In L.G. Christophorou (Ed.), Gaseous Dielectrics III, Pergamon Press, New York, pp.151-163.

Christophorou, L.G., R.A. Mathis, S.R. Hunter, and J.G. Carter (1987). Effect of temperature on the uniform field breakdown strength of electronegative gases. In L.G. Christophorou, and D.W. Bouldin (Eds.), Gaseous Dielectrics V, Pergamon Press, New York, pp.88-95.

Cookson, A.H. (1980). Electrical breakdown studies of $SF_6/CO_2/$fluorocarbon mixtures. In L.G. Christophorou (Ed.), Gaseous Dielectrics II, Pergamon Press, New York, pp.169-178.

Feser, K., and J. Schmid (1987). Influence of atmospheric conditions on the impulse breakdown of rod-plane gaps. Proc. 5th Int. Symp. on High Voltage Engineering (ISH), Braunschweig, Aug. 24-28, Paper 11.01. See also many other contributed papers on this subject in the same proceeding.

Fletcher, J. (1981). Recent measurements of electron transport coefficients. In L.G. Christophorou (Ed.), Electron and Ion Swarms, Pergamon Press, New York, pp.1-10.

Francis, G. (1960). Ionization Phenomena in Gases. London, Butterworths Scientific Publication.

Frommhold, L. (1963). Simultaneous determination of the electron attachment and detachment rates in oxygen. In M.R.C. McDowell (Ed.), Atomic Collision Processes: Proc. 3rd Int. Conf. on Phys. of Electronic and Atomic Collisions, London, July 22-26, 1963, North-Holland, Amsterdam, 1964, pp.556-564.

Frommhold, L. (1968). Resonance scattering and the drift motion of electrons through gases. Phys. Rev., Vol. 172, pp.118-123.

Gallimberti, I., E. Poli, S. Stangherlin, and T.H. Teich (1988). Photodetachment probing of negative oxygen ion populations. Proc. 9th Int. Conf. on Gas Discharges and Their Applications, Venezia, Sept. 19-23, Benetton, Padova, pp.351-354.

Garrity, T.F., and J.P. Vora (1980). The future testing needs of gas-insulated substations. In L.G. Christophorou (Ed.), Gaseous Dielectrics II, Pergamon Press, New York, pp.389-398.

Gilardini, A. (1972). Low Energy Electron Collisions in Gases. John Wiley & Sons, New York.

Grünberg, R. (1967). Bestimmung der Driftgeschwindigkeit von Elektronen in Wasserstoff und Stickstoff bei hohem Druck. Z. für Physik, Vol. 204, pp.12-16.

Grünberg, R. (1968). Messungen der Elektronenbeweglichkeit bei hohen Gasdrucken in Ar, He, N_2 und H_2. Z. für Naturforschung, Vol. 23a, pp.1994-2004.

Hansen, D., H. Jungblut, and W.F. Schmidt (1983). Electron detachment from negative ions in sulphur hexafluoride. J. Phys. D: Appl.

Phys., Vol. 16, pp.1623-1634.

Harland, P.W., and J.C.J. Thynne (1972). Dissociative capture in perfluoropropylene and perfluoropropane. Int. J. Mass Spectrom. and Ion Phys., Vol. 9, pp.253-266.

Hunter, S.R., and L.G. Christophorou (1984). Pressure-dependent electron attachment and breakdown strengths of unitary gases, and synergism of binary gas mixtures: a relationship. In L.G. Christophorou and M.O. Pace (Eds.), Gaseous Dielectrics IV, Pergamon Press, New York, pp.115-127.

Hunter, S.R., and L.G. Christophorou (1985). Pressure-dependent electron attachment and breakdown strengths of unitary gases and synergism of binary gas mixtures: a relationship. J. Appl. Phys., Vol. 57, No. 9, pp.4377-4385.

Hunter, S.R., L.G. Christophorou, D.R. James, and R.A. Mathis (1982). Pressure-dependent electron attachment rates in perfluoroalkanes and perfluoropropylene $(1-C_3F_6)$ and their effect on the breakdown strength of these gases. In L.G. Christophorou (Ed.), Gaseous Dielectrics III, Pergamon Press, New York, pp.7-22.

Hunter, S.R., L.G. Christophorou, D.L. McCorkle, I. Sauers, H. Ellis, and D.R. James (1983). Anomalous electron attachment properties of perfluoropropylene $(1-C_3F_6)$ and their effect on the breakdown strength of this gas. J. Phys. D: Appl. Phys., Vol. 16, pp.573-580.

Huxley, L.G.H., and R.W. Crompton (1974). The Diffusion and Drift of Electrons in Gases. John Wiley & Sons, New York.

James, D.R., L.G. Christophorou, and R.A. Mathis (1980). New unitary and multicomponent gaseous dielectrics. In L.G. Christophorou (Ed.), Gaseous Dielectrics II, Pergamon Press, New York, pp.115-125.

James, D.R., L.G. Christophorou, R.Y. Pai, M.O. Pace, R.A. Mathis, I. Sauers, and C.C. Chan (1978). Dielectrics strengths of new gases and gas mixtures. In L.G. Christophorou (Ed.), Proc. 1st Int. Symp. on Gaseous Dielectrics, Knoxville, Tennessee, March 6-8, pp.224-251.

Kailash Kumar, H.R. Skullerud, and R.E. Robson (1980). Kinetic theory of charged particle swarm in neutral gases. Aust. J. Phys., Vol. 33, pp.343-448.

Lifshitz, C., and R. Grajower (1972). Dissociative electron capture and dissociative ionization in perfluorocyclobutane. Int. J. Mass Spectrom. and Ion Phys., Vol. 10, pp.25-37.

Llewellyn-Jones, F. (1967). Ionization Avalanches & Breakdown. Methuen, London, Science Paperbacks, Vol. 37.

Llewellyn-Jones, F. (1983). The development of theories of the electrical breakdown of gases. In E.E. Kunhardt, and L.H. Luessen (Eds.), Electrical Breakdown and Discharges in Gases, Part A: Fundamental Processes and Breakdown. Plenum Press, New York and London, pp.1-71.

Lowke, J.J. (1962). Errors due to diffusion in drift velocity measurements. Aust. J. Phys., Vol. 15, pp.39-58.

Märk, T.D. (1984). Ionization of molecules by electron impact. In L.G. Christophorou (Ed.), Electron-Molecule Interactions and Their Applications, Vol. 1, Academic Press, pp.251-334.

McDaniel, E.W. (1964). Collision Phenomena in Ionized Gases, John Wiley & Sons, New York.

Meek, J.M., and J.D. Craggs (Eds.) (1978). Electrical Breakdown of Gases. John Wiley & Sons, New York.

Morrow, R. (1986). A survey of the electron and ion transport properties in SF_6. IEEE Trans. on Plasma Science, Vol. PS-14, No. 3, pp.234-239.

Ohmori, Y., M. Shimozuma, and H. Tagashira (1988). Boltzmann equation analysis of electron swarm behaviour in nitrogen. J. Phys. D: Appl. Phys., Vol. 21, pp.724-729.

O'Neill, B.C., and J.D. Craggs (1973a). Collisional detachment of electrons and ion molecule reactions in oxygen. J. Phys. B: Atom. Molec. Phys., Vol. 6, pp.2625-2633.

O'Neill, B.C., and J.D. Craggs (1973b). Collisional detachment of electrons in sulphur hexafluoride. J. Phys. B: Atom. Molec. Phys., Vol. 6, pp.2634-2640.

Raether, H. (1964). Electron Avalanches and Breakdown in Gases. London, Butterworths.

Ramo, S. (1939). Currents induced by electron motion. Proc. IRE, Vol. 27, pp.584-585.

Ritchie, R.H., and J.E. Turner (1967). Electron capture and loss in electron swarm experiments. Z. für Physik, Vol. 200, pp.259-269.

Saff, E.B., and A.D. Snider (1976). Fundamentals of Complex Analysis for Mathematics, Science, and Engineering. Prentice-Hall, Englewood Cliffs, New Jersey. Chapter 6.

Sakai, Y., H. Tagashira, and S. Sakamoto (1977). The development of electron avalanches in argon at high E/N values: I. Monte Carlo simulation. J. Phys. D: Appl. Phys., Vol. 10, pp.1035-1049.

Satoh, K., H. Itoh, Y. Nakao, and H. Tagashira (1988). Electron swarm development in SF_6: II. Monte Carlo simulation. J. Phys. D: Appl. Phys., Vol. 21, pp.931-936.

Schlumbohm, H. (1965). Elektronenlawinen bei hohen E/p. Zur Bestimmung der Driftgeschwindigkeiten von Elektronen und Ionen, der Elektronenstoβionisierung und der Elektronenenergien. Z. für Physik, Vol. 182, pp.306-316.

Schmidt, W.F., H. Jungblut, and D. Hansen (1980). Ionic and electronic processes in sulfur hexafluoride. In L.G. Christophorou (Ed.), Gaseous Dielectrics II, Pergamon Press, New York, pp.1-11.

Schmidt, W.F., and R.J. Van Brunt (1982). Comments on the effect of electron detachment in initiating breakdown in gaseous dielectrics. In L.G. Christophorou (Ed.), Gaseous Dielectrics III, Pergamon Press, New York, pp.561-563.

Shockley, W. (1938). Currents to conductors induced by a moving point charge. J. Appl. Phys., Vol. 9, pp.635-636.

Skullerud, H.R. (1977). Progress in the transport theory of weakly ionized gases. Proc. 13th Int. Conf. on Phen. in Ionized Gases (ICPIG), Berlin, Sept. 12-17, Invited Lectures, pp.303-319.

Somerville, I.C., and D.J. Tedford (1982). Negative ion detachment and its effect on the statistical time-lag in gases. Proc. 7th Int. Conf. on Gas Discharges and Their Applications. London, Aug. 31-Sept. 3, Peter Peregrinus, London, pp.325-327.

Spiegel, M.L. (1968). Mathematical Handbook of Formulas and Tables. McGraw-Hill, New York, Part II.

Steutel, F.W. (1986). Avalanches of electrons in a gas. J. Appl. Prob., Vol. 23, pp.867-879.

Tagashira, H. (1981). Development of electron avalanches at high electric fields. Proc. 15th Int. Conf. on Phen. in Ionized Gases (ICPIG), Minsk, July 14-18, Invited Papers, pp.377-394.

Tagashira, H. (1985). Principles of the measurement of electron drift

velocities. In L.C. Pitchford, B.V. Mckoy, A. Chutjian, and
S. Trajmar (Eds.), Swarm Studies and Inelastic Electron-Molecule
Collisions, Springer-Verlag, New York, pp.55-61.

Tagashira, H., Y. Miyamoto, and M. Shimozuma (1987). Pressure
dependence of electrical breakdown voltage in c-C_4F_8. Proc. 18th
Int. Conf. on Phen. in Ionized Gases, Swansea, July 13-17,
pp.680-681.

Tagashira, H., Y. Sakai, and S. Sakamoto (1977). The development of
electron avalanches in argon at high E/N values: II. Boltzmann
equation analysis. J. Phys. D: Appl. Phys., Vol. 10, pp.1051-1063.

Tagashira, H., A. Taneda, and M. Shimozumas (1985). The measurement
of the ionization and attachment coefficients in 1-C_3F_6 and SF_6
mixtures. Proc. 17th Int. Conf. on Phen. in Ionized Gases,
Budapest, July 8-12, Vol. 1, pp.632-634.

Taniguchi, T., H. Tagashira, and Y. Sakai (1978). Boltzmann equation
analysis of the electron swarm development in nitrogen. J. Phys.
D: Appl. Phys., Vol. 11, pp.1757-1768.

Teich, T.H. (1981). Electrons and ions in sulphur hexafluoride. In
L.G. Christophorou (Ed.), Electron and Ion Swarms, Pergamon Press,
New York, pp.241-250.

Teich, T.H., and D.W. Branston (1974). Time resolved observation of
ionization and electron detachment in SF_6. Proc. 3rd IEE Int.
Conf. on Gas Discharges, London, Sept. 9-12, IEE Conf. Publ.
No. 118, pp.109-113.

Teich, T.H., and E.C.A. Morris (1987a). Laser-produced photon-
detachment from ion swarms in dry and moist oxygen. Proc. 18th
Int. Conf. on Phen. in Ionized Gases (ICPIG), Swansea, July 13-17,
pp.50-51.

Teich, T.H., and E.C.A. Morris (1987b). Galvanooptical measurement of
photodetachment from negative ion swarms in oxygen. In
L.G. Christophorou and D.W. Bouldin (Eds.), Gaseous Dielectrics V,
Pergamon Press, New York, pp.18-26.

de Urquijo-Carmona, J. (1983). Ion mobilities and clustering in SF_6
at high pressures. J. Phys. D: Appl. Phys., Vol. 16, pp.1603-1609.

de Urquijo-Carmona, J., I. Alvarez, and C. Cisneros (1985). Transient
analysis of the drift and longitudinal diffusion of ions in a
uniform-field discharge gap. J. Phys. D: Appl. Phys., Vol. 18,

pp.29-40.

de Urquijo-Carmona, J., I. Alvarez, and C. Cisneros (1986). Time-resolved study of charge transfer in SF_6. J. Phys. D: Appl. Phys., Vol. 19, L207-210.

Verhaart, H.F.A. (1982). Avalanches in Insulating Gases. Ph.D thesis, Eindhoven University of Technology, The Netherlands.

Verhaart, H.F.A., and P.C.T. van der Laan (1982). Fast current measurements for avalanche studies. J. Appl. Phys., Vol. 53, No. 3, pp.1430-1436.

Verhaart, H.F.A., and P.C.T. van der Laan (1983). Fast avalanche measurements in C_3F_6. Proc. 4th Int. Symp. on High Voltage Engineering (ISH), Athens, Sept. 5-9, Paper 33.12.

Verhaart, H.F.A., and P.C.T. van der Laan (1984). The influence of water vapor on avalanches in air. J. Appl. Phys., Vol. 55, No. 9, pp.3286-3292.

Wagner, K.H. (1971). Ionization, electron attachment-detachment, and charge-transfer in oxygen and air. Z. für Physik, Vol. 241, pp.258-270.

Wedding, A.B., H.A. Blevin, and J. Fletcher (1985). The transport of electrons through nitrogen gas. J. Phys. D: Appl. Phys., Vol. 18, pp.2361-2373.

Wen, C., and J.M. Wetzer (1988a). Swarm parameters in Hexafluoro-propene $1-C_3F_6$. Proc. IEEE Int. Symp. on Electrical Insulation, Boston, June 5-8, pp.108-111.

Wen, C., and J.M. Wetzer (1988b). Electron avalanches influenced by detachment and conversion processes. IEEE Trans. on Electrical Insulation, Vol. 23, No. 6, pp.999-1008.

Wetzer, J.M., and C. Wen (1987). Detachment and conversion processes in C_3F_6, analysis and observation from fast swarm experiments. Proc. 5th Int. Symp. on High Voltage Engineering (ISH), Braunschweig, Aug. 24-28, Paper 15.06.

Wootton, R.E., S.J. Dale, and N.J. Zimmerman (1980). Electric strength of some gases and gas mixtures. In L.G. Christophorou (Ed.), Gaseous Dielectrics II, Pergamon Press, New York, pp.137-146.

CURRICULUM VITAE

Date of birth : April 23, 1960.

Place of birth : Xi'an, China.

9.1966~7.1978 : Primary and middle school education in Xi'an, China.

    Prize : *Shaanxi provincial middle-school mathematics contest.*

9.1978~7.1982 : University education at the Dept. of Electrical Engineering, Xi'an Jiaotong University, China, finished with a Bachelor's degree of electrical engineering (B. Eng.).

Bachelor project : *Measurement and calculation of electrostatic field in substations (High-Voltage Group).*

9.1982~5.1985 : Postgraduate study and research at the High-Voltage Group, Dept. of Electrical Engineering, Xi'an Jiaotong University, China, finished with a Master's degree of electrical engineering (M. Eng.).

 Master project : *Investigation of ionized field under HVDC transmission lines.*

   Prize : *Prof. Chen Da-Xie's Award, Xi'an Jiaotong University.*

5.1985~9.1985 : Assistant teacher at the High-Voltage Group, Dept. of Electrical Engineering, Xi'an Jiaotong University, China.

10.1985~9.1989 : Ph.D research at the High-Voltage Group, Dept. of Electrical Engineering, Eindhoven University of Technology, The Netherlands.

 Ph.D project : *Time-resolved swarm studies in gases with emphasis on electron detachment and ion conversion.*

STELLINGEN

behorende bij het proefschrift

TIME-RESOLVED SWARM STUDIES IN GASES
WITH EMPHASIS ON
ELECTRON DETACHMENT AND ION CONVERSION

door

WEN, CHUAN

⟨1⟩

The boundary condition that presumes a zero density of the charged particles at all times at the electrodes of an avalanche setup, as was used by, for example, Huxley and Crompton (1974), is inconsistent with the currents observed in the external circuit.

Huxley, L.G.H., and R.W. Crompton (1974). *The Diffusion and Drift of Electrons in Gases*. John Wiley & Sons, New York.

This thesis, chapter 2.

⟨2⟩

The mechanism for the positive synergism observed in the gas mixture $1-C_3F_6/c-C_4F_8$, as proposed by Hunter and Christophorou (1985), is incomplete because of the neglect of unstable negative ions in $c-C_4F_8$ which have been found to be present in considerable numbers.

Hunter, S.R., and L.G. Christophorou (1985). *J. Appl. Phys.*, Vol. 57, No. 9, pp.4377-4385.

This thesis, chapter 5.

⟨3⟩

The swarm parameters determined by Naidu and co-workers (1972) for $c-C_4F_8$ at very low pressures cannot be extrapolated to higher pressures because of the pronounced occurrence of electron detachment and ion conversion processes.

Naidu, M.S., A.N. Prasad, and J.D. Craggs (1972). *J. Phys. D: Appl. Phys.*, Vol. 5, pp.741-746.

This thesis, chapter 5.

⟨4⟩

The critical remark of Phelps (1987) on the discrepancy between the values for the effective ionization coefficient in humid air calculated by himself, and the values found experimentally by Verhaart and van der Laan (1984), is not significant because Phelps disregards the difference between the "real" and "apparent" coefficients.

Phelps, A.V. (1987). In L.G. Christophorou, and D.W. Bouldin (Eds.), *Gaseous Dielectrics V*, Pergamon Press, New York, pp.1-9.

Verhaart, H.F.A., and P.C.T. van der Laan (1984). *J. Appl. Phys.*, Vol. 55, No. 9, pp.3286-3292.

As in mixtures of some insulating gases where a positive synergism has been observed (the dielectric strength of the mixture is higher than that of either of the constituent gases, see chapter 5 of this thesis), an optimum political system may be found by properly mixing socialism and capitalism.

The intention of avoiding mathematical equations in "A Brief History of Time" (1988, Bantam Press, London) by Stephen W. Hawking is overdone; when combined properly, mathematical equations and physical interpretations can describe science and technology more easily and more clearly than either of the two.

In science management one should bear in mind the statement of Feshbach (1986): "The arrogant pronouncement that some field is no longer interesting has been made often and has been wrong just as often.".
Feshbach, H. (1986). _Physics Today_, *June, 1986, p.7.*

Competition of any kind may or may not be beneficial to the development of society, but is certainly harmful to the competitors, both physically and psychologically, if they have to spend most of their time and effort on the competition itself.

The letter of the "College van Bestuur" (1989) concerning "Beleid ter voorkoming van ongewenste intimiteiten" may make people feel uncomfortable at dealing with normal relationships.
College van Bestuur (1989). No. CvB 163, 410 d.d. 12.06.1989.

Real democracy and freedom can only be achieved through a non-violent approach.

<11>

Music is an empty box in which you can put your own feeling, emotion and imagination, and get a full box which might be completely different from the one that somebody else has obtained.

<12>

The abbreviation of terms both in daily life and in technology often leads to misunderstanding and should be limited in use. For example, NS can mean Nederlandse Spoorwegen or Never Stop; Chinese Airlines Always Cancel (Crash!) is certainly not the original meaning of CAAC (Civil Aviation Administration of China); and Ph.D (Doctor of Philosophy) means more than only Pain, Headache and Disease. For myself, I will never abbreviate my own name!

Eindhoven, 26 September 1989.
Wen, Chuan